



POLITECNICO DI MILANO

SCUOLA DI INGEGNERIA INDUSTRIALE E DELL'INFORMAZIONE
Corso di Laurea Magistrale in Ingegneria Aeronautica

TESI DI LAUREA MAGISTRALE

**An adjoint based topology optimization for flows including
heat transfer**

Relatore
Prof. Marco VERANI

Candidato
Emiliano Ruberto
Matr. 837569

Correlatore
Prof. Nicola PAROLINI

Anno Accademico 2016 - 2017

Ringraziamenti

Ai professori Marco Verani e Nicola Parolini va la mia gratitudine per avermi guidato in questo mio lavoro, e rivolgo loro un sentito ringraziamento per avermi dato l'opportunità di dedicarmi con passione al conseguimento dei risultati ottenuti.

A Laura e alla mia famiglia che mi hanno sempre sostenuto con fiducia nei momenti di maggiore difficoltà.

Ai miei cari amici Giuseppe e Francesco da cui ho ricevuto amicizia e preziosi consigli.

Contents

1	Introduction	12
2	The optimal control problems	16
2.1	Abstract optimal control problem	16
2.2	Governing equations for natural convection problems	18
2.3	<i>Control Problem 1</i>	20
2.4	<i>Control Problem 2</i>	22
2.5	Non-dimensional form of the state equations	23
2.5.1	Non-dimensional <i>Control Problem 1</i>	23
2.5.2	Non-dimensional <i>Control Problem 2</i>	24
3	Optimality conditions	26
3.1	Optimal control problem 1	27
3.1.1	Adjoint equations	27
3.1.2	Adjoint boundary conditions	30
3.1.3	Gradient of the cost function	34
3.2	Optimal control problem 2	34
3.2.1	Adjoint equations	34
3.2.2	Adjoint boundary conditions	36
3.2.3	Gradient of the cost function	36
3.3	Dimensionless form of the <i>adjoint</i> equations	37
3.3.1	Non-dimensional <i>Control Problem 1</i>	37
3.3.2	Non-dimensional <i>Control Problem 2</i>	38
4	Solver algorithm description	39
4.1	The SIMPLE algorithm	39
4.2	Optimal control problem solver: <i>Algorithm 1</i>	40
4.3	Optimal control problem solver: <i>Algorithm 2</i>	42
4.3.1	Line Search method: Backtracking	44
4.3.2	Intermediate control values penalization	47

<i>CONTENTS</i>	4
4.3.3 Volume constraint	48
4.3.4 q-parametrized interpolation functions	49
5 Numerical Tests	52
5.1 A simpler optimal control problem	52
5.1.1 1D Thermal problems	53
5.1.2 2D Thermal problems	62
5.2 Natural convection in a cavity	69
5.2.1 <i>Solver Algorithm 1</i> : a first natural convection study	69
5.2.2 <i>Solver Algorithm 2</i> : a second natural convection study	72
5.2.3 A third natural convection study	76
6 Conclusions	86
A Adjoint equations	88
A.1 Integration by parts	88
A.2 Adjoint boundary conditions	91

List of Figures

1.1	Schematical representation of the porous media domain. Red areas with a non-zero porosity value ($\rho = 1$) correspond to the “solid body” domain (practically, with zero flow within those regions). Blue areas ($\rho = 0$) indicate the flow passage.	14
2.1	Detail of cavity	20
4.1	Block scheme for the <i>Algorithm 1</i>	41
4.2	Block scheme for the <i>Algorithm 2</i>	43
4.3	Illustration of the sufficient condition (4.2)	44
4.4	Penalization function	48
4.5	Interpolation function (4.20) plotted for different q values	50
4.6	Derivatives (4.24) and (4.25) for q equal to 0.1 and 10	51
5.1	Reference temperature T^* and associated control variable ρ^* for 1D thermal problem	54
5.2	Final solutions for unconstrained 1D optimization (<i>Control Problem 1</i>)	55
5.3	Final solutions for 1D volume constraint optimization (<i>Control Problem 1</i>)	56
5.4	Final solutions for unconstrained 1D optimization (<i>Control Problem 2</i>)	58
5.5	$J(\rho^k)$ corresponding to the k-th iteration (ρ^k is close to the final one) for two different values of q	59
5.6	Comparison of analytical and numerical solutions of adjoint and primal temperature equations relative to a fixed K distribution . . .	60
5.7	Slope of T (m_s) as function of K_s for a 1D thermal problem with fixed temperature at the boundary and K distribution given in fig (5.6a)	61
5.8	Reference control and associated temperature for 2D thermal problem	63
5.9	Unconstrained optimization results for the 2D thermal problem . .	65

5.10	Constrained optimization results for 2D thermal problem	66
5.11	Constrained optimization results for 2D thermal problem (<i>Control Problem2 K-limit</i>)	68
5.12	Initial control and <i>filt</i> field. The red regions in (b) form the admissible control domain Ω_ρ : that one the right is the <i>cold</i> one, the other is the <i>hot</i> one	70
5.13	Optimization results for the <i>first natural convection study (Control Problem 1)</i>	71
5.14	Optimization results for the <i>first natural convection study (Control Problem 2)</i>	72
5.15	Reference control and relative temperature, filtering field: the red regions in (c) form the admissible control domain Ω_ρ	73
5.16	Optimization results for the <i>second natural convection study (Control Problem 1)</i>	75
5.17	Optimization results for the <i>second natural convection study (Control Problem 2)</i>	77
5.18	Cavity layout	78
5.19	Initial conditions in the cavity	79
5.20	All optimal $K(\rho)$ and $\alpha(\rho)$ for different values of T^*	82
5.21	Final velocity and temperature field for different values of T^*	83
5.22	Comparison of initial temperature T_0 and final T on the heated wall Γ_q for different values of T^*	84
5.23	Comparison of filtered and non filtered sensibilities in the same case setup ($T^* = 2$), at the 40 th iteration	85

List of Tables

5.1	Settings of the parameters for 1D unconstrained optimization (<i>Control Problem 1</i>)	55
5.2	Initial and final values of cost function (J_0 and J_{opt} respectively), number of optimization iterations, execution time (unconstrained 1D optimization, <i>Control Problem 1</i>)	55
5.3	Settings of the parameters for 1D constrained optimization (<i>Control Problem 1</i>)	56
5.4	Initial and final values of cost function $J = J_{obj} + J_v$, number of optimization iterations, execution time (constrained 1D optimization, <i>Control Problem1</i>)	57
5.5	Settings of the parameters for 1D unconstrained optimization (<i>Control Problem 2</i>)	58
5.6	Initial and final values of cost function (J_0 and J_{opt} respectively), number of optimization iterations, execution time (unconstrained 1D optimization, <i>Control Problem 2</i>)	61
5.7	Settings of the parameters for 2D thermal <i>Control Problem 2</i> unconstrained optimization	64
5.8	Initial and final values of cost function (J_0 and J_{opt}), number of optimization iterations, execution time (unconstrained 2D thermal optimization, <i>Control Problem 2</i>)	64
5.9	Settings of the parameters for 2D thermal <i>Control Problem2 K-limit</i> constrained optimization	67
5.10	Initial and final values of cost function $J = J_{obj} + J_p$, number of optimization iterations, execution time (constrained 2D thermal optimization, <i>Control Problem2 K-limit</i>)	67
5.11	Settings of the tolerances of primal and adjoint equations (<i>second natural convection study, Control Problem 1</i>)	74
5.12	Settings of the solver parameters for the <i>second natural convection study</i> (constrained optimization, <i>Control Problem 1</i>)	74

5.13	Initial and final values of cost function $J = J_{obj} + J_v + J_p$, number of optimization iterations, execution time (<i>second natural convection study</i> constrained optimization, <i>Control Problem 1</i>)	74
5.14	Settings of the parameters for the <i>second natural convection study</i> (constrained optimization, <i>Control Problem 2 K-limit</i>)	76
5.15	Initial and final values of cost function $J = J_{obj} + J_p$, number of optimization iterations, execution time (<i>second natural convection study</i> constrained optimization, <i>Control problem 2</i>)	76
5.16	Settings of the parameters for the <i>third natural convection study</i> . .	81
5.17	Settings of the tolerances of primal and adjoint equations	81
5.18	$T^* = 2.1$: initial and final values of cost function $J = J_{obj} + J_p$, number of optimization iterations, execution time	81
5.19	$T^* = 2.05$: initial and final values of cost function $J = J_{obj} + J_p$, number of optimization iterations, execution time	81
5.20	$T^* = 2$: initial and final values of cost function $J = J_{obj} + J_p$, number of optimization iterations, execution time	82

Abstract

The continuous adjoint approach to topology optimization is a new and active area of research in computational fluid dynamics, particularly for internal flows applications. The present work addresses the development of an *open source* CFD solver for topology optimization of fluids with heat transfer. One possible ultimate industrial application for such optimization tool is the design of heat exchangers. The professional finite volume library OpenFOAM has been used for the solver implementation. The study of optimization methods is the central topic of this work: two control problems are presented and specialized to the study case of natural convection in a 2D cavity, in laminar regime. A different treatment of the thermal properties on the solid portion of the domain distinguishes the two control problems. Their continuous adjoint formulations are derived for a chosen cost function. Two algorithms are also proposed for the iterative resolution of the problems. Finally a series of test cases is meant to validate the results of these studies. The two control problems give satisfactory results, providing a good starting point for further applications in more complex cases.

Keywords: Topology Optimization, Continuous Adjoint, OpenFOAM, Flows with Heat Transfer

Sommario

I problemi di ottimizzazione sono un argomento trattato con molto interesse in diversi campi di studio ed in particolare in molte scienze applicate. In ingegneria, il tema dell'ottimizzazione è generalmente legato alla ricerca di un "design ottimo" che massimizzi le prestazioni di un dato sistema rispetto ad un obiettivo specifico. Questo lavoro in particolare è incentrato sullo sviluppo di un codice CFD *open source* per l'ottimizzazione topologica (mediante operatore aggiunto) di problemi fluidodinamici incomprimibili con scambio termico. L'obiettivo è quello di creare i presupposti di base per l'utilizzo del codice in problemi di rilevanza ingegneristica e industriale, quali ad esempio la progettazione di scambiatori di calore. Trattandosi di uno studio rivolto prevalentemente ai metodi di ottimizzazione, si è considerato come unico problema modello quello della convezione naturale in una cavità 2D, in regime laminare. Tale scelta è legata essenzialmente a due motivi: il primo è quello di voler sviluppare un modello termo-fluidodinamico più completo, comprendente cioè l'effetto delle forze di galleggiamento sul moto complessivo del fluido, trascurabile nel caso di convezione forzata. Il secondo motivo è invece legato ai vantaggi di lavorare con una geometria chiusa, fra i quali la semplicità delle condizioni al contorno.

L'obiettivo del problema di ottimizzazione è minimizzare un dato funzionale, detto di costo, dipendente dalla soluzione del problema fluidodinamico oggetto di studio. A tal fine, è necessario introdurre una funzione di controllo, la cui variazione ha effetto sulla soluzione del problema fluidodinamico e dunque sul funzionale costo. Nell'ottimizzazione topologica la funzione di controllo è definita come un campo di porosità che determina in quale regione del dominio dovrebbe esserci fluido e in quale invece dovrebbe esserci solido, affinché il funzionale costo venga minimizzato. Il design ottimo emerge infine dalla distribuzione di porosità nel dominio.

Un tema centrale dei problemi di ottimizzazione è il calcolo del gradiente della funzione costo rispetto al controllo. Infatti, molti metodi di ricerca di minimo funzionale si basano sulle informazioni contenute nel gradiente per trovare la soluzione ottima. Se si considerano i classici schemi alle differenze finite, il calcolo del gradiente risulta solitamente piuttosto oneroso ed il suo costo aumenta proporzionalmente all'aumentare del numero di variabili di controllo. Il metodo aggiunto

costituisce la migliore alternativa al calcolo del gradiente, in quanto permette di svincolarlo dal numero di variabili di controllo: il gradiente viene calcolato a partire dalle soluzioni del problema primale (cioè il problema fluidodinamico) e aggiunto (ricavato dal primale). Poichè il costo unitario di una simulazione CFD è elevato ed il numero di variabili di design è piuttosto alto in un tipico problema di ottimizzazione topologica, il metodo aggiunto è certamente una scelta vincente.

Nel presente lavoro vengono presentati due distinti problemi di controllo e per ciascun problema le formulazioni aggiunte sono ricavate e dettagliate seguendo un approccio Lagrangiano. Per la risoluzione iterativa dei problemi di controllo si considerano due algoritmi: il primo, descritto in [16], è detto approccio “one shot” e consiste in una valutazione del gradiente ad ogni iterazione del problema primale ed aggiunto, utilizzando quantità solo parzialmente a convergenza. Il secondo si propone come approccio più “classico” in cui il gradiente viene calcolato dopo che il problema primale ed aggiunto sono a convergenza. Inoltre, per questo secondo approccio, sono state studiate alcune soluzioni per migliorare le prestazioni del processo di ottimizzazione.

I problemi di stato (primale ed aggiunto) e l’ intero processo di ottimizzazione sono stati risolti con la libreria a volumi finiti OpenFOAM.

Sono stati condotti alcuni test numerici i cui risultati mostrano la bontà delle formulazioni e delle implementazioni dei problemi di controllo. In particolare il secondo algoritmo si è dimostrato più affidabile e robusto del primo, a dimostrazione dell’ efficacia del lavoro svolto per migliorarne le prestazioni.

Parole chiave: Ottimizzazione Topologica, Problema Aggiunto, OpenFOAM, Fluidodinamica con Scambio Termico

Chapter 1

Introduction

A generic optimization problem deals with the minimization of a certain cost function, say J , depending on a *state system* governed by algebraic or differential equations. Minimization of J is made possible by controlling these equations through a set of *design (or control) parameters* which behave as input to the *state system* and ultimately to the cost function J . In other words a variation of the control produces a variation of the cost function: the goal of an optimization process is to find those control variations that make J decrease as much as possible. This information is enclosed in the gradient of the cost function with respect to the control parameters, also known as sensitivity. The adjoint approach to optimal design consists of computing the gradient of the cost function via a so called *adjoint state*. A Gradient-based optimization can of course be employed without making use of the adjoint formalism. In this case however the conventional way to compute the sensitivities consists of a finite difference scheme such as,

$$\frac{dJ}{d\rho_k} \approx \frac{J(\rho_k + \Delta\rho_k) - J(\rho_k)}{\Delta\rho_k} \quad \text{for } k = [1, \dots, n]$$

being ρ_k , the k-th design parameter. Each evaluation of $J(\rho_k)$ needs the *state system* to be solved at first: that means one solver call. So for the complete gradient information, $n + 1$ solver calls are requested. The large computational cost puts an hard constraint on the affordable number of design variables. On the other hand the adjoint approach has the great advantage of computing the whole sensitivity with the effort of one call to the *primal solver* and one call to the *adjoint solver*, i.e via only two solvers calls, independently from the number of design parameters n . The adjoint method has therefore established as the best method of choice for the computation of sensitivities, although its complexity, both in the mathematical formulation of the adjoint equations and boundary conditions and in their numerical implementation, has limited its application to the favour of simpler methods. In the last decades however a renewed interest in the adjoint method, especially in

fluid dynamics, is manifested by the large number of publications on adjoint-based shape optimization, concerning both external and internal flows. These two applications commonly bring to a first distinction between two possible approaches to the optimization methods, concerning the choice of the control variables: *surface shape optimization* and *topology optimization*. In external applications, *surface shape optimization* is usually employed: the control variables are the normal displacements over a parametrized surface, whose optimal deformation corresponds to the minimization of a merit function. The sensitivity is therefore defined over the controlled surface. Once its shape has been modified, mesh deformation is needed to fit the new design: this operation can be quite computationally expensive and puts a constraint on the number of iterations affordable. In internal applications instead, a more recent optimization method, fluid dynamic *topology optimization* [21], is often preferred. The notion of *topology optimization* was introduced in structural mechanics, by formulating and numerically solving equations in terms of material density in order to identify areas in which material should be added so as to increase structural stiffness. Later, the same idea was adapted to fluid dynamic problems. Here, as opposed to conventional *shape optimization*, the geometry is not described via a parametrized surface, but with a volume mesh of the entire installation space. The control variable on each cell can be interpreted as a porosity (or impedance) field that determines what portion of the domain should be fluid and what should be solid, according to the sensitivity with respect to the chosen cost function. The optimal topology of the domain emerges from the final porosity distribution. Given the large number of cells usually employed in a standard optimization application, it becomes clear that the only possibility to cope with a design space of such dimension is via an adjoint method. The main advantage of *topology optimization* is that the design modifications are accomplished without changing the mesh, saving a lot of computational effort. On the other hand an inherent feature of *topology optimization* is the ragged surface of the resulting geometries; in order to obtain a more accurate surface refinement, a *shape optimization* method can be employed after *topology optimization* has been performed.

Another important distinction concerns the way the adjoint equations are derived, that is by using the *continuous* or the *discrete* approach. Both of the approaches start from the analytical form of the primal equations. In the *continuous* approach the primal equations are first linearized, the adjoint equations are then derived analytically from the linearized primal equations and finally the adjoint equations are discretized. The *discrete* method instead is operating on code level: the discrete adjoint equations are directly derived from the algebraic system resulting from primal equations discretization. The respective advantages and disadvantages of

these two alternatives are not discussed in this work: details can be found in [5, 13, 18]. However, one of the main advantages of the *continuous* method is that it is not discretization dependent; therefore adjoint equations can be implemented in a straightforward manner in a C++ framework such as OpenFOAM: that is the main reason whereby the *continuous* approach has been used in this work.

Fluid dynamics optimal design problems are a very popular topic in engineering and several applications can be found in many industrial sectors. The present work focuses on the development of a computational-fluid-dynamics (CFD) optimization tool suitable to solve incompressible fluid problems with heat transfer. Design optimization is carried out using the topology optimization approach. The information of “where to put fluid” and “where to put solid” is enclosed in the *sensitivity* surface (or volume) function. The cheaper way to obtain the topological sensitivity is via an adjoint method, as detailed further on.

Several studies can be found in literature on topology optimization, [2, 4, 7, 12, 15]. Inspired by some of these works [7, 12, 15], two optimal control problems are considered in the context of natural convection in a 2D cavity, in laminar regime. More precisely, the problems consist on finding an optimal shape design in terms of solid material distribution inside the heated cavity, in order to minimize a chosen objective function. A representation of a possible final topology of fluid and solid regions in a closed domain is schematically depicted in figure 1.1. The two optimal control problems object of study differ from the the way the thermal problem in the solid portion of the domain is treated. The numerical solution of the opti-

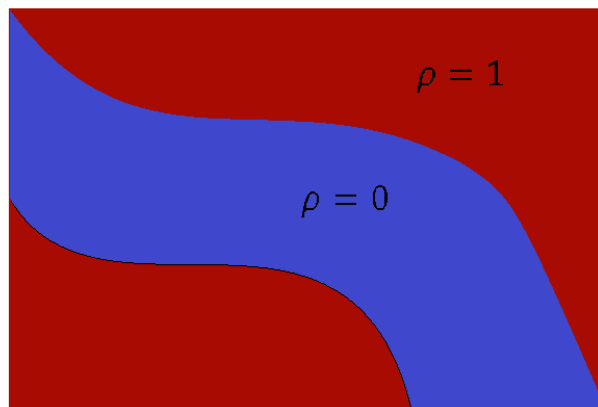


Figure 1.1: Schematical representation of the porous media domain. Red areas with a non-zero porosity value ($\rho = 1$) correspond to the “solid body” domain (practically, with zero flow within those regions). Blue areas ($\rho = 0$) indicate the flow passage.

mization problems has been performed using the open source finite volume library OpenFOAM combined with gradient type algorithms. The relatively simple implementation of custom solvers and its increasing popularity in industry are the main reasons behind the choice of OpenFOAM as CFD toolbox.

The outline of the thesis is as follows. In *Chapter 2* an introduction to the problem of natural convection in a cavity and its governing equations allows the complete definition of the optimal control problems. In *Chapter 3* the continuous adjoint formulations for the control problems are derived. In *Chapter 4* we look into the main aspects of the solvers implementation. In *Chapter 5* some numerical tests are performed on simple thermal 1D and 2D problems and on the case of natural convection in a cavity. These tests are meant to be proof-of-concept studies, where the results of the two control problems are compared and discussed. In the last chapter we draw some conclusions.

Chapter 2

The optimal control problems

In this chapter the complete definition of the optimal control problems under investigation is given. First an abstract optimal control problem is introduced. Then an insight into the governing equations for the natural convection problem in a cavity is given: the problem layout is specified and the relative boundary conditions are also showed. Two possible control problems are proposed and discussed. Finally the dimensionless form of the state equations is derived.

2.1 Abstract optimal control problem

This section is devoted to the presentation of the fundamentals of the optimal control theory for partial differential equations based on the adjoint formalism. In particular a Lagrangian approach is considered. We start introducing the mathematical entities which play the main role in the theory of control problems. We call ρ the control function, defined in an appropriate space function, also known as space of *admissible controls*, whose definition depends on the specific problem object of study. The state variables vector $\mathbf{y}(\rho)$, depending on the control, is the solution of the set of partial differential equations $\mathbf{R}(\mathbf{y}, \rho) = 0$, completed with boundary conditions $\mathbf{B}(\mathbf{y}) = 0$. Denoting by $J(\mathbf{y}, \rho)$ the cost function to be minimized, the optimization problem can be stated as follows:

Find the optimal control ρ that minimizes $J(\mathbf{y}, \rho)$ subjected to the constraint $\mathbf{R}(\mathbf{y}, \rho) = 0$

We therefore have a constrained optimization problem, with the constraints being the state equations. Such problems are commonly tackled by introducing a Lagrangian function L given by:

$$L(\mathbf{y}, \boldsymbol{\lambda}, \rho) = J(\mathbf{y}(\rho), \rho) + \langle \boldsymbol{\lambda}^T, \mathbf{R}(\mathbf{y}, \rho) \rangle \quad (2.1)$$

where the notation $\langle \cdot, \cdot \rangle$ denotes the inner product on a Hilbert space, whereas $\boldsymbol{\lambda}^T$ is the vector of Lagrangian multipliers. Differentiation of L with respect to ρ yields:

$$\begin{aligned} \frac{\partial L}{\partial \rho}[\delta \rho] &= \frac{\partial J}{\partial \mathbf{y}} \frac{\partial \mathbf{y}}{\partial \rho}[\delta \rho] + \frac{\partial J}{\partial \rho}[\delta \rho] + \left\langle \boldsymbol{\lambda}^T, \frac{\partial \mathbf{R}}{\partial \mathbf{y}} \frac{\partial \mathbf{y}}{\partial \rho}[\delta \rho] + \frac{\partial \mathbf{R}}{\partial \rho}[\delta \rho] \right\rangle \\ &= \frac{\partial J}{\partial \mathbf{y}}[\delta \mathbf{y}] + \left\langle \boldsymbol{\lambda}^T, \frac{\partial \mathbf{R}}{\partial \mathbf{y}}[\delta \mathbf{y}] \right\rangle + \frac{\partial J}{\partial \rho}[\delta \rho] + \left\langle \boldsymbol{\lambda}^T, \frac{\partial \mathbf{R}}{\partial \rho}[\delta \rho] \right\rangle . \end{aligned} \quad (2.2)$$

We denote with $\mathcal{L} = \frac{\partial \mathbf{R}}{\partial \mathbf{y}}$ the linearized state equations evaluated on $\mathbf{y}(\rho)$ such that $\mathbf{R}(\mathbf{y}, \rho) = 0$. We choose the Lagrangian multipliers in order to get rid of the terms in (2.2) depending on the state variable variations. Since $\frac{\partial J}{\partial \mathbf{y}}[\delta \mathbf{y}]$ is linear in $\delta \mathbf{y}$, the vanishing terms in $\delta \mathbf{y}$ reads:

$$\left\langle \frac{\partial J}{\partial \mathbf{y}}, \delta \mathbf{y} \right\rangle = - \langle \boldsymbol{\lambda}^T, \mathcal{L} \delta \mathbf{y} \rangle \quad \forall \delta \mathbf{y} . \quad (2.3)$$

Then according to the definition of adjoint operator of \mathcal{L} ,

$$\langle \boldsymbol{\lambda}^T, \mathcal{L} \delta \mathbf{y} \rangle = \langle \mathcal{L}^* \boldsymbol{\lambda}^T, \delta \mathbf{y} \rangle \quad (2.4)$$

equation (2.3) reads,

$$\left\langle \frac{\partial J}{\partial \mathbf{y}}, \delta \mathbf{y} \right\rangle = - \langle \mathcal{L}^* \boldsymbol{\lambda}^T, \delta \mathbf{y} \rangle \quad \forall \delta \mathbf{y} . \quad (2.5)$$

This is the weak form of the so called adjoint equations. When defining the adjoint operator of \mathcal{L} and the derivative $\frac{\partial J}{\partial \mathbf{y}}$, boundary terms may also appear, that should be vanished, namely:

$$\int_{\partial \Omega} C(\boldsymbol{\lambda}^T, \delta \mathbf{y}; \mathbf{y}) = 0 \quad \forall \text{admissible } \delta \mathbf{y} . \quad (2.6)$$

The admissible variations of the state variable at the boundary are deduced from the primal boundary conditions,

$$\mathbf{B}(\mathbf{y}) = 0 \quad (2.7)$$

where, considering linear boundary conditions, their variation yields:

$$\delta \mathbf{B}(\mathbf{y}) = \mathbf{B}(\delta \mathbf{y}) = 0 . \quad (2.8)$$

Once admissible $\delta \mathbf{y}$ on $\partial \Omega$ are deduced, the adjoint boundary conditions are computed from equation (2.6).

Equation (2.5), completed with proper boundary conditions, define the adjoint

problem that can now be turned into the strong formulation,

$$\mathcal{L}^* \boldsymbol{\lambda}^T = -\frac{\partial J}{\partial \mathbf{y}} \quad (2.9)$$

that is a linear equation for the Lagrangian multipliers $\boldsymbol{\lambda}^T$. When primal equations and adjoint ones are fulfilled, the sensitivity of the objective function with respect to the control variable is given by:

$$J'(\rho)[\delta\rho] = \frac{\partial L}{\partial \rho}[\delta\rho] = \frac{\partial J}{\partial \rho}[\delta\rho] + \left\langle \boldsymbol{\lambda}^T, \frac{\partial \mathbf{R}}{\partial \rho}[\delta\rho] \right\rangle . \quad (2.10)$$

Then, since $J'(\rho)[\delta\rho]$ is linear in $\delta\rho$, we have

$$J'(\rho)[\delta\rho] = \langle J'(\rho), \delta\rho \rangle . \quad (2.11)$$

The evaluation of $J'(\rho)$ gives an indication of the variation δJ due to a control variation $\delta\rho$. This information can be used in a gradient-based optimization method, whose general implementation for the control variable ρ at the step k , is given by:

$$\rho^{k+1} = \rho^k + \tau^k d^k \quad (2.12)$$

where d^k represents the descent direction, such that

$$\langle J'(\rho^k), d^k \rangle < 0 \quad \text{if} \quad J'(\rho^k) \neq 0 \quad (2.13)$$

and τ^k is the step length along the prescribed direction. According to the possible choices of d^k one can obtain different gradient-based schemes, such as the simplest *steepest descent method*, or the *Newton method*, or the *conjugate gradient method*. We choose the *steepest descent* in which the search direction is simply:

$$d^k = -J'(\rho^k) \quad (2.14)$$

so equation (2.12) becomes:

$$\rho^{k+1} = \rho^k - \tau^k J'(\rho^k) . \quad (2.15)$$

The iterative procedure stops when a stationary point is achieved, where $J'(\rho) = 0$.

2.2 Governing equations for natural convection problems

In natural convection problems the driven force is given by changes in fluid density due to temperature evolution. A consistent description of natural convection

should involve compressible flows, where an energy equation is solved together with momentum and continuity equations. However, a common approximation, known as *Boussinesq approximation*, allows to use methods for incompressible flows: even though the thermodynamic properties of the fluid are assumed to be constant, a buoyancy body force term in the momentum equation is added, allowing to relate density changes to temperature. This relation is assumed to be linear, according to:

$$\Delta\rho = \rho_0 \beta (T - T_0) \quad (2.16)$$

where ρ_0 is the reference density, β is the coefficient of thermal expansion and T_0 is a reference temperature. Taking into account variations of density only in the gravitational term \mathbf{g} of the momentum equation, the following steady incompressible equations are obtained, [14]:

$$(\mathbf{v} \cdot \nabla)\mathbf{v} + \nabla p - \nabla \cdot (2\nu D(\mathbf{v})) - \mathbf{g}(1 - \beta(T - T_0)) = 0 \quad (2.17a)$$

$$\nabla \cdot \mathbf{v} = 0 \quad (2.17b)$$

where \mathbf{v} is the fluid velocity, p is the pressure divided by the constant density ρ_0 , ν is the cinematic viscosity and $D(\mathbf{v}) = \frac{1}{2}(\nabla\mathbf{v} + (\nabla\mathbf{v})^T)$ is the rate of strain tensor. The energy equation is recast into a transport-diffusion equation for the temperature:

$$\mathbf{v} \cdot \nabla T - \nabla \cdot (K \nabla T) = 0 \quad (2.18)$$

where $K := \frac{k}{\rho_0 c_p}$ is the thermal diffusivity of the fluid, being $\rho_0 c_p$ the density and the specific heat coefficient of the fluid, considered as constant, and k the thermal conductivity coefficient. The Boussinesq approximation holds for limited temperature variations, say about 2K for water or 15K for air, see [11]. In the remainder of this work we will refer to equations (2.17) and (2.18) as Navier-Stokes equations with heat exchange.

Figure 2.1 displays the typical layout of a simple natural convection problem. The closed domain $\Omega(x, y) = (0, L) \times (0, L) \in \mathbb{R}^2$ represents the square cavity of side L . The horizontal walls are thermally isolated, and the vertical sides are kept at different temperatures, T_h and T_c , with $T_h > T_c$. We refer to the walls with fixed temperature as $\Gamma_T = \Gamma_{T_h} \cup \Gamma_{T_c}$ and to the adiabatic ones as Γ_A , that is

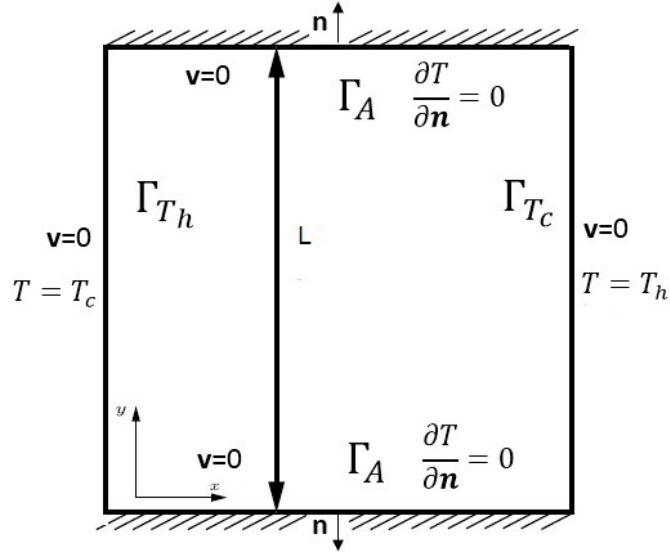


Figure 2.1: Detail of cavity

$\partial\Omega = \Gamma_T \cup \Gamma_A$. The boundary conditions for velocity and temperature read:

$$\mathbf{v} = 0 \quad \text{on } \partial\Omega \quad (2.19a)$$

$$T = T_h \quad \text{on } \Gamma_{T_h} \quad (2.19b)$$

$$T = T_c \quad \text{on } \Gamma_{T_c} \quad (2.19c)$$

$$\frac{\partial T}{\partial \mathbf{n}} = 0 \quad \text{on } \Gamma_A \quad (2.19d)$$

Since fully Dirichlet boundary conditions on velocity are considered, the pressure will be defined up to a constant. The reference temperature T_0 can be defined as $T_0 = \frac{T_h - T_c}{2}$.

2.3 Control Problem 1

After the introduction of the governing equations for the natural convection in a cavity, in the current section we introduce the first control problem we are interested in. First of all we define the cost function to be minimized:

$$J = \frac{1}{2} \int_{\Omega} (T - T^*)^2 \quad (2.20)$$

where T^* is an objective temperature distribution. The control variable $\rho : \Omega \mapsto \mathbb{R}$ is a bounded function on Ω , say $\rho \in [0, 1]$, whose distribution on Ω determines what portion of the domain is fluid and what is solid. The goal is to find the distribution of the solid material that minimizes the cost function or, in other words, that makes the temperature distribution inside the cavity as close as possible to the desired

one, as schematically depicted in figure 1.1.

Let us denote with $\mathbf{y} = (\mathbf{v}, p, T)$ the state variables vector, including velocity, pressure and temperature. The controlled state equations $\mathbf{R}(\mathbf{y}, \rho) = 0$ are defined by:

$$(R_1, R_2, R_3)^T = (\mathbf{v} \cdot \nabla) \mathbf{v} + \nabla p - \nabla \cdot (2\nu D(\mathbf{v})) - \mathbf{g}(1 - \beta(T - T_0)) + \alpha(\rho) \mathbf{v} = 0 \quad (2.21a)$$

$$R_4 = -\nabla \cdot \mathbf{v} = 0 \quad (2.21b)$$

$$R_5 = \mathbf{v} \cdot \nabla T - \nabla \cdot (K \nabla T) + \alpha(\rho)(T - T_D) = 0 \quad (2.21c)$$

Let us comment on the presence of the extra terms $\alpha(\rho)$ and $\alpha(\rho)(T - T_D)$. A popular strategy in topology optimization for fluids is to include the porosity control field in the momentum equation through the Darcy term $\alpha(\rho) \mathbf{v}$, so that the velocity is penalized in the solid part where $\alpha(\rho)$ assumes large values. We extend this idea to the temperature equation also, adding the term $\alpha(\rho)(T - T_D)$, where $T_D(\mathbf{x}) \in \Omega$ is a fixed function to be assigned, depending on temperature along the solid walls surrounding the flow. The function $\alpha(\rho)$ is a generic increasing monotone and continuously differentiable function of ρ such that $\alpha(0) = 0$ in fluid regions and $\alpha(1) = \alpha_{max}$ in the solid portions of the domain. In this way in the fluid region, the Darcy penalization terms $\alpha(\rho) \mathbf{v}$ and $\alpha(\rho)(T - T_D)$ are negligible compared to the other terms of equations (2.21a) and (2.21c), respectively. Consequently, the Navier-Stokes equations with heat exchange are recovered. In the solid region instead, for sufficiently large values of α_{max} , the Darcy penalization terms are dominating and equations (2.21a) and (2.21c) reduce to

$$\begin{aligned} \alpha_{max} \mathbf{v} &= 0 \\ \alpha_{max}(T - T_D) &= 0 \end{aligned}$$

constraining the velocity to be zero and the temperature to be T_D in the solid region. Consequently, the no-slip boundary condition at the solid surface is imposed, as well as the Dirichlet boundary condition for temperature. Thus physically correct flow motions near solid obstacles can be obtained. Mathematical justification of this method is derived in [3].

Summarizing, the resulting optimal control reads:

Find the optimal control ρ that minimizes $J(T)$ in (2.20), subjected to the constraint $\mathbf{R}(\mathbf{v}, p, T, \rho) = 0$ defined by (2.21)

2.4 Control Problem 2

In the current section we introduce the second control problem we are interested in. The cost function J , as well as the control variable ρ , are the same as those introduced in the previous section for the *Control Problem 1*.

The controlled state equations $\mathbf{R}(\mathbf{y}, \rho) = 0$ are given by:

$$(R_1, R_2, R_3)^T = (\mathbf{v} \cdot \nabla)\mathbf{v} + \nabla p - \nabla \cdot (2\nu D(\mathbf{v})) - \mathbf{g}(1 - \beta(T - T_0)) + \alpha(\rho)\mathbf{v} = 0 \quad (2.22a)$$

$$R_4 = -\nabla \cdot \mathbf{v} = 0 \quad (2.22b)$$

$$R_5 = \mathbf{v} \cdot \nabla T - \nabla \cdot (K(\rho)\nabla T) = 0 \quad (2.22c)$$

The Darcy term $\alpha(\rho)\mathbf{v}$ still allows the porosity field ρ to control the momentum equation as described in section 2.3. The temperature equation instead is controlled by the field $K(\rho)$, a generic increasing monotone and continuously differentiable function of $\rho \in [0, 1]$, such that $K(0) = K_f$ in fluid areas and $K(1) = K_s$ in the solid portions of the domain, being generally $K_s > K_f$. Based on the temperature equation (2.18), the function $K(\rho)$ can be defined as:

$$K(\rho) := \frac{k(\rho)}{(\rho_0 c_p)_f} \quad (2.23)$$

being $(\rho_0 c_p)_f$ the density and specific heat coefficient of the fluid, considered as constant, and $k(\rho)$ the thermal conductivity coefficient, depending on the control variable. When $\rho = 0$ the fluid diffusivity coefficient $K_f = \frac{k_f}{(\rho_0 c_p)_f} = \frac{\nu}{Pr}$ (being $Pr := \frac{\nu}{K_f}$ the Prandtl number) is recovered, possibly including the contribution of an eddy viscosity turbulent model. For $\rho = 1$ instead, we have $K_s = \frac{k_s}{(\rho_0 c_p)_f}$, being k_s the solid thermal conductivity. In the solid region, the fluid velocity \mathbf{v} becomes zero due to the Darcy penalization, therefore the equation (2.22c) becomes a pure conduction equation without the convective term as

$$-\nabla \cdot (K_s \nabla T) = 0 \quad (2.24)$$

The fact that $K_s = \frac{k_s}{(\rho_0 c_p)_f}$ may sound a bit weird, since we expect equation (2.24) to describe the conduction law in a solid. However the problem is well posed, since energy conservation is fulfilled at the interface between a solid and a fluid portion of the domain, where the following condition holds:

$$\int_{\Gamma_I} \frac{k_s}{(\rho_0 c_p)_f} \frac{\partial T}{\partial \mathbf{n}} = - \int_{\Gamma_I} \frac{k_f}{(\rho_0 c_p)_f} \frac{\partial T}{\partial \mathbf{n}} \quad (2.25)$$

being Γ_I the interface between fluid and solid.

In the fluid region, the temperature equation (2.22c) maintains the original form with the thermal diffusivity of fluid as

$$\mathbf{v} \cdot \nabla T - \nabla \cdot (K_f \nabla T) = 0 \quad . \quad (2.26)$$

Differently from the *Control Problem 1*, this approach allows to solve the temperature equation in both solid and fluid regions, actually making heat conduction in a solid be considered along with heat convection in the adjacent fluid.

Summarizing, the resulting optimal control reads:

Find the optimal control ρ that minimizes $J(T)$ in (2.20), subjected to the constraint $\mathbf{R}(\mathbf{v}, p, T, \rho) = 0$ defined by (2.22)

2.5 Non-dimensional form of the state equations

The non-dimensional form of the equations $\mathbf{R}(\mathbf{v}, p, T, \rho) = 0$, for both control approaches, is useful to a deeper and more general understanding of the governing equations in natural convection phenomena. To write the dimensionless form of a natural convection problem we consider the following reference quantities:

- length of the square cavity side: L [m]
- diffusivity coefficient of the fluid: K_f [m^2/s]
- wall temperature difference: $T_h - T_c$ [K]

In the next two paragraphs we report the results for the *Control Problem 1* and *Control Problem 2* respectively.

2.5.1 Non-dimensional *Control Problem 1*

Using nominal values given by equations (2.27),

$$\begin{aligned} \mathbf{X} &= \frac{\mathbf{x}}{L}; & \mathbf{V} &= \frac{\mathbf{v}L}{K_f}; & \Theta &= \frac{T - T_c}{T_h - T_c}; & P &= \frac{pL^2}{K_f^2}; \\ & & & & \hat{g} &= \frac{gL^3}{K_f^2}; & \hat{\alpha} &= \frac{\alpha L^2}{K_f}; \end{aligned} \quad (2.27)$$

the non-dimensional form of equations (2.21) reads:

$$\mathbf{U} \cdot \hat{\nabla} \mathbf{U} + \hat{\nabla} P - \hat{\nabla} \cdot (2Pr \hat{D}(\mathbf{U})) - \hat{g} \hat{\mathbf{y}} + Ra Pr \Theta + \hat{\alpha}(\rho) \mathbf{U} = 0 \quad (2.28a)$$

$$- \hat{\nabla} \cdot \mathbf{U} = 0 \quad (2.28b)$$

$$\mathbf{U} \cdot \hat{\nabla} \Theta - \hat{\Delta} \Theta + \hat{\alpha}(\rho)(\Theta - \Theta_D) = 0 \quad (2.28c)$$

where $\hat{\nabla}$ is the dimensionless form of the differential operator ∇ , $\hat{\mathbf{y}}$ is the unit vector on vertical direction. The non-dimensional boundary conditions for the cavity case yield:

$$\begin{aligned} \mathbf{U} &= 0 && \text{on } \Gamma \\ \Theta &= \Theta_D && \text{on } \Gamma_T \\ \frac{\partial \Theta}{\partial \mathbf{n}} &= 0 && \text{on } \Gamma_A \end{aligned}$$

where $\Theta_D(X = 0) = 1$ and $\Theta_D(X = L) = 0$. In equations (2.28) the two non-dimensional numbers

$$\begin{aligned} Ra &= \frac{g L^3 \beta (T_h - T_c)}{\nu K_f} \\ Pr &= \frac{\nu}{K_f} \end{aligned}$$

are the Rayleigh and Prandtl numbers. The latter is often taken as constant and for a laminar air flow $Pr = 0.71$. The Ra number can be interpreted physically as the ratio between the buoyancy and viscous forces and it allows to distinguish laminar from turbulent flows, accomplishing the role of the Reynolds number in natural convection phenomena.

2.5.2 Non-dimensional Control Problem 2

In the same fashion of the previous paragraph, the non-dimensional form of equations (2.22) reads:

$$\mathbf{U} \cdot \hat{\nabla} \mathbf{U} + \hat{\nabla} P - \hat{\nabla} \cdot (2Pr \hat{D}(\mathbf{U})) - \hat{g} \hat{\mathbf{y}} + Ra Pr \Theta + \hat{\alpha}(\rho) \mathbf{U} = 0 \quad (2.29a)$$

$$- \hat{\nabla} \cdot \mathbf{U} = 0 \quad (2.29b)$$

$$\mathbf{U} \cdot \hat{\nabla} \Theta - \hat{\nabla} \cdot (\hat{K}(\rho) \hat{\nabla} \Theta) = 0 \quad (2.29c)$$

where, reminding the definition of $K(\rho)$ given in section 2.4, $\hat{K}(\rho)$ yields:

$$\hat{K}(\rho) = \frac{K(\rho)}{K_f} = \frac{\frac{k(\rho)}{(\rho_0 c_p)_f}}{\frac{k_f}{(\rho_0 c_p)_f}} = \frac{k(\rho)}{k_f}$$

that is the ratio between the controlled thermal conductivity and the fluid one. Its extremities values are:

$$\hat{K}(\rho) = \begin{cases} 1 & \text{for } \rho = 0 \\ \frac{k_s}{k_f} & \text{for } \rho = 1 \end{cases}$$

The non-dimensional boundary conditions are the same as those deduced in the previous paragraph.

Chapter 3

Optimality conditions

Following the guidelines of section 2.1, in this chapter we report the derivation of the the adjoint equations with relative boundary conditions for both the control problems 1 and 2 introduced in the previous chapter. The respective sensitivities (i.e. gradients) of the objective function with respect to the control variable are also computed. In the end the dimensionless form of adjoint equations is derived.

Based on the definition of the cost function J and of the state equations $\mathbf{R}(\mathbf{v}, p, T, \rho) = 0$ introduced in the previous chapter for *Control Problem 1* and *Control Problem 2* the correspondent Lagrangian functional reads:

$$L(\mathbf{y}, \boldsymbol{\lambda}, \rho) = J + \int_{\Omega} (\mathbf{u}, q, T_a) \mathbf{R}(\mathbf{v}, p, T, \rho) \quad (3.1)$$

being \mathbf{y} the vector of the state variables (\mathbf{v}, p, T) and $\boldsymbol{\lambda}$ the vector of Lagrangian multipliers (\mathbf{u}, q, T_a) , that is the adjoint vector. The constrained optimization problems in the Lagrangian approach can be stated as:

Find $(\mathbf{y}, \boldsymbol{\lambda}, \rho)$ *such that* $\nabla L(\mathbf{y}, \boldsymbol{\lambda}, \rho) = 0$

that is,

$$\begin{cases} \partial_{\mathbf{y}} L[\delta \mathbf{y}] = 0 & \forall \delta \mathbf{y} \\ \partial_{\boldsymbol{\lambda}} L[\delta \boldsymbol{\lambda}] = 0 & \forall \delta \boldsymbol{\lambda} \\ \partial_{\rho} L[\delta \rho] = 0 & \forall \delta \rho \end{cases}$$

where we have used the notation $\partial_{\mathbf{y}} L[\delta \mathbf{y}]$ to indicate the Gâteaux derivative of $L(\mathbf{y}, \boldsymbol{\lambda}, \rho)$ w.r.t. \mathbf{y} , that is:

$$\partial_{\mathbf{y}} L[\delta \mathbf{y}] = \lim_{h \rightarrow 0} \frac{L(\mathbf{y} + h \delta \mathbf{y}, \boldsymbol{\lambda}, \rho) - L(\mathbf{y}, \boldsymbol{\lambda}, \rho)}{h}$$

In a similar way, the derivatives $\partial_{\lambda}L[\delta\boldsymbol{\lambda}]$ and $\partial_{\rho}L[\delta\rho]$ can be defined.

We can observe that $\partial_{\mathbf{y}}L[\delta\mathbf{y}] = 0$ corresponds to the weak form of the adjoint equations for the Lagrangian multipliers, $\partial_{\lambda}L[\delta\boldsymbol{\lambda}] = 0$ is the weak form of the state equations and $\partial_{\rho}L[\delta\rho] = 0$ is the optimality condition.

Generally it is convenient to achieve the derivative of the objective function $J'(\rho)$ from the Gâteaux derivative of the Lagrangian $\partial_{\rho}L[\delta\rho]$, which is linear in the variation $\delta\rho$, so the following relation holds:

$$\partial_{\rho}L[\delta\rho] = \int_{\Omega} J'(\rho) \delta\rho \quad . \quad (3.2)$$

Then, as hinted in section 2.1, the sensitivity can be employed into an iterative gradient-based method (*steepest descent*) until the optimality condition $\partial_{\rho}L[\delta\rho] = 0$, i.e. $J'(\rho) = 0$, is achieved.

In the following sections we derive the equations for the adjoint variables, necessary for the computation of the sensitivity of the objective function.

3.1 Optimal control problem 1

3.1.1 Adjoint equations

In this section we derive the adjoint system and the sensitivity for the *Control Problem 1*. We recall the state equations $\mathbf{R}(\mathbf{v}, p, T, \rho) = 0$ for the *Control Problem 1*, namely

$$(\mathbf{v} \cdot \nabla)\mathbf{v} + \nabla p - \nabla \cdot (2\nu D(\mathbf{v})) - \mathbf{g}(1 - \beta(T - T_0)) + \alpha(\rho)\mathbf{v} = 0 \quad (3.3a)$$

$$-\nabla \cdot \mathbf{v} = 0 \quad (3.3b)$$

$$\mathbf{v} \cdot \nabla T - \nabla \cdot (K\nabla T) + \alpha(\rho)(T - T_D) = 0 \quad . \quad (3.3c)$$

We can deduce the weak form of the adjoint equations requiring the derivative of L w.r.t. the state variables to be zero, as follows:

$$\partial_{\mathbf{y}}L[\delta\mathbf{y}] = \partial_{\mathbf{v}}L[\delta\mathbf{v}] + \partial_pL[\delta p] + \partial_TL[\delta T] = 0 \quad . \quad (3.4)$$

We now develop separately the three terms of the previous relation. The first one gives:

$$\begin{aligned}
\partial_{\mathbf{v}}L[\delta\mathbf{v}] &= \partial_{\mathbf{v}}J[\delta\mathbf{v}] + \int_{\Omega} (\mathbf{u}, q, T_a) \partial_{\mathbf{v}}\mathbf{R}[\delta\mathbf{v}] \\
&= \partial_{\mathbf{v}}J[\delta\mathbf{v}] + \int_{\Omega} (\mathbf{u}, q, T_a) \begin{bmatrix} (\delta\mathbf{v} \cdot \nabla)\mathbf{v} + (\mathbf{v} \cdot \nabla)\delta\mathbf{v} - \nabla \cdot (2\nu D(\delta\mathbf{v})) + \alpha(\rho)\delta\mathbf{v} \\ -\nabla \cdot \delta\mathbf{v} \\ \delta\mathbf{v} \cdot \nabla T \end{bmatrix} \\
&= \partial_{\mathbf{v}}J[\delta\mathbf{v}] + \int_{\Omega} \mathbf{u} \cdot \left((\delta\mathbf{v} \cdot \nabla)\mathbf{v} + (\mathbf{v} \cdot \nabla)\delta\mathbf{v} - \nabla \cdot (2\nu D(\delta\mathbf{v})) + \alpha(\rho)\delta\mathbf{v} \right) \\
&\quad + \int_{\Omega} -q \nabla \cdot \delta\mathbf{v} + T_a \delta\mathbf{v} \cdot \nabla T \quad .
\end{aligned}$$

Here, we have neglected the variation of the eddy viscosity. This is correct only for laminar flow regimes, which are considered in the present work. For turbulent flows, neglecting this variation constitutes a common approximation which is known as “frozen turbulence” [1, 18]. The second term of (3.4) is:

$$\begin{aligned}
\partial_p L[\delta p] &= \partial_p J[\delta p] + \int_{\Omega} (\mathbf{u}, q, T_a) \partial_p \mathbf{R}[\delta p] \\
&= \partial_p J[\delta p] + \int_{\Omega} (\mathbf{u}, q, T_a) \begin{bmatrix} \nabla \delta p \\ 0 \\ 0 \end{bmatrix} \\
&= \partial_p J[\delta p] + \int_{\Omega} \mathbf{u} \cdot \nabla \delta p \quad .
\end{aligned}$$

Finally, the last contribution can be developed as follows:

$$\begin{aligned}
\partial_T L[\delta T] &= \partial_T J[\delta T] + \int_{\Omega} (\mathbf{u}, q, T_a) \partial_T \mathbf{R}[\delta T] \\
&= \partial_T J[\delta T] + \int_{\Omega} (\mathbf{u}, q, T_a) \begin{bmatrix} \mathbf{g} \beta \delta T \\ 0 \\ \mathbf{v} \cdot \nabla \delta T - \nabla \cdot (K \nabla \delta T) + \alpha(\rho) \delta T \end{bmatrix} \\
&= \partial_T J[\delta T] + \int_{\Omega} \mathbf{u} \cdot \mathbf{g} \beta \delta T + T_a \mathbf{v} \cdot \nabla \delta T - T_a \nabla \cdot (K \nabla \delta T) + T_a \alpha(\rho) \delta T \quad .
\end{aligned}$$

Equation (3.4) can therefore be written in extended form as:

$$\begin{aligned}
& \partial_{\mathbf{v}} J[\delta \mathbf{v}] + \partial_p J[\delta p] + \partial_T J[\delta T] \\
& + \int_{\Omega} \mathbf{u} \cdot \left((\delta \mathbf{v} \cdot \nabla) \mathbf{v} + (\mathbf{v} \cdot \nabla) \delta \mathbf{v} - \nabla \cdot (2\nu D(\delta \mathbf{v})) + \alpha(\rho) \delta \mathbf{v} \right) \\
& + \int_{\Omega} -q \nabla \cdot \delta \mathbf{v} + T_a \delta \mathbf{v} \cdot \nabla T \\
& + \int_{\Omega} \mathbf{u} \cdot \nabla \delta p \\
& + \int_{\Omega} \mathbf{u} \cdot \mathbf{g} \beta \delta T + T_a \mathbf{v} \cdot \nabla \delta T - T_a \nabla \cdot (K \nabla \delta T) + T_a \alpha(\rho) \delta T = 0 \quad \forall \delta \mathbf{v}, \delta p, \delta T \quad .
\end{aligned} \tag{3.7}$$

We consider now the cost function defined in chapter 2 for the control problem, i.e.

$$J = \frac{1}{2} \int_{\Omega} (T - T^*)^2 \quad . \tag{3.8}$$

Using integration by parts in equation (3.7) the derivatives of the variations can be eliminated and the equation can be written as follows (see appendix A.1 for details):

$$\begin{aligned}
& \int_{\Omega} \left(-(\nabla \mathbf{u}) \mathbf{v} - (\mathbf{v} \cdot \nabla) \mathbf{u} - \nabla \cdot (2\nu D(\mathbf{u})) + \alpha(\rho) \mathbf{u} + \nabla q + T_a \nabla T \right) \cdot \delta \mathbf{v} \\
& + \int_{\Omega} (-\nabla \cdot \mathbf{u}) \delta p \\
& + \int_{\Omega} \left(\beta \mathbf{u} \cdot \mathbf{g} - \mathbf{v} \cdot \nabla T_a - \nabla \cdot (K \nabla T_a) + T_a \alpha(\rho) + (T - T^*) \right) \delta T \\
& + \int_{\Gamma} \left((\mathbf{u} \cdot \mathbf{v}) \mathbf{n} + \mathbf{u} (\mathbf{v} \cdot \mathbf{n}) + 2\nu \mathbf{n} \cdot D(\mathbf{u}) - q \mathbf{n} \right) \cdot \delta \mathbf{v} - \int_{\Gamma} 2\nu \mathbf{n} \cdot D(\delta \mathbf{v}) \mathbf{u} \\
& + \int_{\Gamma} (\mathbf{u} \cdot \mathbf{n}) \delta p \\
& + \int_{\Gamma} \left(T_a \mathbf{v} \cdot \mathbf{n} + K \mathbf{n} \cdot \nabla T_a \right) \delta T + \int_{\Gamma} K \mathbf{n} \cdot \nabla \delta T T_a = 0 \quad \forall \delta \mathbf{v}, \delta p, \delta T \quad .
\end{aligned} \tag{3.9}$$

Since the previous relation has to be fulfilled for every variations $\delta \rho$, then for any $\delta \mathbf{v}, \delta p, \delta T$, each integral must vanish individually. For the integrals over the domain Ω , this requirement gives rise to the adjoint equations; in a similar fashion the adjoint boundary conditions are deduced from the boundary integrals on Γ .

The resulting adjoint equations are:

$$-(\nabla \mathbf{u}) \mathbf{v} - (\mathbf{v} \cdot \nabla) \mathbf{u} - \nabla \cdot (2\nu D(\mathbf{u})) + \alpha(\rho) \mathbf{u} + \nabla q + T_a \nabla T = 0 \quad (3.10a)$$

$$\nabla \cdot \mathbf{u} = 0 \quad (3.10b)$$

$$\beta \mathbf{u} \cdot \mathbf{g} - \mathbf{v} \cdot \nabla T_a - \nabla \cdot (K \nabla T_a) + T_a \alpha(\rho) + T - T^* = 0 \quad . \quad (3.10c)$$

Although linear by definition, the structure of the equations governing the adjoint velocities and pressure is very similar to that of the primal Navier–Stokes equations. Moreover, the adjoint velocity is also solenoidal, as the primal one. Also the adjoint and primal temperature equations are quite similar. The main difference between primal and adjoint equations is the different sign of convective terms, that means the adjoint variables are convected upstream with respect to the primal ones.

3.1.2 Adjoint boundary conditions

The boundary conditions for adjoint velocity, pressure and temperature are also derived from equation (3.9) considering the boundary integrals:

$$\int_{\Gamma} \left((\mathbf{u} \cdot \mathbf{v}) \mathbf{n} + \mathbf{u} (\mathbf{v} \cdot \mathbf{n}) + 2\nu \mathbf{n} \cdot D(\mathbf{u}) - q \mathbf{n} \right) \cdot \delta \mathbf{v} - \int_{\Gamma} 2\nu \mathbf{n} \cdot D(\delta \mathbf{v}) \mathbf{u} = 0 \quad (3.11a)$$

$$\int_{\Gamma} (\mathbf{u} \cdot \mathbf{n}) \delta p = 0 \quad (3.11b)$$

$$\int_{\Gamma} \left(T_a \mathbf{v} \cdot \mathbf{n} + K \mathbf{n} \cdot \nabla T_a \right) \delta T + \int_{\Gamma} K \mathbf{n} \cdot \nabla \delta T T_a = 0 \quad . \quad (3.11c)$$

Equations (3.11) must be fulfilled for all admissible boundary variations $\delta \mathbf{v}$, δp , δT , which are deduced from primal boundary conditions, as specified further on. Before discussing the adjoint boundary conditions in details, in the following we start considering the boundary terms (3.11) that involve the rate of strain tensor D . Following [15] and considering solenoidal variations $\delta \mathbf{v}$, one can write (see appendix A.2 for details):

$$\begin{aligned} \int_{\Gamma} 2\nu \mathbf{n} \cdot (D(\mathbf{u}) \delta \mathbf{v} - D(\delta \mathbf{v}) \mathbf{u}) &= \int_{\Gamma} \nu ((\mathbf{n} \cdot \nabla) \mathbf{u} \cdot \delta \mathbf{v} - (\mathbf{n} \cdot \nabla) \delta \mathbf{v} \cdot \mathbf{u}) \\ &\quad - \int_{\Gamma} \nabla \nu (u_n \delta \mathbf{v} - \delta v_n \mathbf{u}) \end{aligned} \quad (3.12)$$

being $u_n = \mathbf{u} \cdot \mathbf{n}$ e $v_n = \mathbf{v} \cdot \mathbf{n}$. For laminar fluxes $\nabla \nu$ is null. Considering the above results, we rewrite for the sake of clarity the “boundary equations” (3.11):

$$\int_{\Gamma} \left((\mathbf{u} \cdot \mathbf{v}) \cdot \mathbf{n} + \mathbf{u}(\mathbf{v} \cdot \mathbf{n}) + \nu((\mathbf{n} \cdot \nabla)\mathbf{u} - q\mathbf{n}) \right) \cdot \delta \mathbf{v} - \int_{\Gamma} \nu (\mathbf{n} \cdot \nabla) \delta \mathbf{v} \cdot \mathbf{u} = 0 \quad (3.13a)$$

$$\int_{\Gamma} (\mathbf{u} \cdot \mathbf{n}) \delta p = 0 \quad (3.13b)$$

$$\int_{\Gamma} \left(T_a \mathbf{v} \cdot \mathbf{n} + K \mathbf{n} \cdot \nabla T_a \right) \delta T - \int_{\Gamma} K (\mathbf{n} \cdot \nabla \delta T) T_a = 0 \quad (3.13c)$$

From equations (3.13), the following adjoint boundary conditions can be derived for the problem of natural convection in a cavity:

$$\mathbf{u} = 0 \quad \text{on } \Gamma \quad (3.14a)$$

$$T_a = 0 \quad \text{on } \Gamma_T \quad (3.14b)$$

$$\frac{\partial T_a}{\partial \mathbf{n}} = 0 \quad \text{on } \Gamma_A \quad (3.14c)$$

where the boundary $\Gamma = \Gamma_T \cup \Gamma_A$ represents the two walls with fixed temperature Γ_T and the other two adiabatic walls Γ_A , see figure 2.1. In the next two paragraphs the derivation of (3.14) is presented in full details.

Wall with fixed temperature

On Γ_T we have two Dirichlet conditions for velocity and temperature, $\mathbf{v} = 0$ e $T = T_D$, from which we deduce their relative variations are null on this boundary:

$$\delta \mathbf{v} = 0, \quad \delta T = 0 \quad \text{on } \Gamma_T$$

Analyzing equations (3.13) we immediately see that the boundary integrals in $\delta \mathbf{v}$ e δT directly vanish. We therefore have only three terms remaining. Let us consider the first one:

$$\int_{\Gamma} (\mathbf{u} \cdot \mathbf{n}) \delta p = 0 \quad \forall \delta p \quad (3.15)$$

which implies

$$u_n = 0 \quad .$$

We thus obtain a condition for the normal component of the adjoint velocity. The second term to be cancelled is:

$$\int_{\Gamma} (\mathbf{n} \cdot \nabla) \delta \mathbf{v} \cdot \mathbf{u} = 0 \quad (3.16)$$

Since a condition for the normal component of \mathbf{u} has been already obtained, we now rewrite the previous relation in terms of normal and tangential component on the boundary:

$$\int_{\Gamma} (\mathbf{n} \cdot \nabla) (\delta v_n \mathbf{n} + \delta \mathbf{v}_t) \cdot (u_n \mathbf{n} + \mathbf{u}_t) = 0 \quad . \quad (3.17)$$

Let us elaborate on equation (3.17), starting from the term $(\mathbf{n} \cdot \nabla)(\delta v_n \mathbf{n})$. Making use of the index notation, this term reads:

$$n_i (\delta v_n n_j)_{,i} = n_i \delta v_{n,i} n_j + \delta v_n n_i n_{j,i} \quad .$$

The second term on the right-hand-side of the previous equation is null, so equation (3.17) becomes:

$$\int_{\Gamma} \mathbf{n} \cdot \nabla \delta v_n u_n + (\mathbf{n} \cdot \nabla) \delta \mathbf{v}_t \cdot \mathbf{u}_t = 0 \quad . \quad (3.18)$$

Now, under the hypothesis of divergence free variations, considering a local reference frame on the boundary, we can write:

$$\nabla_{\perp} \delta v_n + \nabla_{\parallel} \cdot \delta \mathbf{v}_t = 0 \quad (3.19)$$

being ∇_{\perp} e ∇_{\parallel} respectively the normal and tangential component of the ∇ operator on the boundary. Since the tangential component $\delta \mathbf{v}_t$ is null in every point of the boundary, then its tangential derivative will be null as well. Thus the previous equation becomes:

$$\nabla_{\perp} \delta v_n = 0$$

so

$$\mathbf{n} \cdot \nabla \delta v_n = 0 \quad .$$

Then equation (3.18) becomes:

$$\int_{\Gamma} (\mathbf{n} \cdot \nabla) \delta \mathbf{v}_t \cdot \mathbf{u}_t = 0 \quad \forall \delta \mathbf{v} \quad (3.20)$$

thus implying

$$\mathbf{u}_t = 0 \quad .$$

We analyze now the last boundary term:

$$- \int_{\Gamma} K \mathbf{n} \cdot \nabla \delta T T_a = 0 \quad \forall \delta T \quad (3.21)$$

yielding

$$T_a = 0 \quad .$$

In the end, the boundary conditions on Γ_T for the adjoint system are:

$$\mathbf{u} = 0 \quad (3.22a)$$

$$T_a = 0 \quad . \quad (3.22b)$$

Adiabatic wall

On Γ_A the boundary condition for primal velocity and temperature are:

$$\begin{aligned} \mathbf{v} &= 0 \\ \frac{\partial T}{\partial \mathbf{n}} &= 0 \quad . \end{aligned}$$

So the respective variations are deduced:

$$\begin{aligned} \delta \mathbf{v} &= 0 \\ \delta \frac{\partial T}{\partial \mathbf{n}} &= 0 \quad \implies \quad \frac{\partial \delta T}{\partial \mathbf{n}} = 0 \quad . \end{aligned}$$

Since it is still a wall type boundary condition, velocity and pressure on Γ_A are the same as those found in the previous section, while the boundary temperature can be obtained canceling the boundary integrals depending on δT of equation (3.13):

$$\int_{\Gamma} \left(T_a \mathbf{v} \cdot \mathbf{n} + K \mathbf{n} \cdot \nabla T_a \right) \delta T - \int_{\Gamma} K \frac{\partial \delta T}{\partial \mathbf{n}} T_a = 0 \quad \forall \delta T \quad . \quad (3.23)$$

The first term of equation (3.23) is null, since the primal velocity is zero at the wall, as well as the last one. The resulting boundary condition for the adjoint temperature reads:

$$\frac{\partial T_a}{\partial \mathbf{n}} = 0 \quad . \quad (3.24)$$

3.1.3 Gradient of the cost function

The sensitivity of the objective function with respect to the control variable can be evaluated as follows:

$$\begin{aligned}
J'(\rho)[\delta\rho] &= \partial_\rho L[\delta\rho] = \partial_\rho J + \int_\Omega (\mathbf{u}, q, T_a) \partial_\rho \mathbf{R} \\
&= \int_\Omega (\mathbf{u}, q, T_a) \begin{bmatrix} \mathbf{v} h(\rho) \delta\rho \\ 0 \\ (T - T_D) h(\rho) \delta\rho \end{bmatrix} \\
&= \int_\Omega \underbrace{(\mathbf{u} \cdot \mathbf{v} + T_a(T - T_D))}_{\nabla_\rho J} h(\rho) \delta\rho
\end{aligned} \tag{3.25}$$

where $\alpha'(\rho) = h(\rho)\delta\rho$. Here we have supposed the functional $J(\mathbf{y}, \rho)$ does not depend directly from ρ , that is $J = J(\mathbf{y})$. If it is not the case, its contribution should also be taken into account. In practical applications we need to build the discrete form of the gradient of the cost function with respect to the discrete control variable. Considering a typical finite volume approximation and using a mid-point rule, the discrete gradient reads:

$$\begin{aligned}
J'_h(\rho_h)[\delta\rho_h] &= \sum_i ((\mathbf{u}_i \cdot \mathbf{v}_i + T_{a_i}(T_i - T_D)) h(\rho_i) V_i \delta\rho_i \\
&= \nabla J_h \cdot \delta\rho_h
\end{aligned} \tag{3.26}$$

where we have considered values relative to the center of the i -th cell, with V_i being the volume of the i -th cell.

3.2 Optimal control problem 2

3.2.1 Adjoint equations

In this section we derive the adjoint system and the sensitivity for the *Control Problem 2*. We recall the state equations $\mathbf{R}(\mathbf{v}, p, T, \rho) = 0$ for the *Control Problem 2*, namely

$$(\mathbf{v} \cdot \nabla) \mathbf{v} + \nabla p - \nabla \cdot (2\nu D(\mathbf{v})) - \mathbf{g}(1 - \beta(T - T_0)) + \alpha(\rho) \mathbf{v} = 0 \tag{3.27a}$$

$$-\nabla \cdot \mathbf{v} = 0 \tag{3.27b}$$

$$\mathbf{v} \cdot \nabla T - \nabla \cdot (K(\rho) \nabla T) = 0 \quad . \tag{3.27c}$$

We can deduce the weak form of the adjoint equations requiring the derivative of L w.r.t. the state variables to be zero, as follows:

$$\partial_{\mathbf{y}}L[\delta\mathbf{y}] = \partial_{\mathbf{v}}L[\delta\mathbf{v}] + \partial_pL[\delta p] + \partial_TL[\delta T] = 0 \quad . \quad (3.28)$$

Proceeding as in section 3.1.1, considering the cost function defined in chapter 2 for the control problem, i.e.

$$J = \frac{1}{2} \int_{\Omega} (T - T^*)^2$$

the weak form of the adjoint problem yields:

$$\begin{aligned} & \int_{\Omega} \left(-(\nabla\mathbf{u})\mathbf{v} - (\mathbf{v}\cdot\nabla)\mathbf{u} - \nabla\cdot(2\nu D(\mathbf{u})) + \alpha(\rho)\mathbf{u} + \nabla q + T_a\nabla T \right) \cdot \delta\mathbf{v} \\ & + \int_{\Omega} (-\nabla\cdot\mathbf{u})\delta p \\ & + \int_{\Omega} \left(\beta\mathbf{u}\cdot\mathbf{g} - \mathbf{v}\cdot\nabla T_a - \nabla\cdot(K(\rho)\nabla T_a) + T - T^* \right) \delta T \\ & + \int_{\Gamma} \left((\mathbf{u}\cdot\mathbf{v})\mathbf{n} + \mathbf{u}(\mathbf{v}\cdot\mathbf{n}) + 2\nu\mathbf{n}\cdot D(\mathbf{u}) - q\mathbf{n} \right) \cdot \delta\mathbf{v} - \int_{\Gamma} 2\nu\mathbf{n}\cdot D(\delta\mathbf{v})\mathbf{u} \\ & + \int_{\Gamma} (\mathbf{u}\cdot\mathbf{n})\delta p \\ & + \int_{\Gamma} \left(T_a\mathbf{v}\cdot\mathbf{n} + K(\rho)\mathbf{n}\cdot\nabla T_a \right) \delta T + \int_{\Gamma} K(\rho)\mathbf{n}\cdot\nabla\delta T T_a = 0 \quad \forall \delta\mathbf{v}, \delta p, \delta T \quad . \end{aligned} \quad (3.29)$$

Since the previous relation has to be fulfilled for every variations $\delta\rho$, then for any $\delta\mathbf{v}, \delta p, \delta T$, each integral must vanish individually. For the integrals over the domain Ω , this requirement gives rise to the adjoint equations; in a similar fashion the adjoint boundary conditions are deduced from the boundary integrals on Γ . The adjoint equations are:

$$-(\nabla\mathbf{u})\mathbf{v} - (\mathbf{v}\cdot\nabla)\mathbf{u} - \nabla\cdot(2\nu D(\mathbf{u})) + \alpha(\rho)\mathbf{u} + \nabla q + T_a\nabla T = 0 \quad (3.30a)$$

$$\nabla\cdot\mathbf{u} = 0 \quad (3.30b)$$

$$\beta\mathbf{u}\cdot\mathbf{g} - \mathbf{v}\cdot\nabla T_a - \nabla\cdot(K(\rho)\nabla T_a) + T - T^* = 0 \quad . \quad (3.30c)$$

Comparing the adjoint equations of the two control problems, (3.10) and (3.30), we notice just few little differences, the same ones occurring between the two primal formulations. The considerations previously made for the adjoint equations of *Control Problem 1* still hold.

3.2.2 Adjoint boundary conditions

The boundary conditions for adjoint velocity, pressure and temperature are also derived from equation (3.29), considering the boundary integrals:

$$\int_{\Gamma} \left((\mathbf{u} \cdot \mathbf{v}) \mathbf{n} + \mathbf{u} (\mathbf{v} \cdot \mathbf{n}) + 2\nu \mathbf{n} \cdot D(\mathbf{u}) - q \mathbf{n} \right) \cdot \delta \mathbf{v} - \int_{\Gamma} 2\nu \mathbf{n} \cdot D(\delta \mathbf{v}) \mathbf{u} = 0 \quad (3.31a)$$

$$\int_{\Gamma} (\mathbf{u} \cdot \mathbf{n}) \delta p = 0 \quad (3.31b)$$

$$\int_{\Gamma} \left(T_a \mathbf{v} \cdot \mathbf{n} + K(\rho) \mathbf{n} \cdot \nabla T_a \right) \delta T + \int_{\Gamma} K(\rho) \mathbf{n} \cdot \nabla \delta T T_a = 0 \quad . \quad (3.31c)$$

Comparing the correspondent boundary equations (3.11) of the *Control Problem 1*, the only difference concerns the diffusivity coefficients in the third equation which, however, for the natural convection problem under consideration, do not affect the boundary conditions. In fact, proceeding as in section 3.1.2, specification of boundary conditions for the problem of object of study yields,

$$\mathbf{u} = 0 \quad \text{on } \Gamma \quad (3.32a)$$

$$T_a = 0 \quad \text{on } \Gamma_T \quad (3.32b)$$

$$\frac{\partial T_a}{\partial \mathbf{n}} = 0 \quad \text{on } \Gamma_A \quad (3.32c)$$

exactly as for *Control Problem 1*.

3.2.3 Gradient of the cost function

In the following we compute the sensitivity of the objective function with respect to the control variable:

$$\begin{aligned} J'(\rho)[\delta \rho] &= \partial_{\rho} L[\delta \rho] = \partial_{\rho} J + \int_{\Omega} (\mathbf{u}, q, T_a) \partial_{\rho} \mathbf{R} \\ &= \int_{\Omega} (\mathbf{u}, q, T_a) \begin{bmatrix} \mathbf{v} h(\rho) \delta \rho \\ 0 \\ -\nabla \cdot (H(\rho) \nabla T \delta \rho) \end{bmatrix} \\ &= \int_{\Omega} \mathbf{u} \cdot \mathbf{v} h(\rho) \delta \rho - T_a \nabla \cdot (H(\rho) \nabla T \delta \rho) \end{aligned}$$

where we have supposed the functional J does not depend on ρ explicitly. If not its contribution must be added. $H(\rho)$ and $h(\rho)$ are respectively the derivatives of $K(\rho)$ and $\alpha(\rho)$, that is $K'(\rho) = H(\rho) \delta \rho$ and $\alpha'(\rho) = h(\rho) \delta \rho$. Integration by part is necessary to get rid of the derivative of the control variation. The result yields:

$$J'(\rho)[\delta \rho] = \int_{\Omega} \left(\mathbf{u} \cdot \mathbf{v} h(\rho) + \nabla T_a \cdot \nabla T H(\rho) \right) \delta \rho - \int_{\Gamma} T_a H(\rho) \nabla T \cdot \mathbf{n} \delta \rho \quad . \quad (3.33)$$

Equation (3.33) includes a boundary integral which makes the computation of the sensitivity quite harder than its counterpart (3.25), for *Control Problem 1*. However, considering the particular case object of study, the boundary conditions are such that the integral on Γ disappears, making the sensitivity computation straightforward. So considering the case of a null boundary contribution on $J'(\rho)$, the discrete formulation of the sensitivity in a typical finite volume approximation becomes:

$$\begin{aligned} J'_h(\rho_h)[\delta\rho_h] &= \sum_i ((\mathbf{u}_i \cdot \mathbf{v}_i h(\rho_i) + \nabla T_{a_i} \cdot \nabla T_i H(\rho_i)) V_i \delta\rho_i) \\ &= \nabla J_h \cdot \delta\rho_h \end{aligned} \quad (3.34)$$

where we have considered values relative to the center of the i -th cell, with V_i being the volume of the i -th cell.

3.3 Dimensionless form of the *adjoint* equations

As for the two primal problems, we report here the equivalent non-dimensional form of their correspondent adjoint problems, considering the following reference quantities:

- length of the square cavity side: L [m]
- diffusivity coefficient of the fluid: K_f [m^2/s]
- wall temperature difference: $T_h - T_c$ [K]

In the next two paragraphs we report the results for the *Control Problem 1* and *Control Problem 2* respectively.

3.3.1 Non-dimensional *Control Problem 1*

Before defining the non-dimensional adjoint variables, it is necessary to have a look at their effective dimensions, which depends on the choice of J :

$$J = \frac{1}{2} \int_{\Omega} (T - T^*)^2 \quad . \quad (3.35)$$

From the adjoint equations (3.10) one can obtain the following nominal adjoint values:

$$\mathbf{U} = \mathbf{u} \frac{K_f^2}{L^3 (T_h - T_c)^2}; \quad \Theta_a = T_a \frac{K_f}{L^2 (T_h - T_c)}; \quad Q = \frac{q K_f}{(T_h - T_c) L^2};$$

The non-dimensional form of adjoint system (3.10) involved in the *Control Problem 1* finally reads:

$$\hat{\nabla} \mathbf{U} \mathbf{V} - (\mathbf{V} \cdot \hat{\nabla}) \mathbf{U} - \hat{\nabla} \cdot (2 Pr \hat{D}(\hat{\mathbf{U}})) + \hat{\alpha}(\rho) \mathbf{U} + \hat{\nabla} Q + \Theta_a \hat{\nabla} \Theta = 0 \quad (3.36a)$$

$$- \hat{\nabla} \cdot \mathbf{U} = 0 \quad (3.36b)$$

$$\mathbf{U} \cdot \hat{\mathbf{y}} Ra Pr - \mathbf{V} \cdot \hat{\nabla} \Theta_a - \hat{\Delta} \Theta_a + \hat{\alpha}(\rho) \Theta_a = 0 \quad (3.36c)$$

The non-dimensional adjoint boundary conditions (3.14) for the cavity case yield:

$$\begin{aligned} \mathbf{U} &= 0 & \text{on } \Gamma \\ \Theta_a &= 0 & \text{on } \Gamma_T \\ \frac{\partial \Theta_a}{\partial \mathbf{n}} &= 0 & \text{on } \Gamma_A \end{aligned}$$

3.3.2 Non-dimensional *Control Problem 2*

In the same fashion of the previous paragraph, one can obtain the non-dimensional form of adjoint systems (3.30), involved in the *Control Problem 2*:

$$\hat{\nabla} \mathbf{U} \mathbf{V} - (\mathbf{V} \cdot \hat{\nabla}) \mathbf{U} - \hat{\nabla} \cdot (2 Pr \hat{D}(\hat{\mathbf{U}})) + \hat{\alpha}(\rho) \mathbf{U} + \hat{\nabla} Q + \Theta_a \hat{\nabla} \Theta = 0 \quad (3.37a)$$

$$- \hat{\nabla} \cdot \mathbf{U} = 0 \quad (3.37b)$$

$$\mathbf{U} \cdot \hat{\mathbf{y}} Ra Pr - \mathbf{V} \cdot \hat{\nabla} \Theta_a - \hat{\nabla} \cdot (\hat{K}(\rho) \hat{\nabla} \Theta_a) = 0 \quad (3.37c)$$

where,

$$\hat{K}(\rho) = \frac{K(\rho)}{K_f} = \frac{\frac{k(\rho)}{(\rho_0 c_p)_f}}{\frac{k_f}{(\rho_0 c_p)_f}} = \frac{k(\rho)}{k_f}$$

that is the ratio between the controlled thermal conductivity and the fluid one. The boundary conditions are the same as those deduced in the previous paragraph.

Chapter 4

Solver algorithm description

In this chapter some aspects of the OpenFOAM implementations of the optimal control problems are hinted. We start with a brief introduction to the SIMPLE algorithm used for the numerical resolution of primal and adjoint equations. Then we give an insight in the implementation of a solver for the optimal control problems: two algorithms, namely Algorithm 1 and Algorithm 2, are presented. For the latter, a number of optimization tools are described.

4.1 The SIMPLE algorithm

The numerical implementation of the control problems introduced in the previous chapters has been performed using the finite volume library OpenFOAM (version 4.1). This open source CFD software allows the usage of a large number of numerical methods for the resolution of the fluid dynamics equations. Given the steady-state incompressible nature of the controlled problems, we decided to use the SIMPLE algorithm. A brief description of the main features of the latter is given in the following.

Solving general fluids flows requires an algorithm that can deal with pressure and velocity coupling. The solution procedure is based on reformulating the Navier-Stokes equations in terms of a momentum predictor and a pressure correction equation which enforces the satisfaction of the continuity constraint. The discretized equations are solved sequentially in an iterative procedure, that can be summarized as follows:

1. Start with a guessed pressure and velocity fields, say \mathbf{v}^m, p^m .
2. Solve the momentum predictor equation to obtain a new velocity field, say \mathbf{v}^* .

3. Solve the pressure correction (Poisson) equation to find the corrected pressure, say p^* .
4. Update the velocity field to satisfy continuity constraint. Denote with \mathbf{v}^{**} the corrected velocity.
5. Set $\mathbf{v}^m = \mathbf{v}^{**}$, and $p^m = p^*$
6. Go back to step 2 and repeat until convergence.

This sequential solution of the equations is denoted in literature by the segregated approach. For a deeper insight into the finite volume discretized equations and the SIMPLE algorithm, we suggest [8, 11]. The governing equations of the two control problems we are interested in, need however an energy equation to be solved together with momentum and continuity equations. The numerical scheme adopted in OpenFOAM to cope with this kind of coupled problems is actually a SIMPLE algorithm where the energy equation is updated at each iteration, using the current value of velocity, [14].

The segregated algorithm employed for the numerical resolution of the state equations requires an explicit boundary condition for pressure. In problems where it is assigned a full Dirichlet boundary conditions on velocity, as for the case of natural convection in a cavity (see section 2.2), the following Neumann boundary condition applies for pressure:

$$\frac{\partial p}{\partial \mathbf{n}} = 0 \quad \text{on} \quad \partial\Omega \quad .$$

The pressure will be thus defined up to a constant. Justification of this approximated boundary condition can be found in the *projection-methods* theory involved in the numerical resolution of the Navier-Stokes equations, [17].

We conclude underlining that the SIMPLE algorithm introduced in this section for the primal governing equations, is easily extendable to the adjoint equations, since these latter share the same structure of their primal counterpart. Accordingly, a similar boundary condition on the adjoint pressure can be applied, as for primal pressure:

$$\frac{\partial q}{\partial \mathbf{n}} = 0 \quad \text{on} \quad \partial\Omega \quad .$$

4.2 Optimal control problem solver: *Algorithm 1*

The first attempt in the implementation of a new code for topological optimization including heat transfer, is based on a simple merge of two existing solvers

coming from the official release of OpenFOAM. The two solvers in question are *adjointShapeOptimizationFoam*, a topological optimization problem based on the adjoint formulation for incompressible flows, proposed in [15], and *buoyantBoussinesqSimpleFoam*, which couples the incompressible Navier-Stokes equations and a simplified energy equation by means of the Boussinesq's approximation. The solver *Algorithm 1* is reported in the work-flow displayed in figure 4.1. The struc-

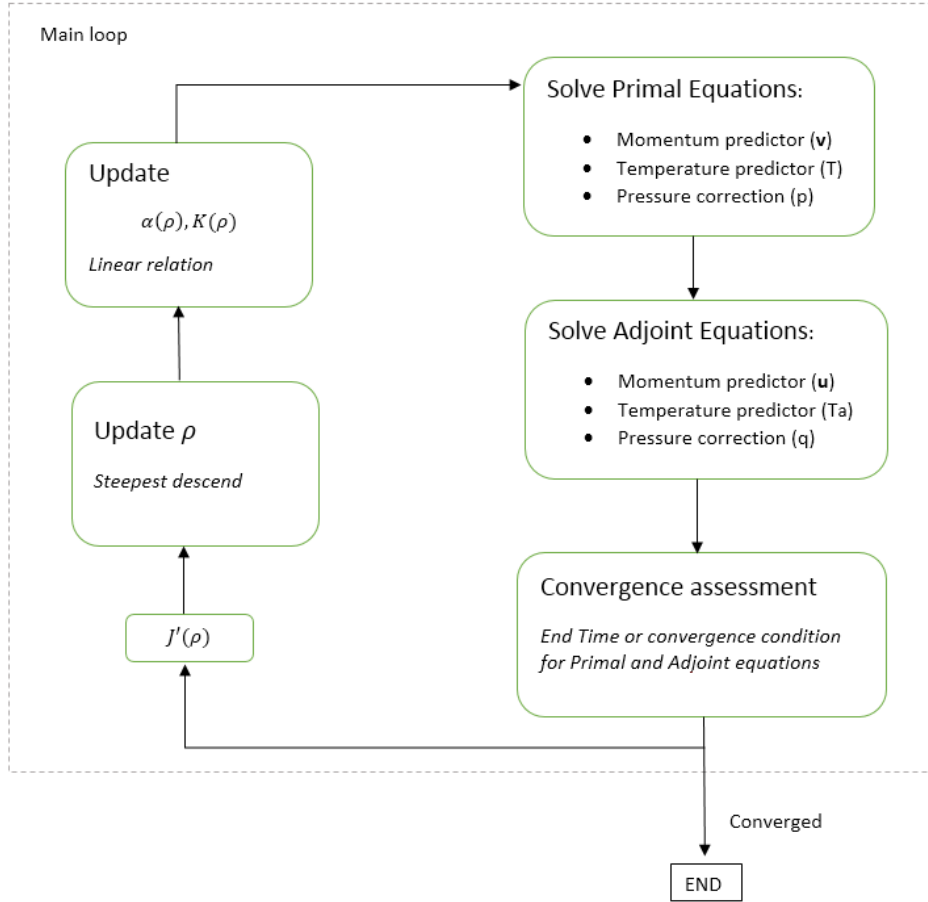


Figure 4.1: Block scheme for the *Algorithm 1*

ture of the *adjointShapeOptimizationFoam* has been taken as reference: primal and adjoint problems are solved sequentially, then the sensitivity is computed and the control variable updated, all within one step of a unique SIMPLE loop. Obviously the sensitivity obtained at each step is not the exact one, since it has been computed using only partially converged quantities. The sensitivity $J'(\rho)$ is then plugged in a *steepest descent* method, that is:

$$\rho^{k+1} = \rho^k - \tau J'(\rho^k) \quad . \quad (4.1)$$

The choice of the step length τ is done in a very simple way by fixing it to a constant value chosen arbitrarily. The boundedness of the control variable is achieved by a *min-max* filter that limits the control values in the interval $[0-1]$. Moreover an under-relaxation factor on ρ is applied to enhance stability. No control on the step effectiveness in decreasing the objective function is done, consequently the only termination criterion that can be developed is about the maximum number of iterations allowed. Although this method seems rather inaccurate, it perfectly fits to the *one shot* architecture of the algorithm, being on the other hand the only reasonable solution applicable.

From figure 4.1 it can be noted that simple linear relations have been used for the controlled functions $\alpha(\rho)$ and $K(\rho)$.

4.3 Optimal control problem solver: *Algorithm 2*

The analysis of the *Algorithm 1* shows some potential weaknesses that can affect the solver performances. The inconsistency of the sensibilities, above all in the first iterations, may cause the divergence of the optimization procedure. Also the continuous update of the control variable could bring undesired fluctuations on the solutions, preventing full convergence to the optimal result. In the section we propose some implementation improvements and also new possible strategies to broaden the solver usability. The solver *Algorithm 2* is schematized in figure 4.2. The first noteworthy change regards the way in which the primal and adjoint problems are solved. Despite the “*one shot*” architecture (*Algorithm 1*) should be good enough to ensure in most cases convergence of primal, adjoint and optimal solutions all together, as suggested in [15, 16], we preferred to split this procedure into three different parts: an outer optimization loop, and two inner SIMPLE loops for solving primal and adjoint problems. First we solve the primal problem up to a chosen tolerance, than the same is done for the adjoint problem. Once primal and adjoint solutions have been separately computed for a given control variable, the sensitivity can be computed. At this time we update the control variable and one step of the optimization loop is concluded. A code structured in this way guarantees a better control on each part of the solution; moreover we assure that the sensitivity is computed only when primal and adjoint systems are fulfilled, according to what prescribed by the theory. This new algorithm structure has another important feature: differently from the “*one shot*” formulation, now it is possible to evaluate the cost functional at each control update. This brings to new possible strategies to develop a more accurate *steepest descent* method,

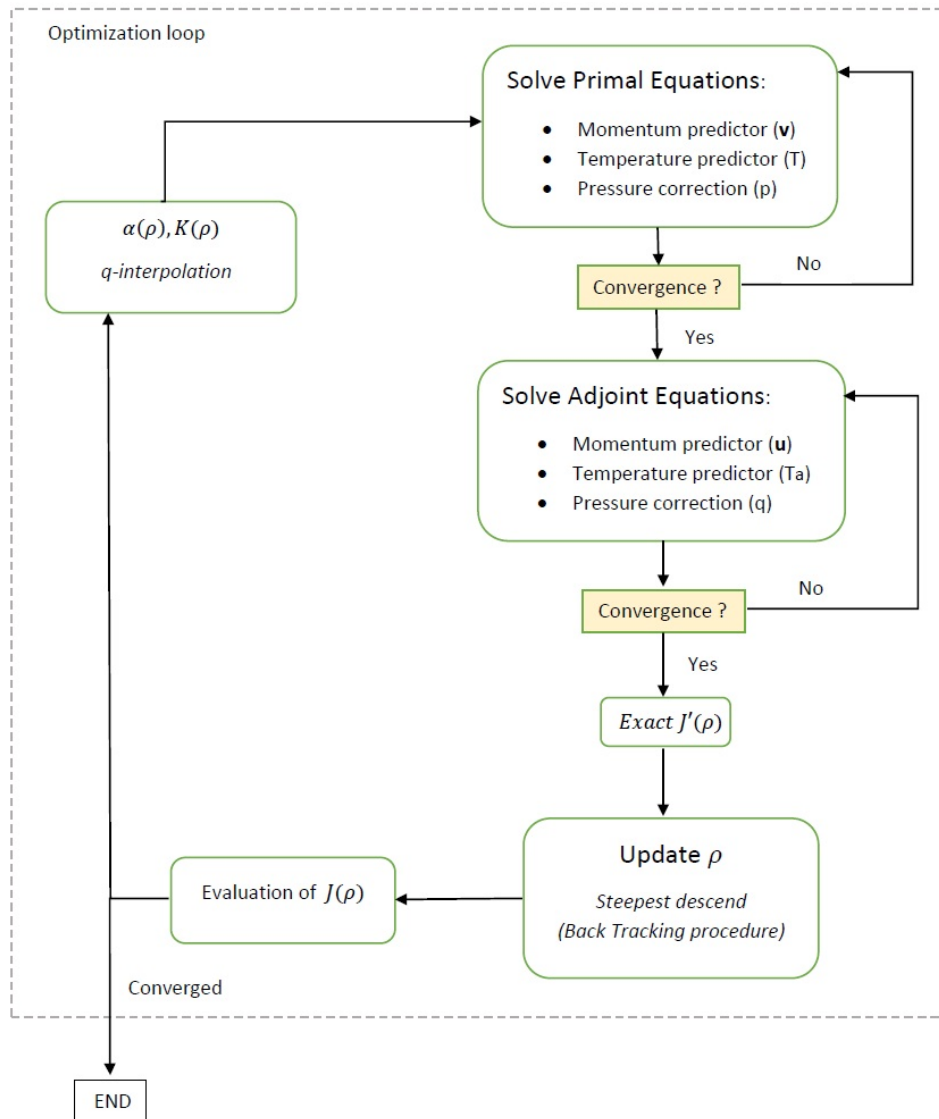


Figure 4.2: Block scheme for the *Algorithm 2*

as discussed in the next section. Other “optimization tools” are presented in the following lines to complete the solver algorithm description.

4.3.1 Line Search method: Backtracking

The update of the control variable is based on the *steepest descent* method, whose general implementation for the discrete control variable $\boldsymbol{\rho}$ at the iteration k , is described as follow:

$$\boldsymbol{\rho}^{k+1} = \boldsymbol{\rho}^k - \tau^k \nabla J(\boldsymbol{\rho}^k)$$

where $\nabla J(\boldsymbol{\rho})$ is the discrete derivative of the objective function w.r.t the control variable, while τ^k is the step length along the prescribed direction. In order to completely define a descent method is necessary to find the parameter τ^k . There are different strategies to assign a value to τ^k and they can all be gathered in the so called “line search methods”, which consist of a 1D optimization problem that can be stated as follows:

$$\text{Find } \tau^k \text{ that minimizes } \phi(\tau^k) = J(\boldsymbol{\rho}^k + \tau^k \mathbf{d}^k)$$

Following the work of Nocedal and Wright [10], we briefly introduce the line search algorithm developed.

A popular line search condition states that τ^k should first of all give sufficient decrease in the objective function J , as measured by the following inequality:

$$J(\boldsymbol{\rho}^k + \tau^k \mathbf{d}^k) \leq J(\boldsymbol{\rho}^k) + c_1 \tau^k \nabla J(\boldsymbol{\rho}^k) \cdot \mathbf{d}^k \quad (4.2)$$

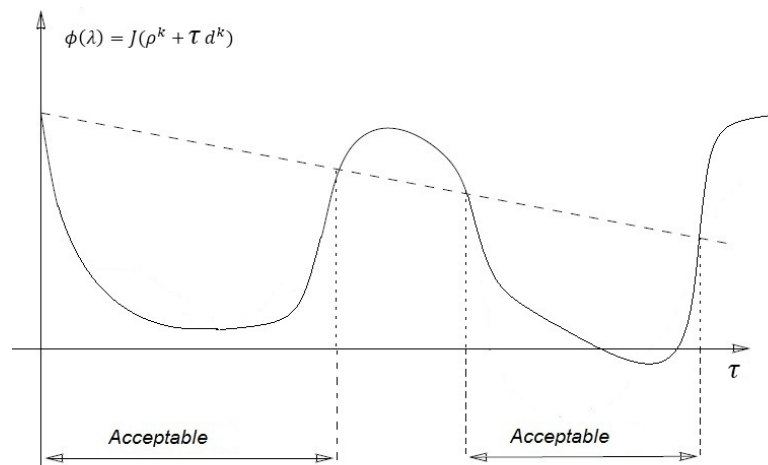


Figure 4.3: Illustration of the sufficient condition (4.2)

for some constant $c_1 \in (0, 1)$. In other words, the reduction in J should be proportional to both the step length τ^k and the directional derivative $\nabla J(\boldsymbol{\rho}^k) \cdot \mathbf{d}^k$. The sufficient decrease condition is not sufficient by itself to ensure that the algorithm makes reasonable progress, because as sketched in figure 4.3, it is satisfied for all sufficiently small values of τ . In order to avoid too small steps along the prescribed direction, the following condition on τ^k , called the curvature condition, is imposed:

$$\nabla J(\boldsymbol{\rho}^k + \tau^k \mathbf{d}^k) \cdot \mathbf{d}^k \geq c_2 \nabla J(\boldsymbol{\rho}^k) \cdot \mathbf{d}^k \quad (4.3)$$

for some constant $c_2 \in (c_1, 1)$. Note that the left-hand side is simply the derivative $\phi'(\tau^k)$, so the curvature condition ensures that the slope of $\phi(\tau^k)$ is greater than c_2 times the slope of $\phi'(0) < 0$. The meaning of this condition can be explained as follows: if the slope $\phi'(\tau^k)$ is strongly negative, it means that we can reduce J significantly by moving further along the chosen direction. On the other hand, if the slope is only slightly negative or even positive, we cannot expect much more decrease in J in this direction, so termination of the line search is reasonable. The main issue in the fulfillment of condition (4.3) is the calculation of $\phi'(\tau^k)$. Considering an iterative 1D line search method to get τ , this would mean computing the sensitivity $J'(\boldsymbol{\rho}^{k+1})$ at each iteration, with a huge increase of computational cost. On the other hand we have mentioned that the decrease condition (4.2) alone is not sufficient to ensure that the algorithm makes reasonable progress along the given search direction. However, by using a so-called backtracking approach, sufficiently large steps length are automatically assured without directly satisfying the extra condition (4.3). Then, just the sufficient decrease condition is employed to terminate the line search procedure. In its most basic form, backtracking proceeds as follows:

Backtracking Procedure:

Choose $\tau_0 > 0, \tau, c \in (0, 1)$; set $\tau_0 \rightarrow \tau$;
repeat until $J(\boldsymbol{\rho}^k + \tau^k \mathbf{d}^k) \leq J(\boldsymbol{\rho}^k) + c\tau^k \nabla J(\boldsymbol{\rho}^k) \cdot \mathbf{d}^k$
 $\gamma\tau \rightarrow \tau$
end
 Terminate with $\tau^k = \tau$

In the following we specify the method adopted to choose the initial step length τ_0 and the contraction factor γ , which stands for a compact notation to describe the way the initial step is iteratively decreased until a correct termination is found.

Initial step length

A popular strategy to evaluate the initial step τ_0 , is to assume that the first-order change in the function at the k -th iteration will be the same as that obtained at the previous step. In other words, we choose the initial guess τ_0 so that $\tau_0 \nabla J(\boldsymbol{\rho}^k) \cdot \mathbf{d}^k = \tau^{k-1} \nabla J(\boldsymbol{\rho}^{k-1}) \cdot \mathbf{d}^{k-1}$. We therefore have:

$$\tau_0 = \tau^{k-1} \frac{\nabla J(\boldsymbol{\rho}^{k-1}) \cdot \mathbf{d}^{k-1}}{\nabla J(\boldsymbol{\rho}^k) \cdot \mathbf{d}^k} \quad . \quad (4.4)$$

Interpolation

In these lines we introduce a method to generate a decreasing sequence of values τ_i starting from the initial guess τ_0 , as described in [10]. In order to reduce the computational effort it is essential that each trial τ_i is chosen accurately, exploiting all possible known information available at iteration i . An interpolation method is here employed to guess the step length value τ_i that satisfies the sufficient decrease condition (4.2). Note that we can write the sufficient decrease condition as:

$$\phi(\tau^k) \leq \phi(0) + c_1 \tau^k \phi'(0) \quad (4.5)$$

and that since the constant c_1 is usually chosen to be small in practice, this condition asks for little more than descent in J . We design the procedure to be “efficient” in the sense that the only requested derivative is the already known $\phi'(0)$. Suppose that the initial guess τ_0 is given. If we have

$$\phi(\tau_0) \leq \phi(0) + c_1 \tau_0 \phi'(0) \quad (4.6)$$

this step length satisfies the condition, and we terminate the search. Otherwise, we know that the interval $[0, \tau_0]$ contains acceptable step lengths. We form a quadratic approximation $\phi_q(\tau)$ to ϕ by interpolating the three pieces of information available, that is $\phi(0)$, $\phi'(0)$ and $\phi(\tau_0)$. In particular we want $\phi_q(\tau)$ to satisfy the interpolation conditions $\phi_q(0) = \phi(0)$, $\phi_q(\tau_0) = \phi(\tau_0)$ and $\phi'_q(0) = \phi'(0)$. The new trial value τ_1 is defined as the minimizer of this quadratic, that is, we obtain:

$$\tau_1 = -\frac{\phi'(0)\tau_0^2}{2[\phi(\tau_0) - \phi(0) - \phi'(0)\tau_0]} \quad . \quad (4.7)$$

If the sufficient decrease condition (4.5) is satisfied at τ_1 , we terminate the search. Otherwise, we construct a cubic function that interpolates the four pieces of information $\phi(0)$, $\phi'(0)$, $\phi(\tau_0)$, $\phi(\tau_1)$, obtaining

$$\phi_c(\tau) = a\tau^3 + b\tau^2 + \phi'(0)\tau + \phi(0) \quad (4.8)$$

being a and b two appropriate coefficients derived from cubic interpolation. By differentiating $\phi_c(\tau)$, the minimizer τ_2 of ϕ_c lies in the interval $[0, \tau_1]$ and is given by

$$\tau_2 = \frac{-b + \sqrt{b^2 - 3a\phi'(0)}}{3a} . \quad (4.9)$$

If necessary, this process is repeated, using a cubic interpolant of $\phi(0)$, $\phi'(0)$ and the two most recent values of ϕ , until a τ_i that satisfies (4.5) is obtained. In this case we put $\tau^k = \tau_i$ and the line search ends. If instead it does not occurs in a fixed maximum number of trials, than the line search is terminated and the optimization procedure too.

4.3.2 Intermediate control values penalization

In topology optimization, the final optimal control should be a discrete valued 0-1 function that distinguishes fluid regions from solid ones. In order to tend to a discrete solution while using a continuous approach, it is necessary that the intermediate values of the control variable are somehow penalized. This penalization can be obtained in different ways, according to the problem we are interested and its formulation. We decided to put the penalization as an explicit constraint in the cost function, as suggested in [20]:

$$J = \epsilon_1 J_{obj} + \epsilon_2 J_p \quad (4.10)$$

where ϵ_1 and ϵ_2 are relative weight coefficients to be properly assigned and J_{obj} is the ordinary objective function augmented with the penalization constraint J_p , defined as

$$J_p(\rho) = \int_{\Omega} g(\rho) = \int_{\Omega} \rho(1 - \rho) . \quad (4.11)$$

The quadratic compact support function $g(\rho): [0, 1] \rightarrow \mathbb{R}$ depicted in figure 4.4, makes the constraint objective function increase for all values of ρ different from 1 or 0. The minimization of J means putting J_p as close to zero as possible. In the case of natural convection in a cavity, the augmented cost functional reads:

$$J(\rho) = \epsilon_1 \frac{1}{2} \int_{\Omega} (T - T^*)^2 + \epsilon_2 \int_{\Omega} \rho(1 - \rho) . \quad (4.12)$$

The sensitivity previously obtained for the unconstrained objective function, now needs to be completed with the addition of a new contribution given from direct

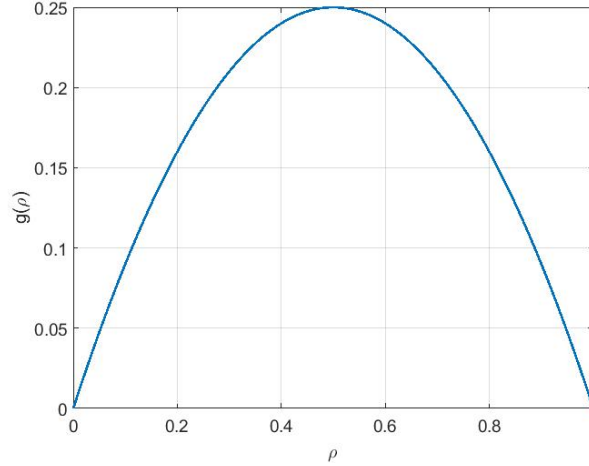


Figure 4.4: Penalization function

differentiation of the penalty constraint w.r.t to ρ :

$$J'(\rho)[\delta\rho] = \underbrace{\int_{\Omega} (\mathbf{u} \cdot \mathbf{v} + T_a(T - T_D)) h(\rho) \delta\rho}_{J'_{obj}(\rho)[\delta\rho]} + \epsilon_2 \underbrace{\int_{\Omega} (1 - 2\rho) \delta\rho}_{J'_p(\rho)[\delta\rho]} \quad (4.13)$$

where we have considered *Control Problem 1*. The same applies to the *Control Problem 2*. Note that the ϵ_1 weight coefficient does not appear directly in the sensitivity expression, but multiplies the right-hand-side source term of the adjoint temperature equation.

4.3.3 Volume constraint

In topology optimization it is common to introduce a constraint on the amount of available control, so as to limit the volume of solid (or fluid) within a prescribed portion of the whole domain, thus avoiding trivial optimal solutions. We decide to express this constraint as an equality constraint:

$$\int_{\Omega} \rho = V_{\rho} \quad (4.14)$$

where V_{ρ} represent the volume of solid to keep constant during the optimization. It can be directly assigned as an external data or computed from a given control ρ_0 whose volume we want to preserve. A simple way to include an equality constraint into a free optimization problem, consist of putting the constraint in the cost function definition, similarly to what performed for intermediate control value penalization. In this case we can define:

$$J = \epsilon_1 J_{obj} + \epsilon_2 J_v \quad (4.15)$$

being

$$J_v(\rho) = \frac{1}{2} \left(\int_{\Omega} \rho - \rho_0 \right)^2 . \quad (4.16)$$

In the case of natural convection in a cavity, the augmented cost functional reads:

$$J(\rho) = \epsilon_1 \frac{1}{2} \int_{\Omega} (T - T^*)^2 + \epsilon_2 \frac{1}{2} \left(\int_{\Omega} \rho - \rho_0 \right)^2 . \quad (4.17)$$

The sensitivity previously obtained for the unconstrained objective function, now needs to be completed with the addition of a new contribution given from direct differentiation of the volume constraint w.r.t. to ρ :

$$J'(\rho)[\delta\rho] = \underbrace{\int_{\Omega} \left(\mathbf{u} \cdot \mathbf{v} + T_a(T - T_D) \right) h(\rho) \delta\rho}_{J'_{obj}(\rho)[\delta\rho]} + \epsilon_2 \underbrace{\int_{\Omega} \left(\int_{\Omega} \rho - \rho_0 \right) \delta\rho}_{J'_v(\rho)[\delta\rho]} \quad (4.18)$$

where we have considered the *Control Problem 1*. The same applies to the *Control Problem 2*. Note that the ϵ_1 weight coefficient does not appear directly in the sensitivity expression, but multiplies the right-hand-side source term of the adjoint temperature equation.

4.3.4 q-parametrized interpolation functions

Another interesting aspect to be analyzed concerns the quantities $\alpha(\rho)$ and $K(\rho)$. A linear relation has been used as first approach, keeping a certain continuity with the original *adjointShapeOptimizationFoam*, but it seems worth exploring other solutions. Following the pioneering work of T. Borrvall and J. Petersson [21], the mapping between ρ and the penalty and conductivity terms can be expressed as follows:

$$\alpha(\rho) = \alpha_{max} - \alpha_{max}(1 - \rho) \frac{1 + q}{1 - \rho + q} \quad (4.19)$$

$$K(\rho) = K_s - (K_s - K_f)(1 - \rho) \frac{1 + q}{1 - \rho + q} \quad (4.20)$$

where K_s and K_f are the solid and fluid thermal conductivities. Figure 4.5 shows how the q parameter affects the function shape of K (being the same obviously for α). It is easily deduced that when q is large the interpolation is close to linear. Despite the differences between [21] and this work, we however take some important advantages from the parametric interpolation proposed. Before giving some hints about the effect of q on the whole problem formulation, let us take into account the complete objective function, augmented with volume and intermediate control

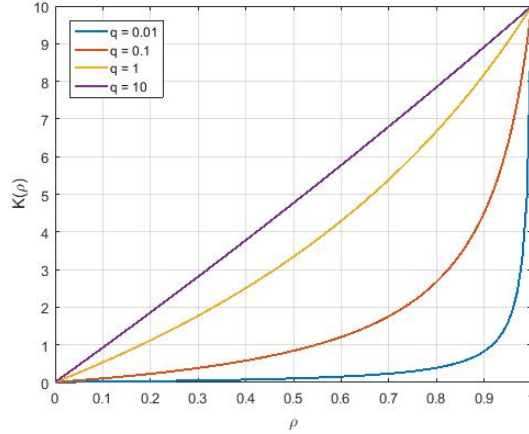


Figure 4.5: Interpolation function (4.20) plotted for different q values

value penalization constraints:

$$J = \epsilon_1 \frac{1}{2} \int_{\Omega} T - T^* + \epsilon_2 \frac{1}{2} \left(\int_{\Omega} \rho - \bar{\rho} \right)^2 + \epsilon_3 \int_{\Omega} \rho(1 - \rho) \quad . \quad (4.21)$$

We can deduce the complete sensitivity as

$$J'(\rho)[\delta\rho] = \int_{\Omega} \left(\mathbf{u} \cdot \mathbf{v} + T_a(T - T_D) \right) h(\rho)\delta\rho + \epsilon_2 \int_{\Omega} S_{\rho}\delta\rho + \epsilon_3 \int_{\Omega} (1 - 2\rho)\delta\rho \quad (4.22)$$

for the *Control Problem 1*, or

$$J'(\rho)[\delta\rho] = \int_{\Omega} \left(\mathbf{u} \cdot \mathbf{v} h(\rho) + \nabla T_a \cdot \nabla T H(\rho) \right) \delta\rho + \epsilon_2 \int_{\Omega} S_{\rho}\delta\rho + \epsilon_3 \int_{\Omega} (1 - 2\rho)\delta\rho \quad (4.23)$$

for the *Control Problem 2*, where $S_{\rho} = \int_{\Omega} (\rho - \bar{\rho})$ and $\epsilon_1, \epsilon_2, \epsilon_3$ are the relative weight coefficients assigned to the augmented functional contributions. From equations (4.19) and (4.20) the derivatives

$$K'(\rho) = (K_s - K_f)(1 + q) \frac{q}{(1 - \rho + q)^2} \delta\rho = H(\rho)\delta\rho \quad (4.24)$$

and

$$\alpha'(\rho) = \alpha_{max}(1 + q) \frac{q}{(1 - \rho + q)^2} \delta\rho = h(\rho)\delta\rho \quad (4.25)$$

are easily deduced. Figure 4.6 shows $H(\rho)$ and $h(\rho)$ for two different values of q . Looking at equations (4.22) and (4.23) we can think of $H(\rho)$ and $h(\rho)$ as variable gains on the unconstrained sensitivity: for sufficiently high q values the $K(\rho)$ and $\alpha(\rho)$ relations are almost linear whereas $H(\rho)$ and $h(\rho)$ are practically constant, with little influence on the sensitivity. But the more q value decreases the more the non linearity of $K(\rho)$ and $\alpha(\rho)$ increases and their derivatives leave the constant

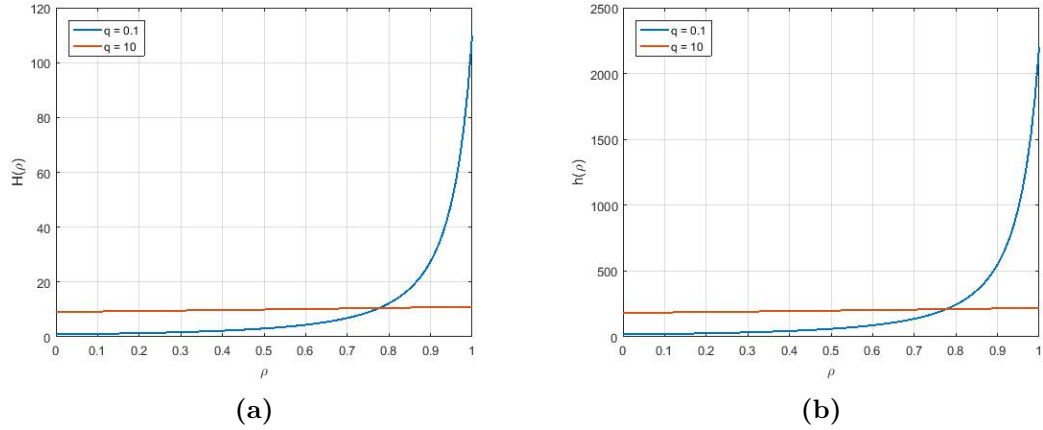


Figure 4.6: Derivatives (4.24) and (4.25) for q equal to 0.1 and 10

trend for a sharper one. These choices for $h(\rho)$ and $\alpha(\rho)$ affect the sensitivity, increasing its value when ρ tends to 1 and decreasing it when ρ tends to 0. This effect is as much higher as smaller is q . Now, let us take into consideration equation (4.22) at first: as the control approaches to 1, the temperature T becomes closer to T_D and the primal velocity \mathbf{v} tends to 0, thus the first term of the sensitivity vanishes, leaving to the constraints the greater contributions on $J'(\rho)$. In a trend of diminishing sensitivity for increasing control, the opposite trend of $h(\rho)$ is useful to mitigate this effect and to balance the weights of the three contributions to $J'(\rho)$. On the other hand, for smaller values of q , the aforementioned effects are excessively amplified and limited on an always narrower interval of ρ close to 1. In the end the q -parametrization reveals to be a good method to regularize the sensitivity, making the optimization process more stable, as it will be highlighted in the numerical results presented in the next chapter. The same applies to equation (4.23) where, however, the way the temperature contribution on the sensitivity approaches to zero for an increasing control, depends on how much is the difference between K_s and K_f values. If this difference is quite great, the temperature distribution over a $\rho = 1$ region is almost constant and its gradient almost zero, as well as the unconstrained sensitivity. Differently, if K_s is close to K_f , this effect is much more mitigated.

Chapter 5

Numerical Tests

We report in this chapter the results of the numerical simulations that have been carried out using the solvers introduced in the previous chapter. First we show the results of simple optimal control thermal problems in 1D and 2D and compare the performances of the different solvers. Then we will move to the more complex case of a 2D natural convection in a cavity. The numerical simulations have been launched on a PC with the following specifications: CPU Intel Core i3 M 370 @2.40GHz, RAM DDR3 2.8GB @1066MHz

5.1 A simpler optimal control problem

The optimization problem always deals with finding the control variable ρ that minimizes the cost functional:

$$J = \frac{1}{2} \int_{\Omega} (T - T^*)^2 \quad (5.1)$$

which means finding the control shape that best fits a given reference solution T^* . The control variable $\rho \in [0, 1]$ is here intended as a porosity field affecting the thermal properties of a solid medium. The problem is defined by *Control Problem 1* and *Control Problem 2* when a null velocity is assumed. The *Solver Algorithm 2* is employed. Problems details are found in each test case that we will discuss. In order to assess the capability of the solver to recover the optimal solution, the reference temperature distribution T^* is computed starting from a reference control variable ρ^* . We expect the optimization process to be able to find the optimal control $\rho_{opt} = \rho^*$ starting from a null initial control ρ^0 far from the reference one. These simplified test cases have been carried out to verify the ability of the adjoint formulations in computing the topological sensitivities.

5.1.1 1D Thermal problems

The problem layout consist of a 1D domain $\Omega(x) = (0, L) \in \mathbb{R}$ of length $L = 1$ [m] with prescribed temperature at the boundary, say T_h in $x = 0$ and T_c in $x = L$, with $T_h > T_c$. The only state variable is temperature T .

The reduced forms of the *Control Problem 1* and *Control Problem 2* are tested on the same problem.

Control Problem 1

The optimization problem can be stated as follow:

Find the optimal control ρ that minimizes $J(T) = \frac{1}{2} \int_0^L (T - T^*)^2$, subjected to the constraint $\mathcal{R}_{\mathcal{G}}(T, \rho) = 0$, defined by the following elliptic equation for the temperature:

$$\begin{cases} \frac{d}{dx} \left(K \frac{dT}{dx} \right) = \alpha(\rho)(T - T_D) \\ T(0) = T_h \\ T(1) = T_c \end{cases}$$

with Dirichlet boundary conditions. Where $\rho = 0$ we have $\alpha(0) = 0$ and the heat equation in a solid is recovered, while where $\rho = 1$, $\alpha(1) = \alpha_{max}$, and temperature is forced to assume the value T_D . In this test $\alpha_{max} = 200$. The conductivity coefficient is constant and equal to $K = 0.01$ [$\frac{W}{mK}$], an indicative value of a thermally insulating material. We take $T_h = 1$ [°C] and $T_c = 0$ [°C]. The function T_D is described by the following relation:

$$T_D(x) = \begin{cases} T_h & \text{per } x \leq \frac{L}{2} \\ T_c & \text{per } x > \frac{L}{2} \end{cases} . \quad (5.2)$$

The reference temperature T^* is obtained from the assigned control distribution:

$$\rho^*(x) = \begin{cases} 1 & \text{per } x \leq \frac{1}{4} \vee x \geq \frac{3}{4} \\ 0 & \text{per } \frac{1}{4} < x < \frac{3}{4} \end{cases} . \quad (5.3)$$

Figure 5.1 shows the reference control and temperature. The adjoint equation with relative boundary conditions can be obtained as simplified version of the adjoint problem (3.10):

$$\begin{cases} \frac{d}{dx} \left(K \frac{dT_a}{dx} \right) = \alpha(\rho)T_a + T - T^* \\ T_a(0) = T_a(1) = 0 \end{cases} . \quad (5.4)$$

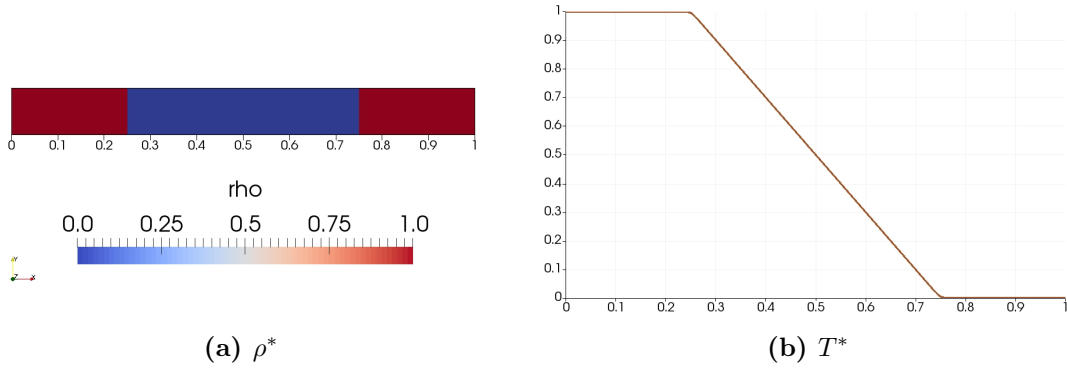


Figure 5.1: Reference temperature T^* and associated control variable ρ^* for 1D thermal problem

The sensitivity is given by:

$$J'(\rho)[\delta\rho] = \int_0^L T_a(T - T_D)h(\rho)\delta\rho \quad (5.5)$$

being $\alpha'(\rho) = h(\rho)\delta\rho$.

Because of the discontinuity of the T_D function (5.2) in $\frac{L}{2}$, also $J'(\rho)$ is discontinuous. It make sense that the control variable is not allowed to act in the interval $[\frac{L}{2} + \epsilon, \frac{L}{2} - \epsilon]$ for an arbitrary small value of ϵ . This is guaranteed by multiplying ρ for the filter field

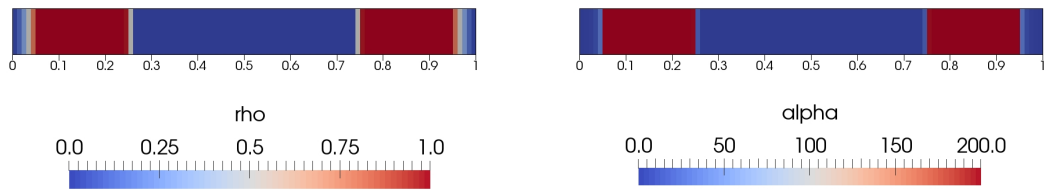
$$filt = \begin{cases} 1 & \text{per } x \leq \epsilon \vee x \geq L - \epsilon \\ 0 & \text{per } \epsilon < x < L - \epsilon \end{cases} \quad (5.6)$$

Despite sounding as an artificial limitation to the control action, the adopted measure is in line with the intrinsic task of this control problem, that is modifying the domain shape through a penalization of the cells next to the boundary, thus extending the boundary properties to the penalized regions inside the domain. In other words the control is not supposed to act in the only middle of the domain anyway. The mesh chosen for this case is a uniform Cartesian grid of 50×1 cells. In table 5.1 we report the parameters used in the simulation, where Tol stands for the chosen tolerance for the solution of primal/adjoint temperature equation, q is the interpolation parameter (see section 4.3.4) and c is the constant employed in the sufficient decrease condition (4.2) introduced in section 4.3.1. Figure 5.2 shows the obtained results of the free optimization (no volume or intermediate control value constraints).

Starting from figure 5.2b and 5.2d, we can appreciate the way the optimal control follows the discontinuities of the reference solution in $x = \frac{1}{4}$ and $x = \frac{3}{4}$,

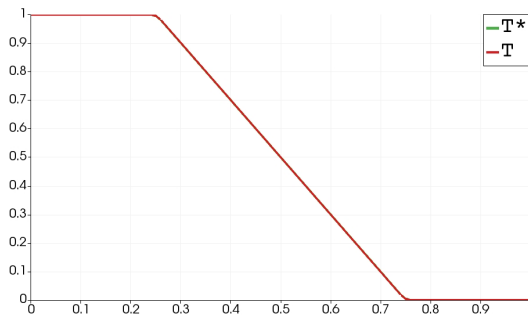
Tol Ta	Tol T	q	c	$K [\frac{W}{mK}]$
1e-6	1e-6	0.04	1e-8	0.01

Table 5.1: Settings of the parameters for 1D unconstrained optimization (*Control Problem 1*)

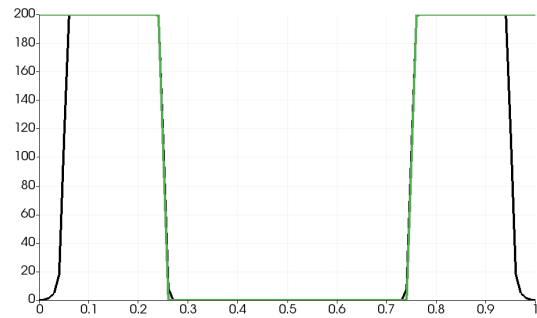


(a) Final result of optimization: ρ

(b) Final result of optimization: $\alpha(\rho)$



(c) Comparison of final temperature distribution T with T^*



(d) Comparison of final $\alpha(\rho)$ (in black) with $\alpha(\rho^*)$ (in green)

Figure 5.2: Final solutions for unconstrained 1D optimization (*Control Problem 1*)

J_0	J_{opt}	iterations	Exec.Time
1.73e-3	6.59e-9	24	0.52s

Table 5.2: Initial and final values of cost function (J_0 and J_{opt} respectively), number of optimization iterations, execution time (unconstrained 1D optimization, *Control Problem 1*)

but an important mismatch appears near the boundaries. Looking at figure 5.2c however, the temperature curves overlap almost perfectly. This behavior can be explained in a simple way: the optimal solution for an unconstrained optimization is not unique. A simple way to recover uniqueness of the solution, at least for the problem object of study, is adding a volume constraint, using as target volume the one corresponding to ρ^* . The results are showed in figure 5.3. In table 5.3

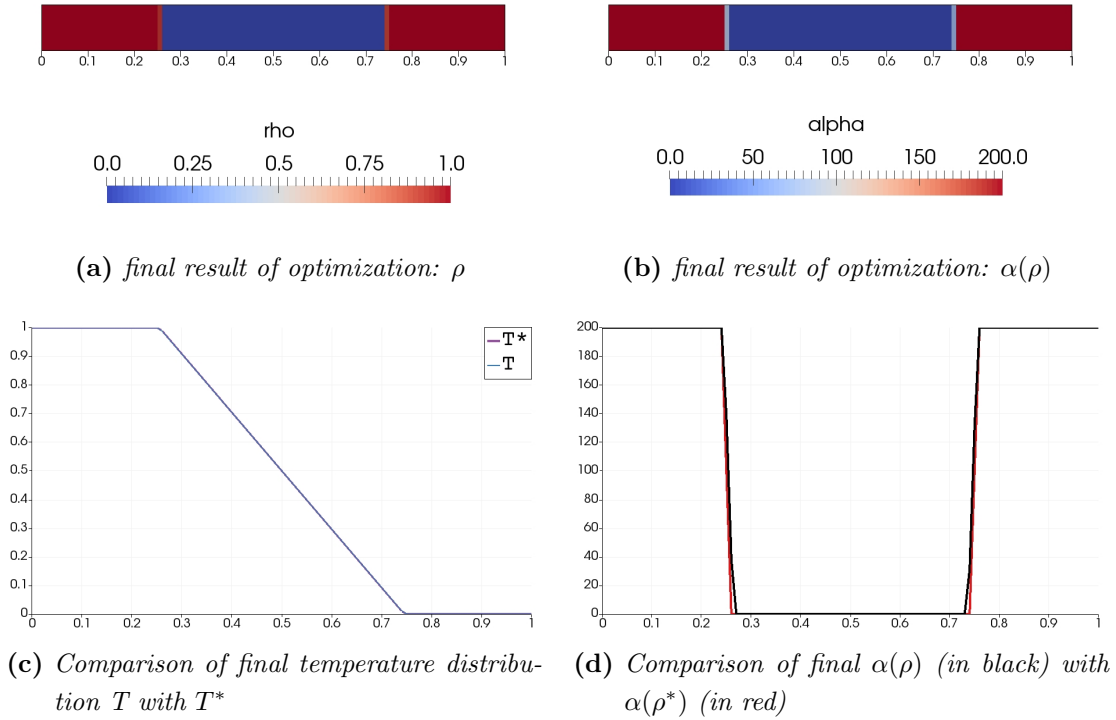


Figure 5.3: Final solutions for 1D volume constraint optimization (*Control Problem 1*)

the setting parameters are reported, where ϵ_1 and ϵ_2 are respectively the weight coefficients of the objective function and volume penalization. The final results of the optimization are summarized in table 5.4.

Tol Ta	Tol T	q	c	$K [\frac{W}{mK}]$	ϵ_1	ϵ_2
1e-6	1e-6	0.04	1e-8	0.01	0.9	0.1

Table 5.3: Settings of the parameters for 1D constrained optimization (*Control Problem 1*)

	J	J_{obj}	J_v	iterations	Exec.Time
Initial	1.87e-3	1.55e-3	3.2e-4	8	0.35s
Final	4.64e-7	1.99e-8	4.44e-7		

Table 5.4: Initial and final values of cost function $J = J_{obj} + J_v$, number of optimization iterations, execution time (constrained 1D optimization, *Control Problem1*)

Control Problem 2

The optimization problem can be stated as follow:

Find the optimal control ρ that minimizes $J(T) = \frac{1}{2} \int_0^L (T - T^*)^2$, subjected to the constraint $\mathcal{R}_{\mathcal{F}}(T, \rho) = 0$, defined by the following equation on temperature:

$$\begin{cases} \frac{d}{dx} \left(K(\rho) \frac{dT}{dx} \right) = 0 \\ T(0) = T_h \\ T(1) = T_c \end{cases} .$$

Where $K(0) = K_f$ is the minimum value of solid thermal conductivity, whereas $K(1) = K_s$ is the maximum, with $\frac{K_s}{K_f} = 1000$. Such a high ratio has been chosen in order to have an almost constant temperature profile where $\rho = 1$, making this control problem be comparable to the previous one. In particular $K_f = 0.01 [\frac{W}{mK}]$ and $K_s = 10 [\frac{W}{mK}]$, being respectively the indicative values of a thermally insulating and conductive material, while $T_h = 1$ [°C] and $T_c = 0$ [°C].

The reference temperature T^* is obtained from the assigned control distribution (5.3) given in the previous section. The temperature profile is practically identical to the one showed in figure 5.1. We can think to the reference temperature T^* as the temperature profile along a slender rod of length L made of two solid materials with very different thermal properties and with fixed temperature at the ends. The aim of our optimization process is to reconstruct the exact distribution of K along the rod that gives the just described temperature solution starting from a null control in the whole domain.

For the computation of the sensitivity, the adjoint equation has to be solved with the correct boundary conditions:

$$\begin{cases} \frac{d}{dx} \left(K(\rho) \frac{dT_a}{dx} \right) = T - T^* \\ T_a(0) = T_a(1) = 0 \end{cases} . \quad (5.7)$$

Then the sensitivity can be deduced as,

$$J'(\rho)[\delta\rho] = \int_0^L \frac{dT_a}{dx} \frac{dT}{dx} H(\rho) \delta\rho \quad . \quad (5.8)$$

Figure 5.4 shows the final result of the free optimization (no volume or intermediate control value constraints). The mesh chosen for this case is a uniform Cartesian grid of 50×1 cells. In table 5.5 we report the parameters used in the simulation.

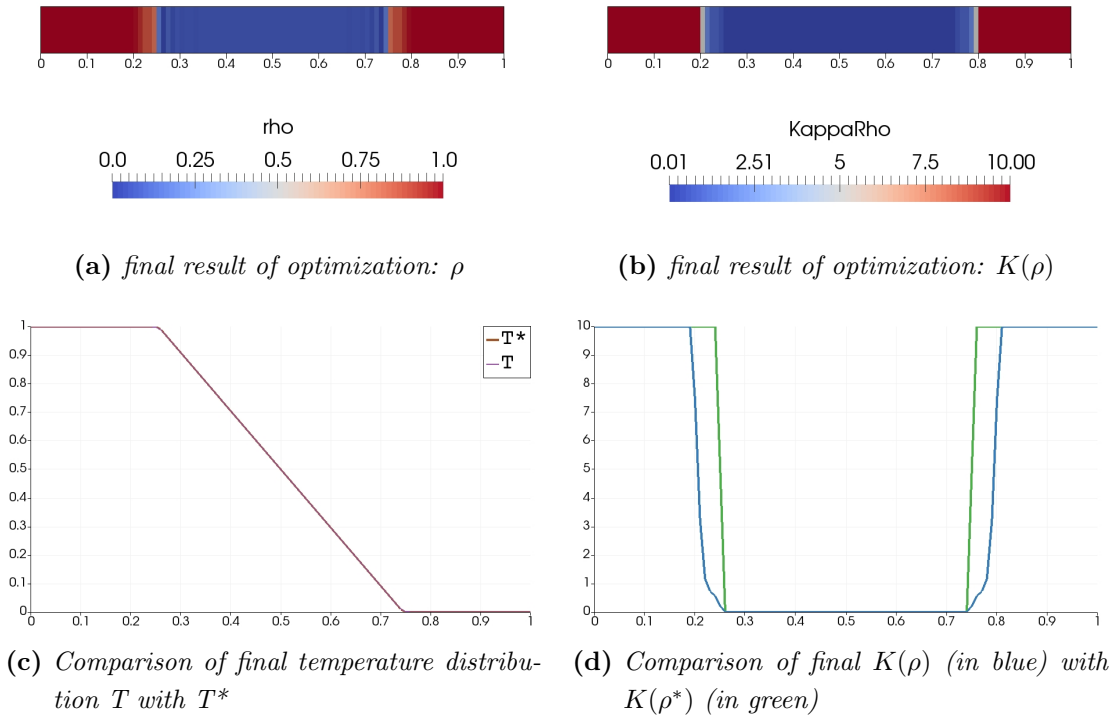


Figure 5.4: Final solutions for unconstrained 1D optimization (*Control Problem 2*)

First of all we notice from pictures 5.4a and 5.4b that the control variable ρ and

Tol Ta	Tol T	q	c	$K_f [\frac{W}{mK}]$	$K_s [\frac{W}{mK}]$
1e-6	1e-6	0.01	1e-8	0.01	10

Table 5.5: Settings of the parameters for 1D unconstrained optimization (*Control Problem 2*)

$K(\rho)$ are slightly different. This is a consequence of the small value of the q parameter employed, which affects the $K(\rho)$ relation and its derivative $H(\rho)$ as described in section 4.3.4. In particular the regularization effect of q on $J'(\rho)$ is

evident from picture 5.5. On the other hand the almost constant profile of $K(\rho; q)$ for sufficiently low control action, brings some oscillation on the solution. As a matter of fact the value of q plays a quite important role in obtaining a good result from the optimization. In picture 5.4d the final K profile and the reference

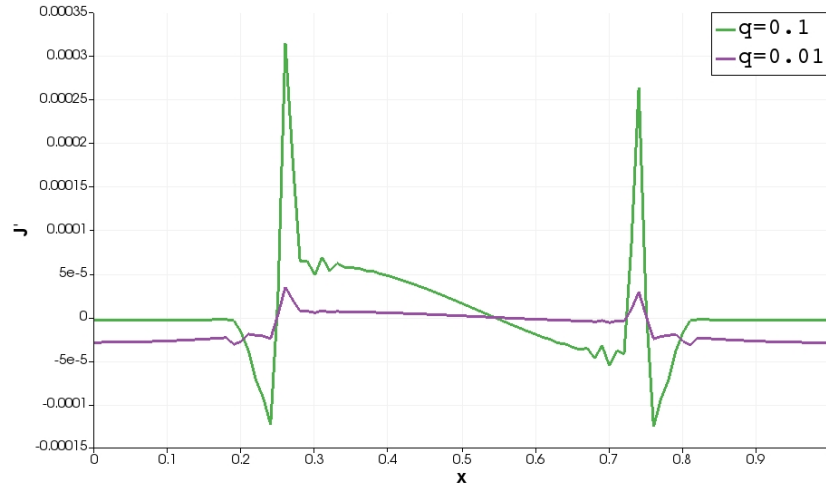


Figure 5.5: $J'(\rho^k)$ corresponding to the k -th iteration (ρ^k is close to the final one) for two different values of q

one are showed: the “optimal” control does not fit exactly the reference one, but the temperature profiles showed in picture 5.4c are very close to each other, with few little differences only around the slope discontinuities. This particular feature of the solution needs deeper investigation. In order to exclude possible numerical errors, we solve primal and adjoint temperature equations both numerically and analytically in a similar but simpler configuration than the current one. Obviously no optimization is performed. For this test we choose:

$$\rho(x) = \begin{cases} 1 & \text{for } x \leq \frac{1}{2} \\ 0 & \text{for } x > \frac{1}{2} \end{cases} .$$

We take $T^* = 0$ in order to have an easier source term in the adjoint temperature equation. Moreover, just for this test, the maximum value of K (K_s) has been reduced to 0.1 (instead of 10), so as to better appreciate the slope in the temperature solution. The minimum value K_f has not been changed. The comparison of numerical and analytical results is showed in figure 5.6. The test not only confirms the goodness of numerical solutions for the two elliptic equations, but also highlights another important issue. Looking at figure 5.6b we can see how the temperature profile is made of two straight lines with two different slopes, say m_s the one relative to $K_s = 0.1$ and m_f the other. We consider now the same configuration of K showed in figure 5.6a but with variable values of K_s and we compute the slope of

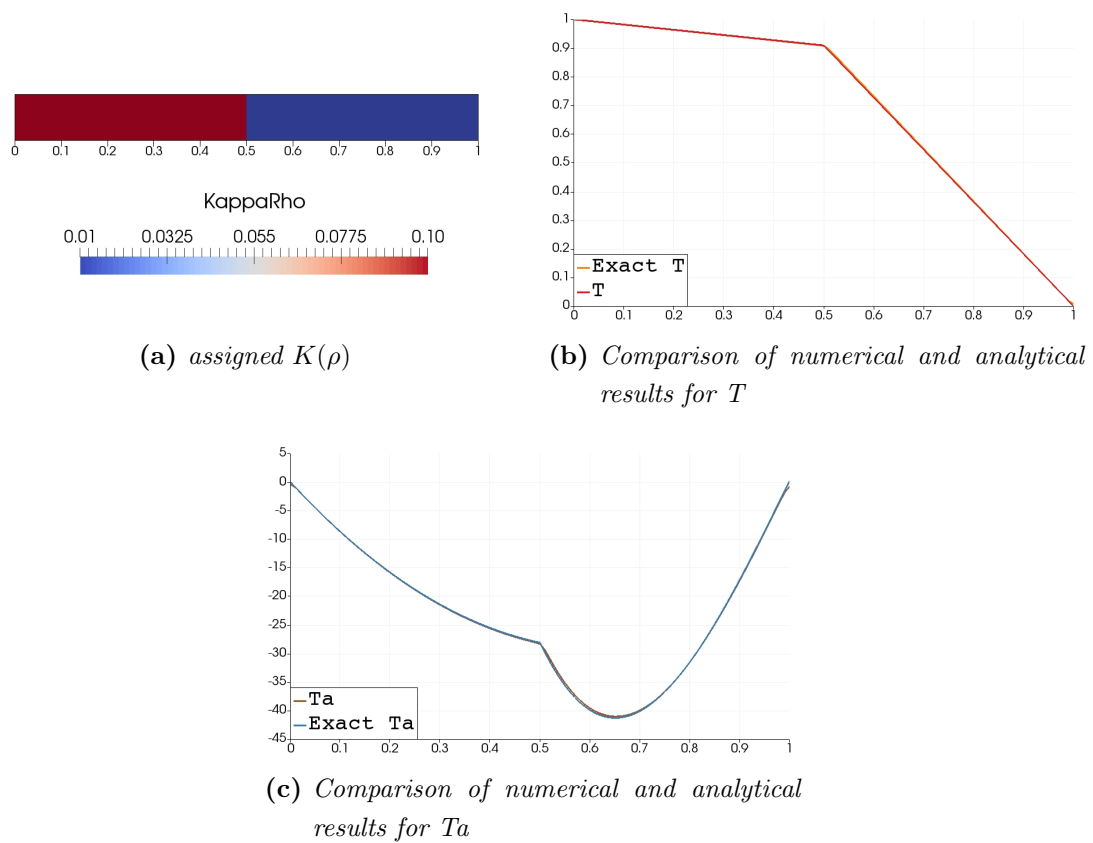


Figure 5.6: Comparison of analytical and numerical solutions of adjoint and primal temperature equations relative to a fixed K distribution

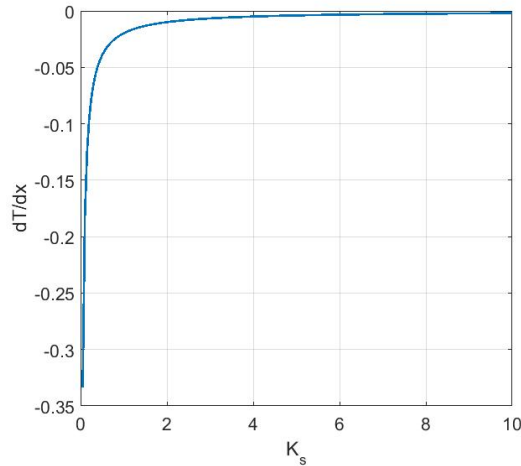


Figure 5.7: Slope of T (m_s) as function of K_s for a 1D thermal problem with fixed temperature at the boundary and K distribution given in fig (5.6a)

the temperature profile m_s as function of K_s . The result is showed in figure 5.7: it is evident that K_s values beyond 2 give an almost constant m_s , compromising the ability of the solver to distinguish from different control actions, causing little sensitivities and a premature end of the optimization process. That's why despite of the consistent difference between the “optimal” control solution and the reference one showed in figure 5.4d, the two relative temperature profiles are almost identical. Moreover this seems to be the cause of the slow rate of convergence of the solver, which takes more than 11000 iterations to get the final solution. Further on we will discuss deeply the question and a cure to improve the solver performances will be proposed. We point out that we are interested in obtaining good results from these thermal problems, using an high ratio $\frac{K_s}{K_f}$, because the same ratio can be employed in the natural convection problem. Finally we conclude reporting in table 5.6 some data about the optimization process.

J_0	J_{opt}	iterations	Exec.Time
1.73e-3	1.98e-08	11067	119.27s

Table 5.6: Initial and final values of cost function (J_0 and J_{opt} respectively), number of optimization iterations, execution time (unconstrained 1D optimization, *Control Problem 2*)

Conclusions

These 1D thermal problems give in the end appreciable results but also show some weaknesses of the control problems: the very slow rate of convergence of the *Control Problem 2*, that could be unbearable for more complex problems, and the inaccuracy of the solution; the non-uniqueness of the solution involving the *Control Problem 1*, that therefore needs a volume constraint to regain uniqueness; finally, a certain dependence of the optimization process on the choice of the parameter q , which therefore requires a fine tuning to prevent an early end of the process. In the next paragraph we propose a solution to speed up the convergence of the *Control Problem 2*.

5.1.2 2D Thermal problems

In this section a 2D thermal problem is presented. The domain $\Omega(x, y) = (0, L) \times (0, L) \in \mathbb{R}^2$ is a square of side $L = 1$ [m], with the two vertical sides at fixed temperature and the horizontal sides adiabatic. It is the same layout employed in the natural convection study, but with no fluid involved.

The reduced form of the *Control Problem 2* with zero velocity has been used for this test.

The statement of the optimization problem is as before:

Find the optimal control ρ that minimizes $J(T) = \frac{1}{2} \int_{\Omega} (T - T^)^2$, subjected to the constraint $\mathcal{R}_{\mathcal{F}}(T, \rho) = 0$, defined by the following equation on temperature:*

$$\left\{ \begin{array}{l} -\nabla \cdot (K(\rho)\nabla T) = 0 \quad \text{in } \Omega \\ T(0, y) = T_h \\ T(1, y) = T_c \\ \frac{\partial T}{\partial y}(x, 0) = -\frac{\partial T}{\partial y}(x, 1) = 0 \quad . \end{array} \right. \quad (5.9)$$

In particular $K(0) = K_f$ is the minimum value of solid thermal conductivity, whereas $K(1) = K_s$ is the maximum, with $\frac{K_s}{K_f} = 1000$. The same high ratio of the 1D problem has been used. In particular $K_f = 0.01 [\frac{W}{mK}]$ and $K_s = 10 [\frac{W}{mK}]$, being respectively the indicative values of a thermally insulating and conductive material, while $T_h = 1$ [°C] and $T_c = 0$ [°C].

The reference temperature chosen for this test case has been computed assuming

the following control:

$$\rho^*(x, y) = \begin{cases} 1 & \text{for } (x - \frac{1}{2})^2 + (y - \frac{1}{2})^2 \leq R \\ 0 & \text{elsewhere} \end{cases}$$

being $R = \frac{1}{4}$ the given radius. The reference temperature and control are showed in figure 5.8. For this particular case it is evident that the *Control Problem 1* cannot be defined since physically inconsistent: on the round centered “island” where $\rho = 1$ no temperature at the boundary can be assigned, neither the hot one or the cold one. For *Control Problem 2*, adjoint equations with relative boundary

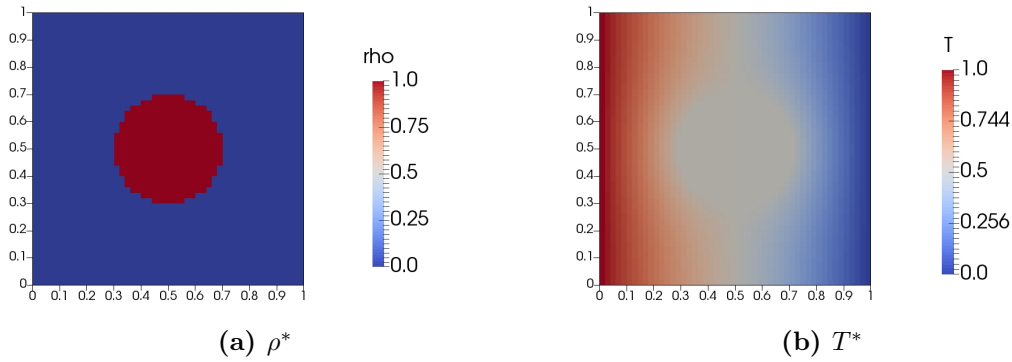


Figure 5.8: Reference control and associated temperature for 2D thermal problem

conditions read:

$$\begin{cases} \nabla \cdot (K(\rho)\nabla T_a) = T - T^* & \text{in } \Omega \\ T_a(0, y) = T_a(1, y) = 0 \\ \frac{\partial T_a}{\partial y}(x, 0) = \frac{\partial T_a}{\partial y}(x, 1) = 0 \end{cases} \quad (5.10)$$

Then the sensitivity can be deduced as,

$$J'(\rho)[\delta\rho] = \int_{\Omega} \nabla T_a \cdot \nabla T H(\rho)\delta\rho \quad . \quad (5.11)$$

where $H(\rho)$ is the derivative of $K(\rho)$, i.e. $K'(\rho) = H(\rho)\delta\rho$.

Unconstrained optimization

An unconstrained optimization has been run at first, using a uniform Cartesian mesh 50×50 : as we expected the convergence rate revealed to be very slow and the optimization process ended after the maximum number of iterations has been reached. Similarly to the 1D case, we can see from table 5.8 the objective function has decreased of six order of magnitude, that means the final temperature distribution is very close to the reference one, but the final control variable does not

match very well to ρ^* , as depicted in figure 5.9b. In figures (5.9c) and (5.9d) the line plots of the sensitivity help to understand the reason of the low performance of the solver. Compared to the initial value, the sensitivity at the 100-th iteration not only loses about two orders of magnitude but also becomes almost constant, despite of the control being still rather far from the reference one. The problem of low sensitivity (as already discussed in the 1D analogous problem) can certainly affect the rate of convergence of the solver.

Tol Ta	Tol T	q	c	$K_f [\frac{W}{mK}]$	$K_s [\frac{W}{mK}]$
1e-6	1e-6	0.04	1e-8	0.01	10

Table 5.7: Settings of the parameters for 2D thermal *Control Problem 2* unconstrained optimization

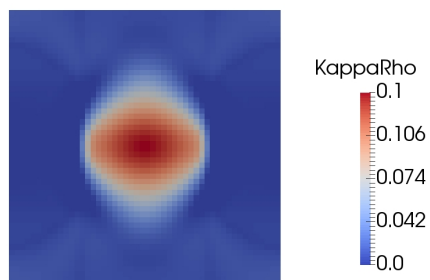
J_0	J_{opt}	iterations	Exec.Time
2.38e-4	1.20e-10	100024	10820.5s

Table 5.8: Initial and final values of cost function (J_0 and J_{opt}), number of optimization iterations, execution time (unconstrained 2D thermal optimization, *Control Problem 2*)

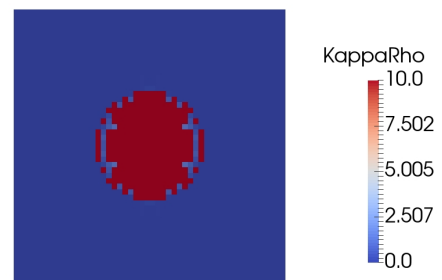
Constrained optimization

The first attempt to improve the solver performances consists of introducing an intermediate control value penalization, as described in section 4.3.2. The relative weight coefficients chosen for this case are $\epsilon_1 = 0.9$ (for the objective function) and $\epsilon_2 = 0.1$ (for the intermediate control value constraint). All the other parameters are the same as the unconstrained case, see table 5.7.

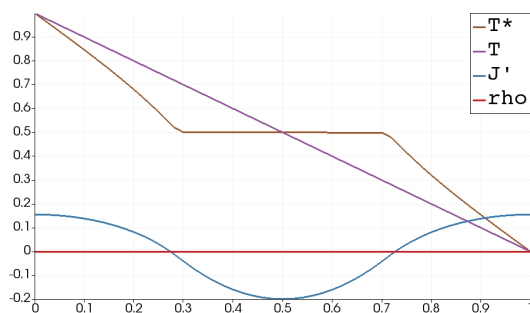
The solution after 37 iterations is showed in figure 5.10. Clearly it is not a good result, since the solution is far from the reference one (the cost function just halved, see figure 5.10a) and the control is not a discontinuous [0-1] function. The reason of this behavior is explained in figure 5.10a: in the first iterations the penalization function $J_p = \int_{\Omega} \rho(1 - \rho)$ acts in opposition to the objective function $J_{obj} = \frac{1}{2} \int_{\Omega} (T - T^*)^2$, tending to reduce the amount of used control as much as possible. As a result J_p increases whereas J_{obj} decreases, making however the total cost function J decrease as well. This behaviour is quite reasonable if we consider the penalization function argument $g(\rho) = \rho(1 - \rho)$ (section 4.3.2): starting from



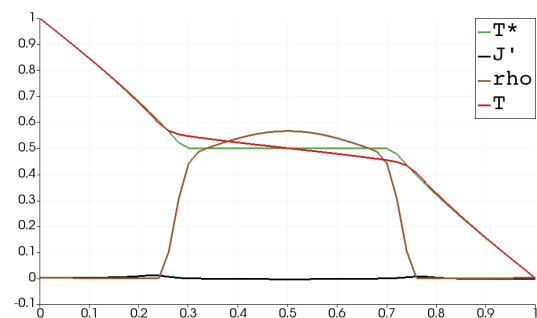
(a) $K(\rho)$ field after 100 iterations



(b) Final $K(\rho)$ field, stopped at the maximum number of iterations allowed, almost equal to 100000



(c) Line plot over the horizontal centerline at the beginning of the optimization process: $\rho_0 = 0$, $T(\rho_0)$, T^* and the sensitivity $J'(\rho_0)$

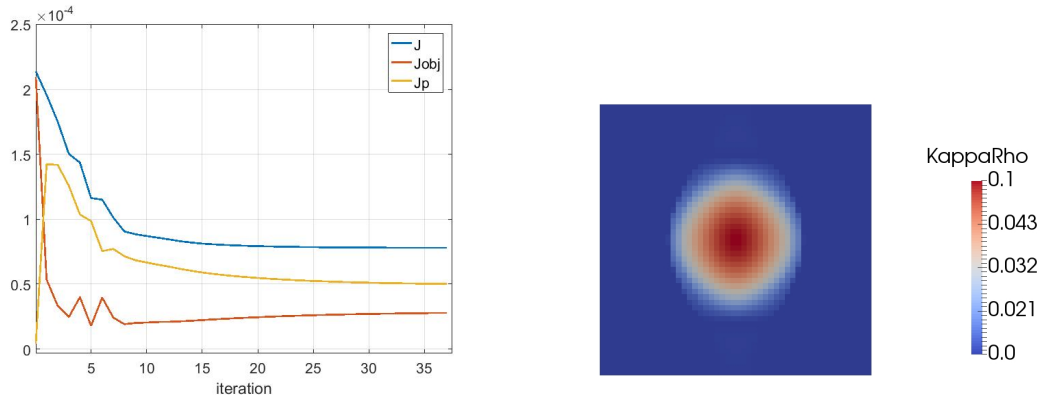


(d) Line plot over the horizontal centerline of fig. (5.9a): $T(\rho_{100})$, T^* and the sensitivity $J'(\rho_{100})$

Figure 5.9: Unconstrained optimization results for the 2D thermal problem

a null control, the slope of $g(\rho)$ is positive and this makes J_p increase in the first iterations. Theoretically, as soon as ρ tends to the threshold value $\rho = \frac{1}{2}$, the penalization should help the objective function to find an optimum [0-1] discontinuous control field. However in the current case the threshold value $\rho = \frac{1}{2}$ is never reached, because the sensitivity of the objective function decreases very rapidly as the control increases (as we have seen in the unconstrained case), leaving the penalization to lead the optimization process after few iterations. This is clearly visible from figure 5.10a, where J_{obj} keeps almost constant when J_p starts decreasing.

Different values on a wide range of weights coefficients ϵ_1 and ϵ_2 have been tried, but the final results always ended in a stalemate, where the opposite effects of J_{obj} and J_p balance each other, leading to no noteworthy solution.



(a) trend of the total cost, objective and penalization functions, J (blue), J_{obj} (red) and J_p (yellow), w.r.t. optimization iterations

(b) final $K(\rho)$ field after 37 iterations

Figure 5.10: Constrained optimization results for 2D thermal problem

The main issue affecting these 1D and 2D tests (concerning *Control Problem 2*) seems to be the low controllability for high ratios $\frac{K_s}{K_f}$, which causes poor gradient information. A simple but effective solution is to fictitiously reduce this ratio, as explained in the following lines. We rewrite the equation for the controlled conductivity coefficient (4.20) using K_l instead of K_s as maximum value:

$$\tilde{K}(\rho) = K_l - (K_l - K_f)(1 - \rho) \frac{1 + q}{1 - \rho + q} . \quad (5.12)$$

The value $K_f < K_l < K_s$ can be arbitrarily chosen, but according to figure 5.7 it seems a good choice to fix it to 1. By doing so, we enforce $\tilde{K}(\rho)$ to vary in the interval $[0.01, 1]$, where the derivative of temperature is very sensible to the control variations. The sensitivity of the cost function (5.11) is thus computed using the

derivative $\tilde{K}'(\rho)$. Then, after control update, we derive a modified form of equation (4.20) for the controlled conductivity coefficient, to be used in primal and adjoint equations:

$$K(\rho) = \begin{cases} \tilde{K}(\rho) & \text{for } 0 \leq \rho < 1 \\ K_s & \text{for } \rho = 1 \end{cases} \quad (5.13)$$

where K_s is the solid conductivity coefficient. In the remainder of this chapter, we will refer to this procedure as *K-limit*. Figure 5.11 and table 5.10 show the results for the constraint optimization (intermediate control value penalization), obtained with the *K-limit* procedure.

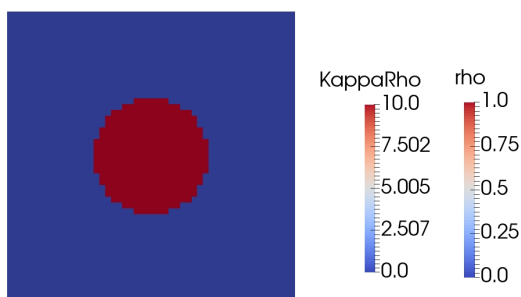
Tol Ta	Tol T	q	c	$K_f [\frac{W}{mK}]$	$K_s [\frac{W}{mK}]$	$K_l [\frac{W}{mK}]$	ϵ_1	ϵ_2
1e-6	1e-6	0.04	1e-8	0.01	10	1	0.999	0.001

Table 5.9: Settings of the parameters for 2D thermal *Control Problem2 K-limit* constrained optimization

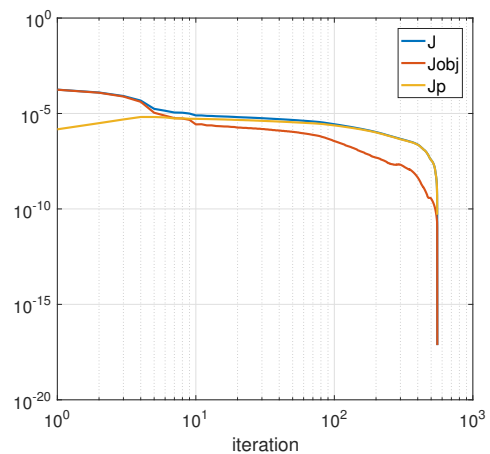
	J	J_{obj}	J_p	iterations	Exec.Time
Initial	2.38e-3	2.38e-3	0	554	63.48s
Final	7.34e-18	7.34e-18	0		

Table 5.10: Initial and final values of cost function $J = J_{obj} + J_p$, number of optimization iterations, execution time (constrained 2D thermal optimization, *Control Problem2 K-limit*)

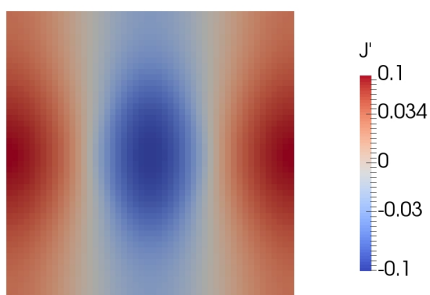
Comparing the obtained results with those of the unconstrained case, reported in table 5.8, we can appreciate the relevant differences in the number of iterations and execution time. Moreover the final value of the cost function is practically zero in the current case, and the penalization function is null at the end of the optimization process since the final control is a discontinuous [0-1] function. The great improvement of the optimization results is due to the *K-limit* method employed, together with intermediate control value penalization, the other parameters being the same in the two cases (see tables 5.7 and 5.9)



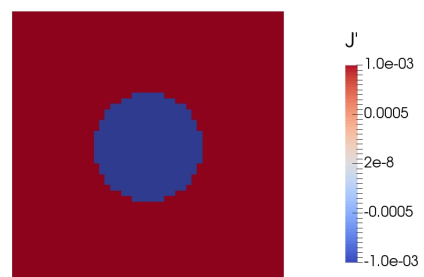
(a) Final $K(\rho)$ and ρ fields



(b) Trend of the total cost, objective and penalization functions, J (blue), J_{obj} (red) and J_p (yellow), w.r.t optimization iterations (in a log-log scale)



(c) Initial sensitivity



(d) Final sensitivity

Figure 5.11: Constrained optimization results for 2D thermal problem (*Control Problem2 K-limit*)

5.2 Natural convection in a cavity

The 1D and 2D thermal cases have been of great importance to understand a lot of aspects concerning the optimization case setup and to solve some crucial aspects that affected the solvers performances. Now we consider the full thermo-fluid dynamic problem introduced in the previous chapters. We begin specifying the fluid properties used in these tests.

The non-dimensional form of primal and adjoint equations suggests that similar solutions to the cavity problem can be found as long as the same Ra and Pr number is achieved. With this idea in mind we list below the parameters chosen, corresponding to $Ra = 1000$ and $Pr = 0.71$:

- side of the cavity [m]: $L = 1$;
- hot side temperature [°C]: $T_h = 1$;
- cold side temperature [°C]: $T_c = 0$;
- thermal expansion coefficient [1/K]: $\beta = 0.071$;
- cinematic viscosity [m^2/s]: $\nu = 0.0071$;
- gravitational acceleration [m/s^2]: $g = -1$;

It follows that the fluid diffusivity coefficient is $K_f = \frac{\nu}{Pr} = 0.01 \left[\frac{m^2}{s}\right]$. For natural convection problems, the critical Ra number is about $10^7 - 10^8$, causing transition from laminar to turbulent regime, [19]. Thus, for $Ra = 1000$ a steady laminar solution is expected.

The section is structured in this way: in the first paragraph a first test case is solved with both *Control Problem 1* and *Control Problem 2*, using the *Solver Algorithm 1*. Later, a second test is worked out with still both control problems, but using the *Solver Algorithm 2*. Finally, a third test case is solved with *Control Problem 2* using the *Solver Algorithm 2*.

5.2.1 *Solver Algorithm 1*: a first natural convection study

The optimization problem consists in finding the optimal control function ρ_{opt} that makes the temperature inside the cavity as close as possible to a desired reference temperature, starting from an assigned initial ρ_0 . Here the reference temperature T^* is constant and equal to the cold temperature at the wall T_c , while ρ_0 is showed in figure 5.12a. The control filtering function (*filt*), defined in (5.6), allows us to limit the design space to a non-connected subset $\Omega_\rho \subset \Omega$ where $filt = 1$, as figure

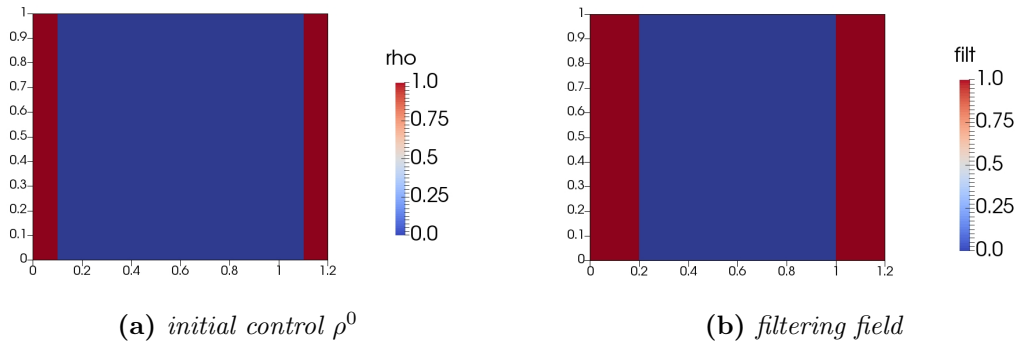


Figure 5.12: Initial control and *filt* field. The red regions in (b) form the admissible control domain Ω_ρ : that one the right is the *cold* one, the other is the *hot* one

5.12b shows. The reason of this choice is mainly because we want to keep the test case as simple as possible.

According to the problem set up, we expect the optimization process to remove ρ from the *hot* region of Ω_ρ and to put it on the *cold* one, keeping unaltered its volume. In order to keep the characteristic dimension of the convective cell equal to $L=1$, the effective x-dimension of the domain as been adapted to the initial control volume.

Control Problem 1

The *Control Problem 1* is here used to perform the optimization. The definition of the control problem requires the specification of the function T_D :

$$T_D = \begin{cases} T_h & \text{per } x \leq \frac{L}{2} \\ T_c & \text{per } x > \frac{L}{2} \end{cases} \quad (5.14)$$

The *filt* field prevent the control to act on the discontinuity in $\frac{L}{2}$. The solution of the optimization process is showed in figure 5.13. As we expected, the control fills the “cold” region on the right of the *admissible* domain Ω_ρ , while the “hot” one on the left is gradually reduced until it completely disappears.

Control Problem 2

The *Control Problem 2* is used to perform the optimization. Here the two values K_f and K_s need to be defined. Recalling the non-dimensional form of the *Control Problem 2*, it is their ratio that affects the solution. We choose a ratio $\frac{K_s}{K_f} = 10$, then considering that $K_f = 0.01 [\frac{m^2}{s}]$, it follows that $K_s = 0.1 [\frac{m^2}{s}]$. We have

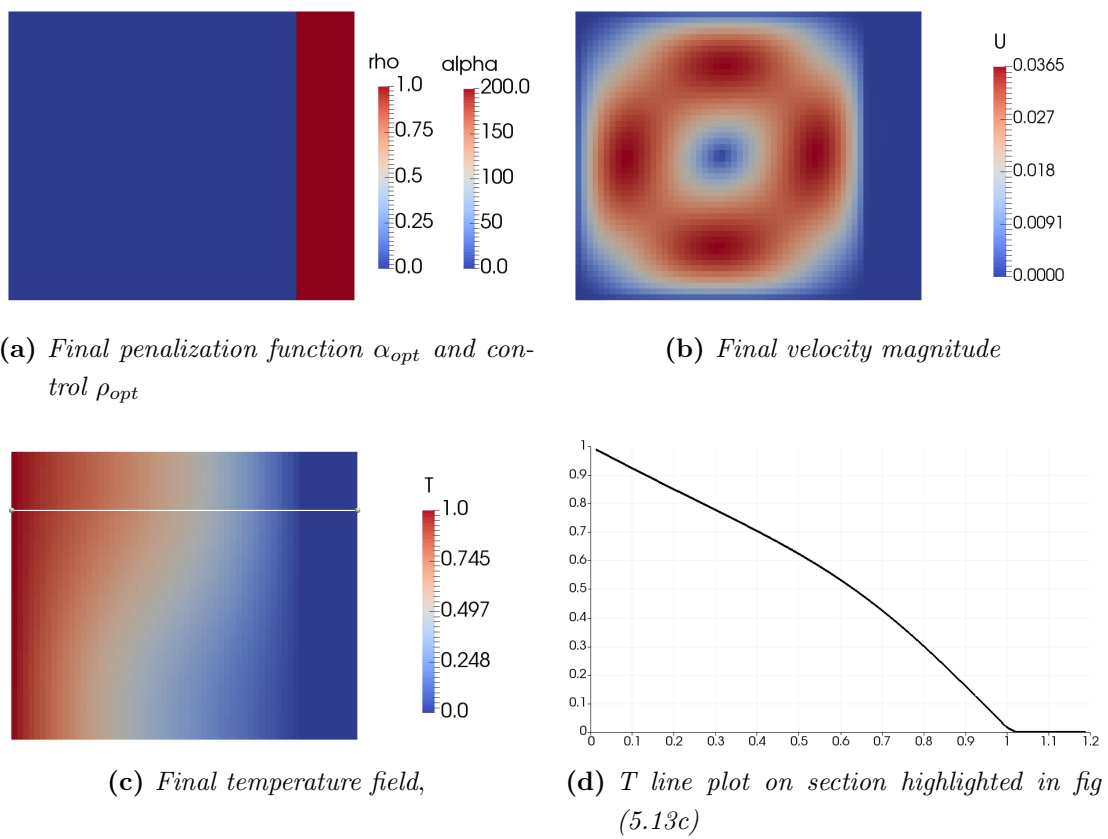


Figure 5.13: Optimization results for the *first natural convection study (Control Problem 1)*

chosen a low ratio so as to not have the same controllability issues faced in the thermal cases. The solution of the optimization process is showed in figure 5.14. The optimal solution is as expected. The difference with the previous case is only

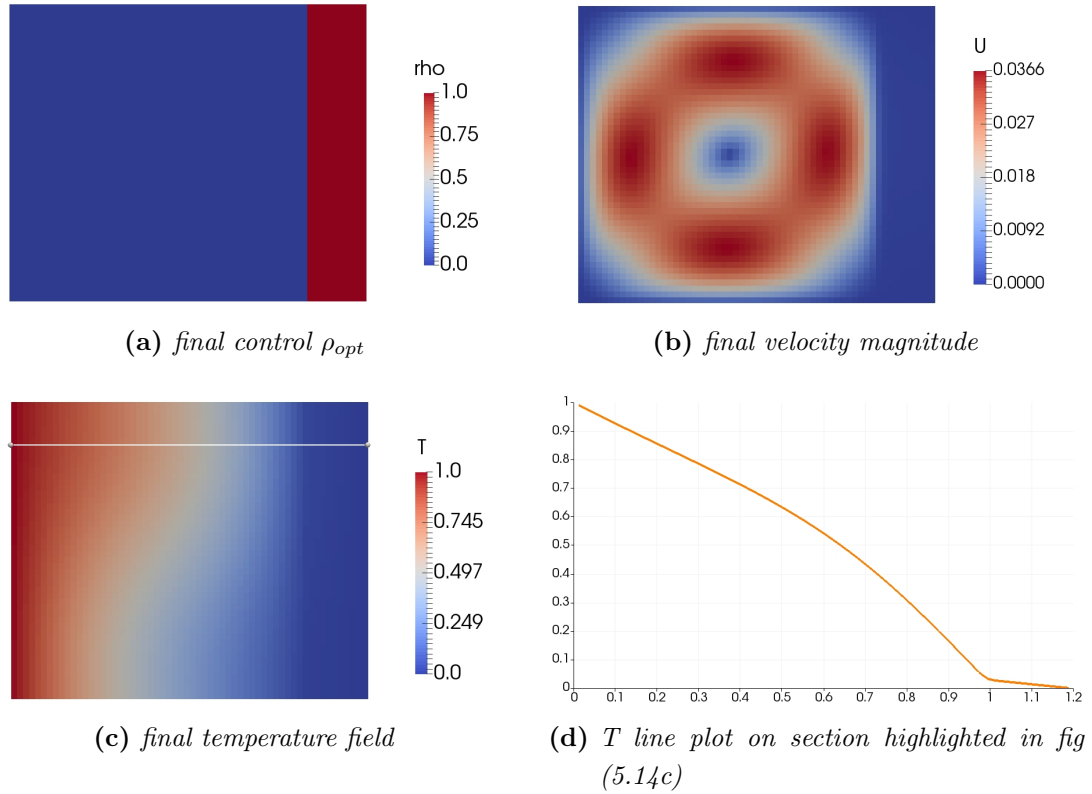


Figure 5.14: Optimization results for the *first natural convection study (Control Problem 2)*

the temperature profile in the solid region, which in this case is linear and not constant, as expected.

5.2.2 Solver Algorithm 2: a second natural convection study

In these study cases the reference temperature distribution T^* is computed starting from a reference control variable ρ^* . We expect the optimization process to find the optimal control $\rho_{opt} = \rho^*$ starting from a null initial control ρ^0 far from the reference one.

$$\rho^*(x, y) = \begin{cases} 1 & \text{for } x \leq A \sin\left(\frac{\pi y}{L}\right) \vee x \geq L - A \sin\left(\frac{\pi y}{L}\right) \\ 0 & \text{elsewhere} \end{cases} \quad (5.15)$$

where $A=0.2$ [m] and $L=1$ [m].

Control Problem 1

Figure 5.15 shows the reference conditions. The definition of the control problem requires the specification of the function T_D , defined as in (5.14). A *filt* field, allowed to filter the control variable, prevents this latter to act on the discontinuity in $\frac{L}{2}$ due to the definition of T_D .

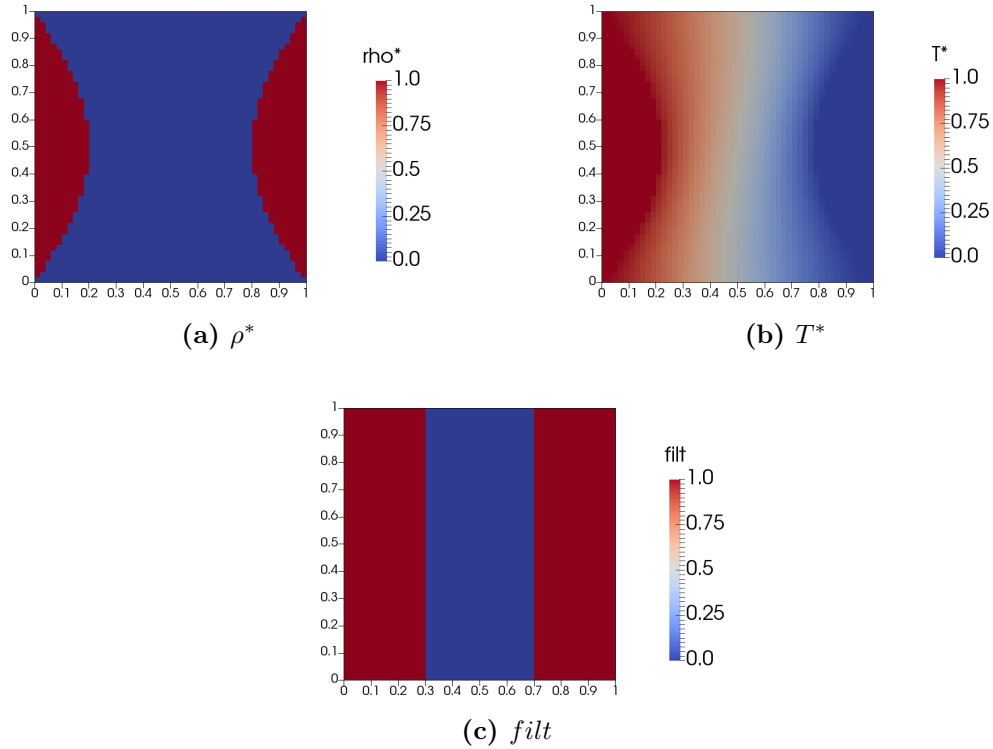


Figure 5.15: Reference control and relative temperature, filtering field: the red regions in (c) form the admissible control domain Ω_ρ

The tolerances used on the primal and adjoint equations are reported in table 5.11. It is well known that the convergence of the adjoint momentum and pressure correction equations is a rather delicate matter and in spite of the regularity of the Cartesian grid used to discretize the domain, this study is not free from convergence troubles: the tolerances of adjoint velocity and pressure have been chosen to be lower than their primal counterparts because of the slower rate of convergence. We decided to use a coarse uniform Cartesian mesh of 50×50 cells in order to keep the problem computationally cheap. This choice is reasonable considering the low Ra number used in this test ($Ra = 1000$). On the other hand the adjoint temperature equation seems not to suffer from any kind of convergence issue, at least for this study.

The solver parameters are summarized in table 5.12. Here we can note that three weight coefficients have been used: ϵ_1 refers to the objective function while

Tol U	Tol T	Tol P	Tol Ua	Tol Ta	Tol Pa
1e-5	1e-5	1e-5	1e-3	1e-5	1e-4

Table 5.11: Settings of the tolerances of primal and adjoint equations (*second natural convection study, Control Problem 1*)

q	c	$K_f [\frac{m^2}{s}]$	α_{max}	ϵ_1	ϵ_2	ϵ_3
0.04	1e-8	0.01	200	0.799	0.2	0.001

Table 5.12: Settings of the solver parameters for the *second natural convection study* (constrained optimization, *Control Problem 1*)

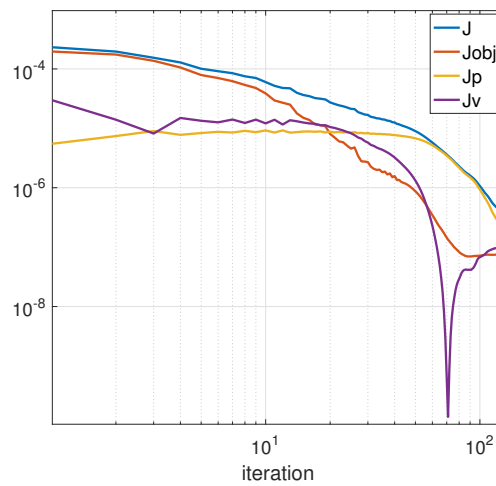
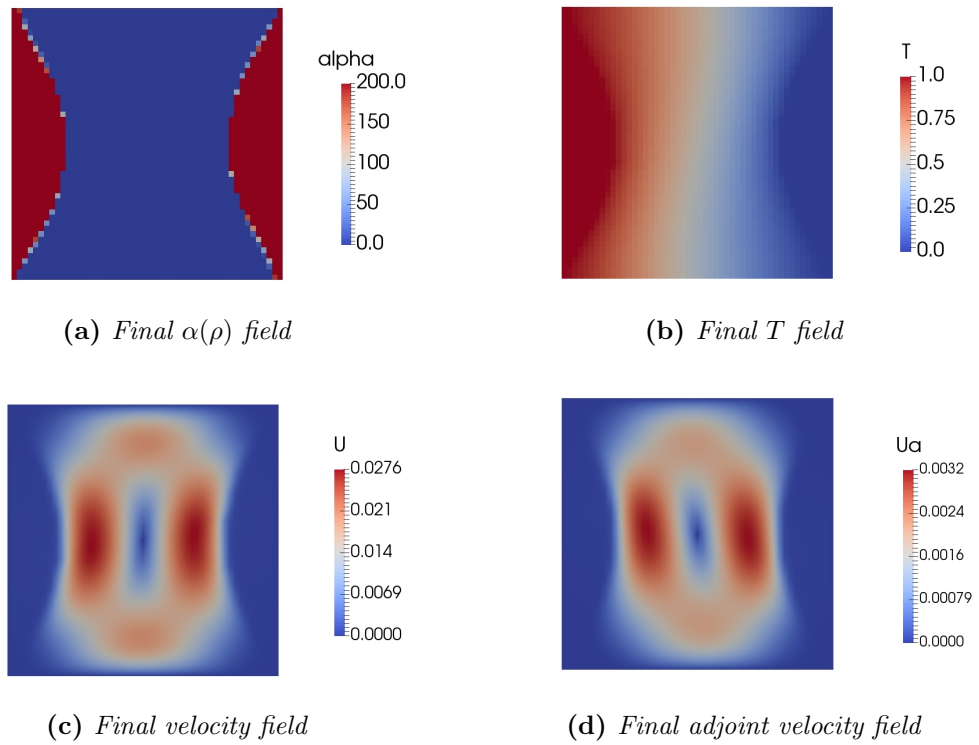
ϵ_2 and ϵ_3 to the volume and penalization constraints respectively. Having three contributes to the augmented cost function to be minimized, makes it quite hard to find the optimal solution. However, looking at table 5.13, we can appreciate the noteworthy reduction of the total cost, objective and volume constraint functionals. The penalization functional keeps very low, since the final control is close to a discontinuous [0-1] function, as figure 5.16a shows. In figure 5.16 we report the results of the optimization problem. The final temperature distribution in the cavity is very similar to the reference one, as suggested by the final value of the objective function, which decreases of almost 4 order of magnitude.

	J	J_{obj}	J_v	J_p	iterations	Exec.Time
Initial	4.64e-4	3.98e-4	6.63e-5	0	122	1310.64 s
Final	4.44e-7	7.54e-8	9.66e-8	2.72e-7		

Table 5.13: Initial and final values of cost function $J = J_{obj} + J_v + J_p$, number of optimization iterations, execution time (*second natural convection study* constrained optimization, *Control Problem 1*)

Control Problem 2

For this test the two values K_f and K_s need to be defined. Recalling the non-dimensional form of the *Control Problem 2*, it is their ratio that affects the solution. We choose a ratio $\frac{K_s}{K_f} = 1000$, that is the one between thermal conductivity of still air and metal (steel). Then, considering that $K_f = 0.01 [\frac{m^2}{s}]$, we obtain



(e) Trend of the total cost, objective and penalization functions, J (blue), J_{obj} (red) and J_p (yellow) and J_v (violet) w.r.t optimization iterations (in a log-log scale)

Figure 5.16: Optimization results for the *second natural convection study (Control Problem 1)*

$K_s = 10 [\frac{m^2}{s}]$. Given the high ratio $\frac{K_s}{K_f}$, the reference temperature given by the reference control (5.3) is practically identical to the one showed in figure 5.15b. In this case no filtering field needs to be defined, so no restrictions to the control domain are imposed.

The experience of the only thermal cases suggests the better way to achieve a good result with the *Control Problem 2* is to enable the *K-limit* function and the intermediate control value penalization constraint. The parameters setting for this case are reported in table 5.14, the tolerances are the same as the previous case (see table 5.11), the computational mesh is 50×50 cells. The results are showed in figure 5.17 and summarized in table 5.15. Similarly to the previous case for *Control Problem 1*, we can appreciate a consistent reduction of total cost and objective functionals. The final controlled functions ($K(\rho)$ and $\alpha(\rho)$) are very close to a discontinuous [0-1] function, as appreciable from the low final value of the the penalization functional. The final temperature distribution is also showed in figure 5.17c, being however very similar to the one obtained in *Control Problem 1*, given the high ratio $\frac{K_s}{K_f}$ employed.

q	c	$K_f [\frac{m^2}{s}]$	$K_l [\frac{m^2}{s}]$	$K_s [\frac{m^2}{s}]$	ϵ_1	ϵ_2
0.04	1e-8	0.01	1	10	0.999	0.001

Table 5.14: Settings of the parameters for the *second natural convection study* (constrained optimization, *Control Problem 2 K-limit*)

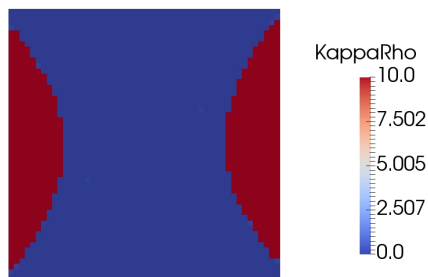
	J	J_{obj}	J_p	iterations	Exec.Time
Initial	6.45e-4	6.45e-4	0		
Final	6.65e-7	5.27e-7	1.38e-7	66	1032.78 s

Table 5.15: Initial and final values of cost function $J = J_{obj} + J_p$, number of optimization iterations, execution time (*second natural convection study* constrained optimization, *Control problem 2*)

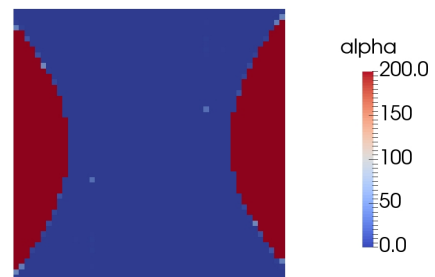
Figures (5.17e) and (5.17f) shows the primal and adjoint velocity fields. The arrows underline the expected opposite directions of the two velocity fields.

5.2.3 A third natural convection study

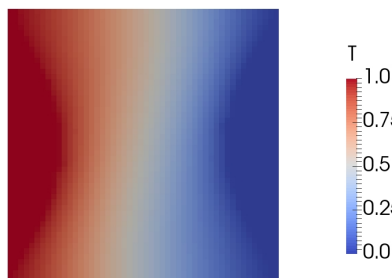
Finally we consider a third natural convection study. The problem still deals with natural convection in a cavity, but the definition of the cost functional and



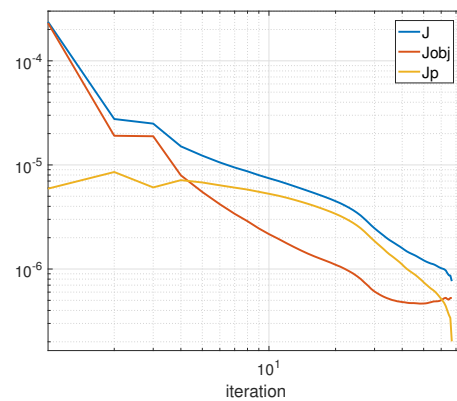
(a) Final $K(\rho)$ field



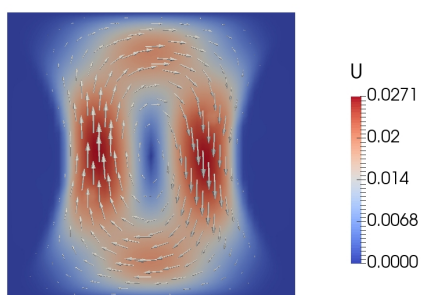
(b) Final $\alpha(\rho)$



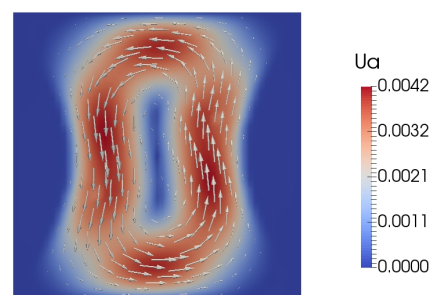
(c) Final T field



(d) Trend of the total cost, objective and penalization functions, J (blue), J_{obj} (red) and J_p (yellow) and J_v (violet) w.r.t optimization iterations (in a log-log scale)



(e) Final velocity field



(f) Final adjoint velocity field

Figure 5.17: Optimization results for the *second natural convection study (Control Problem 2)*

boundary conditions is different from the previous cases. The problem layout is sketched in figure 5.18.

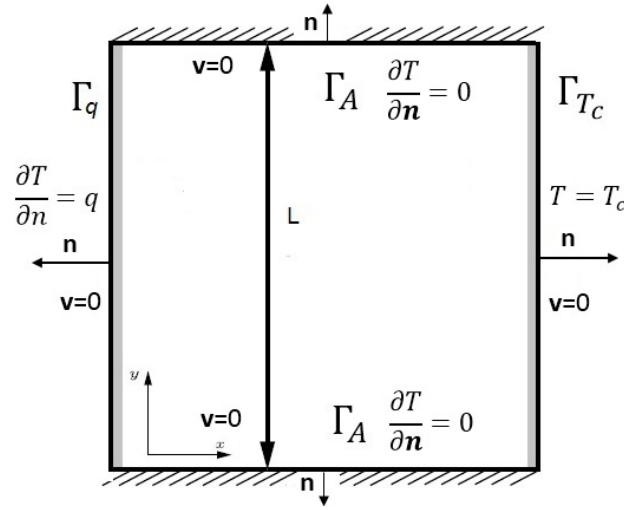


Figure 5.18: Cavity layout

The top and bottom sides are adiabatic, while the vertical side on the right is at fixed temperature and the opposite side on the left has a fixed temperature gradient. The two grey regions represent a fixed solid thickness, where heat conduction is considered. The boundary conditions for velocity and temperature are summarized as follows:

$$\mathbf{v} = 0 \quad \text{on } \partial\Omega \quad (5.16a)$$

$$\frac{\partial T}{\partial \mathbf{n}} = 0.01 \quad \text{on } \Gamma_q \quad (5.16b)$$

$$T = 0 \quad \text{on } \Gamma_{T_c} \quad (5.16c)$$

$$\frac{\partial T}{\partial \mathbf{n}} = 0 \quad \text{on } \Gamma_A \quad (5.16d)$$

Since fully Dirichlet boundary conditions on velocity are considered, the pressure will be defined up to a constant. The steady solution for the described natural convection problem is showed in figure 5.19. The governing equations are numerically solved with a uniform Cartesian mesh of 100×100 cells. Residuals are reduced below $4e-6$ for all variables.

The solution has been obtained using the following parameters:

- side of the cavity [m]: $L = 1$;
- temperature gradient on Γ_q [$^{\circ}\text{C}/\text{m}$]: $\frac{\partial T}{\partial x} = 0.01$;
- cold side temperature [$^{\circ}\text{C}$]: $T_c = 0$;

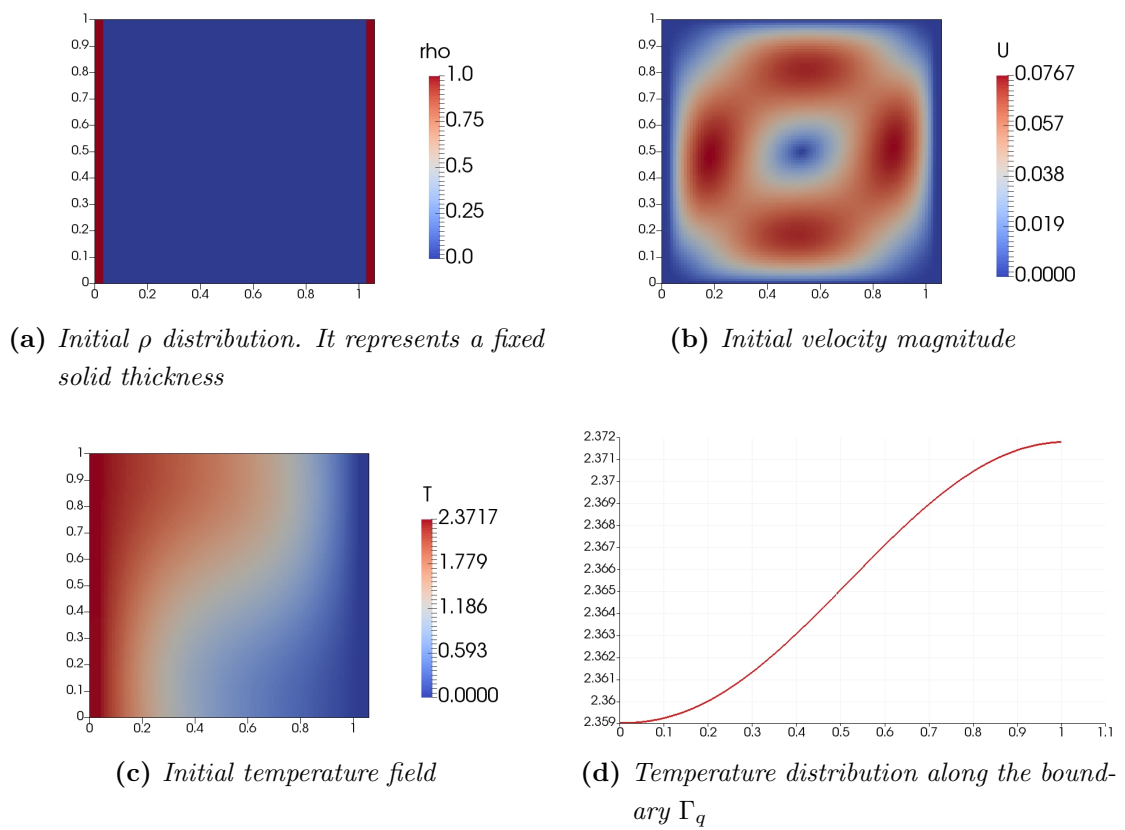


Figure 5.19: Initial conditions in the cavity

- thermal expansion coefficient [1/K]: $\beta = 0.071$;
- cinematic viscosity [m^2/s]: $\nu = 0.0071$;
- gravitational acceleration [m/s^2]: $g = -1$;
- Prandtl number: $Pr = 0.71$;

The Ra number is about 2000, since the temperature at the heated wall is a bit higher than 2 [°C].

The temperature boundary condition on Γ_q represents an imposed uniform heat flux entering the cavity, which causes the temperature on the heated wall to be higher than T_c . We also note that the temperature profile on the boundary is not constant, as expected (see figure 5.19c). The goal of the optimization problem is to find a solid distribution inside the cavity that makes the temperature on Γ_q as close as possible to the objective constant temperature T^* , according to the following definition of the cost functional defined over the boundary Γ_q :

$$J = \frac{1}{2} \int_{\Gamma_q} (T - T^*)^2 \quad . \quad (5.17)$$

We choose a value of T^* smaller than the value obtained in the uncontrolled case. In other words we want to better dissipate the imposed heat flux reducing the temperature on the heated surface to a desired value. The *Control Problem 2* is the best choice to solve the optimization problem, since it is more suitable for this kind of application. Moreover, the *Solver Algorithm 2* is employed. The previously obtained adjoint formulation of the control problem (see section 3.1) needs to be modified since a different objective function has been defined. The resulting adjoint equations are:

$$-(\nabla \mathbf{u}) \mathbf{v} - (\mathbf{v} \cdot \nabla) \mathbf{u} - \nabla \cdot (2\nu D(\mathbf{u})) + \alpha(\rho) \mathbf{u} + \nabla q + T_a \nabla T = 0 \quad (5.18a)$$

$$\nabla \cdot \mathbf{u} = 0 \quad (5.18b)$$

$$\beta \mathbf{u} \cdot \mathbf{g} - \mathbf{v} \cdot \nabla T_a - \nabla \cdot (K(\rho) \nabla T_a) = 0 \quad . \quad (5.18c)$$

and the adjoint boundary conditions read:

$$\mathbf{u} = 0 \quad \text{on } \Gamma \quad (5.19a)$$

$$T_a = 0 \quad \text{on } \Gamma_{T_c} \quad (5.19b)$$

$$\frac{\partial T_a}{\partial \mathbf{n}} = 0 \quad \text{on } \Gamma_A \quad (5.19c)$$

$$\frac{\partial T_a}{\partial \mathbf{n}} = -\frac{T - T^*}{K(\rho)} \quad \text{on } \Gamma_q \quad (5.19d)$$

The sensitivity is defined in section 3.2.3 for the control problem of interest. Some hints about the derivation of the adjoint equations and boundary conditions can be found in appendix A.1, where the complete weak form of the adjoint equations is showed for generic cost functionals.

In this study we have chosen three values of the reference temperature $T^* = 2.1, 2.05$ and 2 [°C]. The parameters used in the simulations are reported in tables 5.16 and 5.17.

q	c	$K_f [\frac{m^2}{s}]$	$K_l [\frac{m^2}{s}]$	$K_s [\frac{m^2}{s}]$	ϵ_1	ϵ_2
0.1	1e-8	0.01	1	10	0.97	0.03

Table 5.16: Settings of the parameters for the *third natural convection study*

Tol U	Tol T	Tol P	Tol Ua	Tol Ta	Tol Pa
4e-6	4e-6	4e-6	1e-4	1e-4	1e-4

Table 5.17: Settings of the tolerances of primal and adjoint equations

Figures (5.20), (5.21) and (5.22), show the final solutions of the optimization. Their results are also reported in tables (5.18), (5.19) and (5.20).

	J	J_{obj}	J_p	iterations	Exec.Time
Initial	3.14e-4	3.14e-4	0	63	6752.37 s
Final	2.88e-6	2.37e-8	2.86e-6		

Table 5.18: $T^* = 2.1$: initial and final values of cost function $J = J_{obj} + J_p$, number of optimization iterations, execution time

	J	J_{obj}	J_p	iterations	Exec.Time
Initial	4.54e-4	4.54e-4	0	78	16370.67 s
Final	2.78e-6	1.55e-8	2.76e-6		

Table 5.19: $T^* = 2.05$: initial and final values of cost function $J = J_{obj} + J_p$, number of optimization iterations, execution time

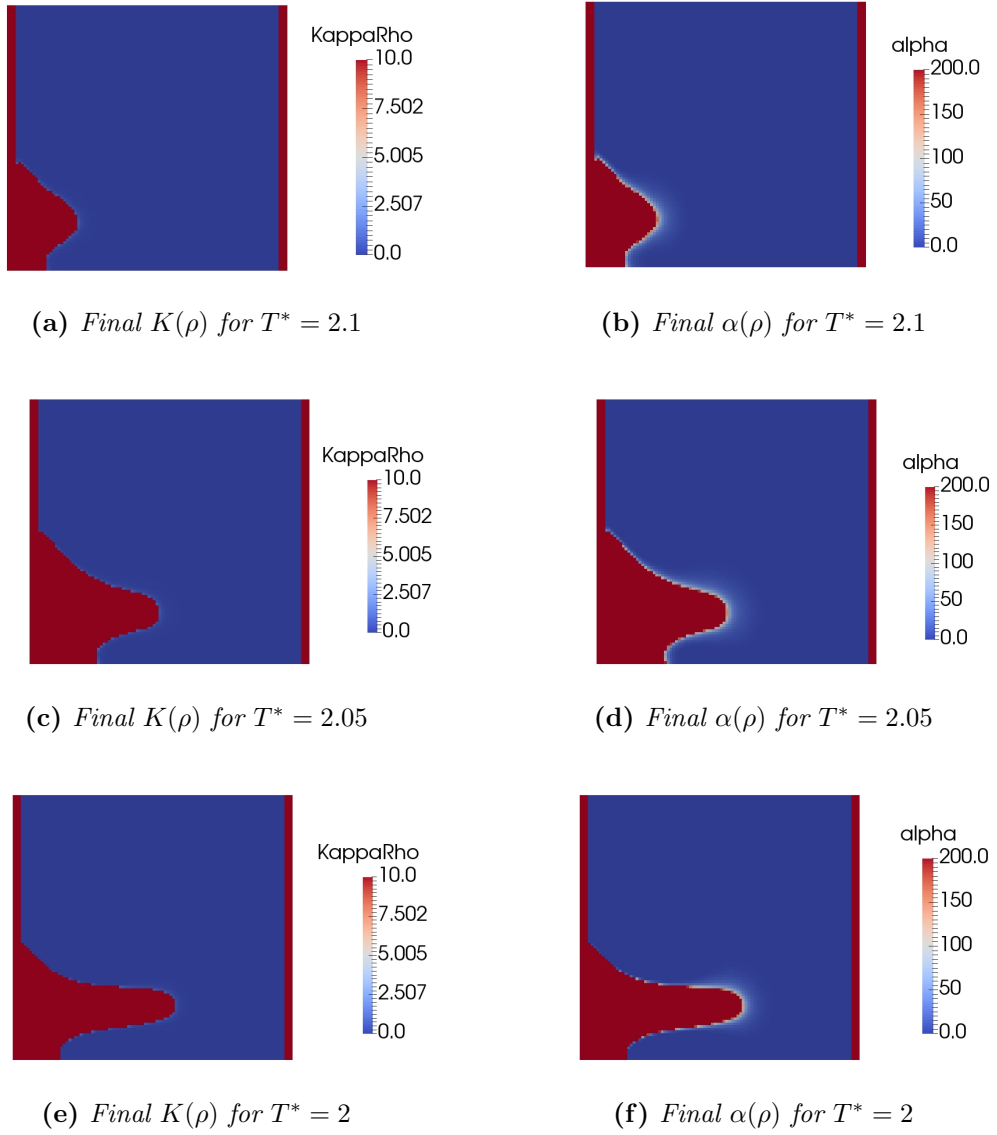


Figure 5.20: All optimal $K(\rho)$ and $\alpha(\rho)$ for different values of T^*

	J	J_{obj}	J_p	iterations	Exec.Time
Initial	6.09e-4	6.09e-4	0	111	14311.3 s
Final	2.93e-6	3.20e-8	2.90e-6		

Table 5.20: $T^* = 2$: initial and final values of cost function $J = J_{obj} + J_p$, number of optimization iterations, execution time

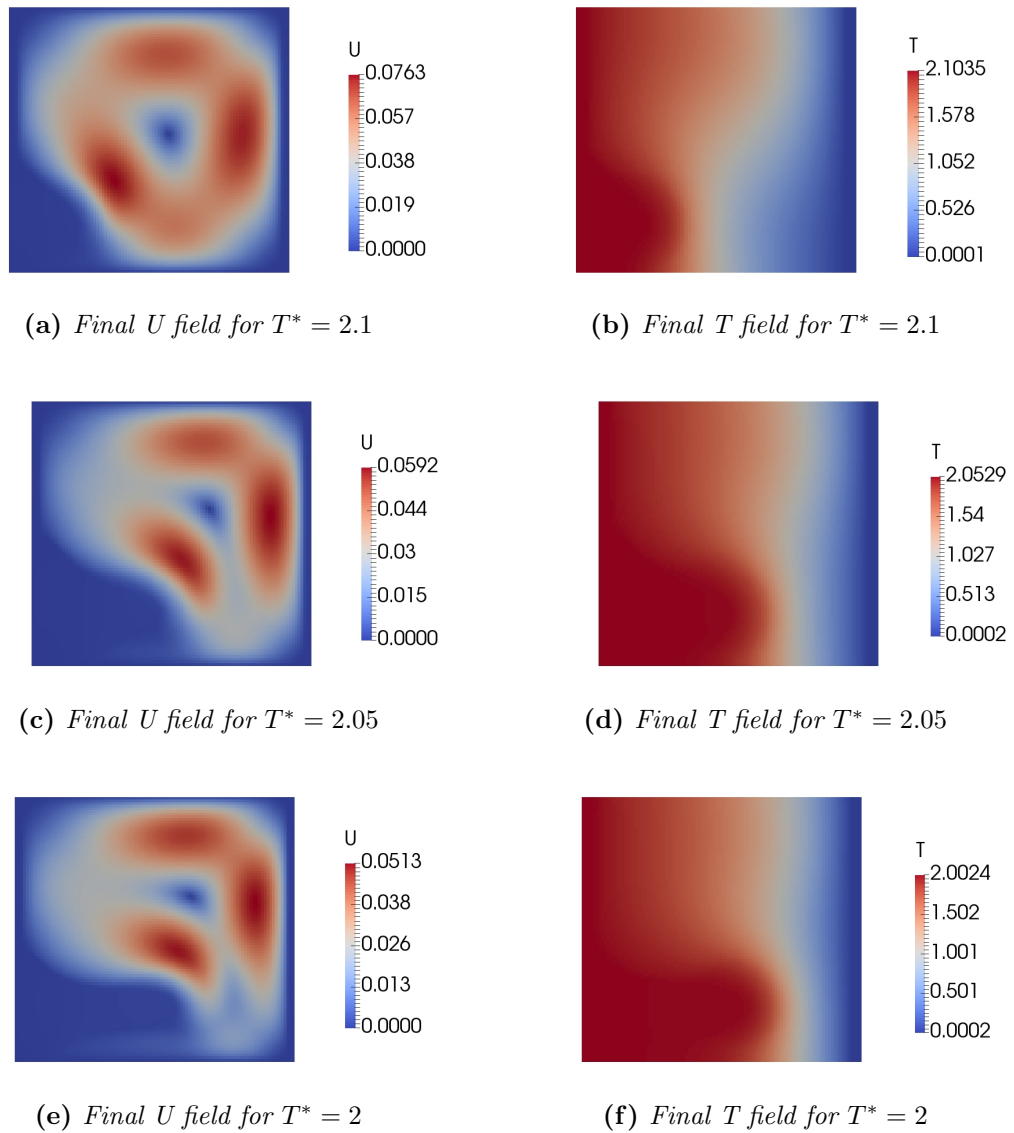


Figure 5.21: Final velocity and temperature field for different values of T^*

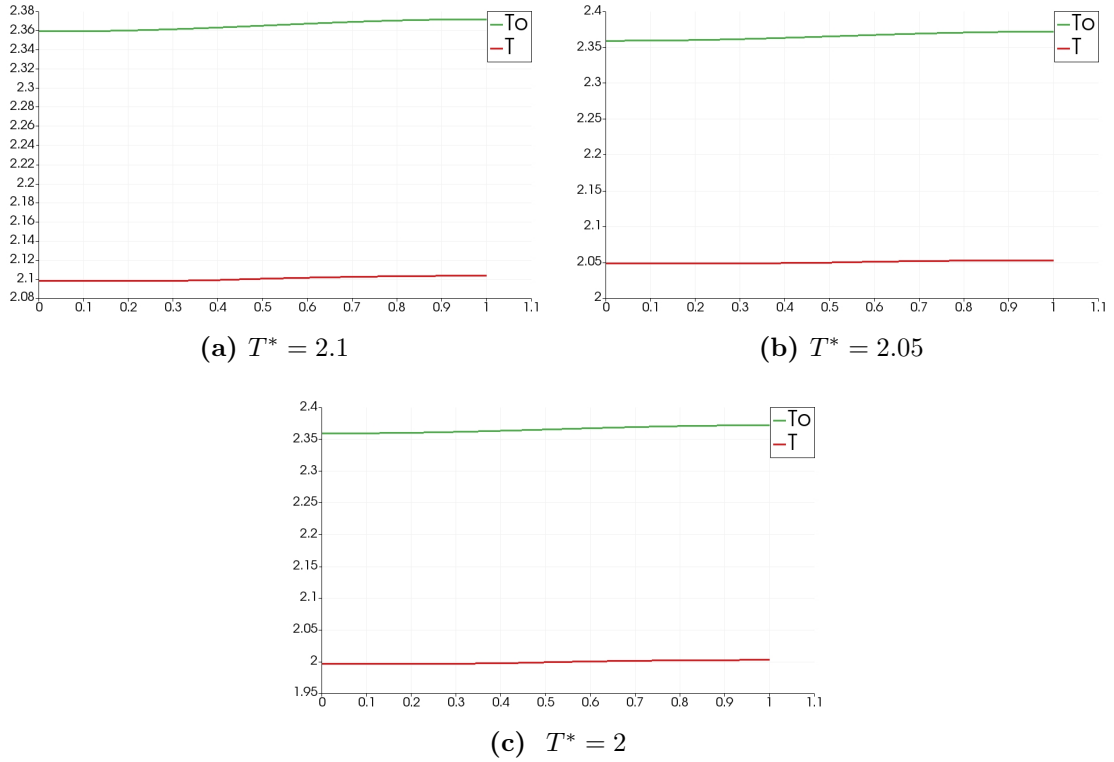
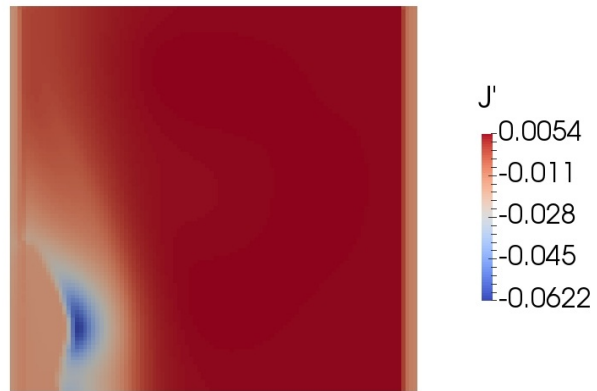


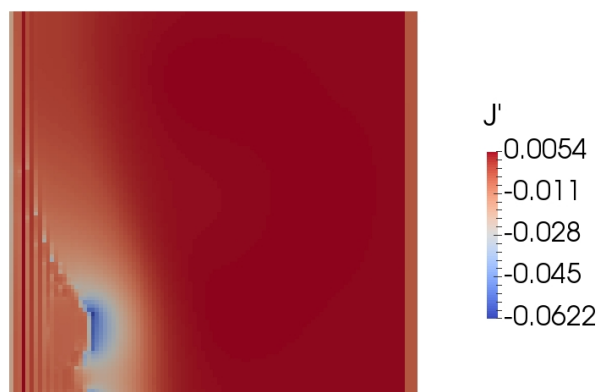
Figure 5.22: Comparison of initial temperature T_0 and final T on the heated wall Γ_q for different values of T^*

The reference temperature at the wall is matched in all three cases: the consistent reduction of the objective functional confirms what is clearly visible from picture 5.22. Moreover it can be noted that the temperature profile on the heated wall is more uniform than the initial one. The shape of the added solid material is quite reasonable: since the cold temperature is convected downward, adding solid medium (with high thermal conductivity) in that region allows a better cooling of the heated wall.

Finally we point out that these results have been obtained by averaging the sensitivity on each cell with its values on the neighbour cells. The reason of this filtering is due to some oscillations of the sensitivity close to the heated wall, as showed in figure 5.23, which can pollute the final control.



(a) *Filtered sensitivity*



(b) *Non filtered sensitivity*

Figure 5.23: Comparison of filtered and non filtered sensibilities in the same case setup ($T^* = 2$), at the 40th iteration

Chapter 6

Conclusions

The present work has introduced two different control problems, *Control Problem 1* and *Control Problem 2*, for topology optimization of steady incompressible Navier-Stokes equations including heat transfer. The control problems have been specialized to the study case of natural convection in a cavity. Moreover, two solver algorithms have been developed, namely *Solver Algorithm 1*, described in [15], and *Solver Algorithm 2*, which includes some optimization tools to enhance the solver performances.

First, the results of the two control problems have been compared on a series of numerical tests on 1D and 2D thermal problems. Only the *Solver Algorithm 2* has been employed for this preliminary studies. These tests gave us the opportunity to tune the solver algorithm on problems simpler than natural convection, obtaining at last noteworthy results. Then we moved to the more complex case of natural convection in a 2D cavity.

The *Solver Algorithm 1* has been tested on a *first test case*. The obtained results of *Control Problem 1* and *Control Problem 2* suggest a robust capability of the algorithm to manage the optimization process. Also *Solver Algorithm 2* has been tested on the same problem giving identical results, which therefore were not shown.

The *Solver Algorithm 2* has been employed to work out a *second test case*. Satisfactory results have been obtained with both *Control Problem 1* and *Control Problem 2*: volume and/or intermediate control values constraints have been used to enhance the optimization results. Also *Solver Algorithm 1* has been tested, but it showed some limitations in tackling this *second test case* and no result has converged to the optimal solution.

The *Solver Algorithm 2* therefore definitely establishes as the preferable algorithm implementation, proving the importance of the work done to enhance robustness and stability of the optimization process.

In light of the obtained results, we can summarize the main features of the two control problems developed in this work as follows.

The *Control Problem 1* formulation needs the definition of an admissible control domain Ω_ρ which limits the control action on a portion of the entire domain close to the boundaries. The a priori definition of Ω_ρ puts a constraint on the final solid (or fluid) topology; however many practical applications require modification of only some portions of the domain, whereby the definition of Ω_ρ can be included as part of the problem setup. A volume constraint is also necessary to achieve uniqueness of the optimal solution.

The *Control Problem 2* on the other hand does not impose any a priori limitation to the control action and no volume constraint is necessary. Moreover it allows heat equation to be solved either in the fluid and in the solid medium. Several applications could take advantage from the more accurate modeling of the heat transfer phenomena. Consequently *Control Problem 2* establishes as the best choice.

Finally, *Solver Algorithm 2* and *Control problem 2* are tested on a *third test case*. The results increase the confidence in the optimization process and confirm the potentiality of the implemented finite volume CFD solver.

The results obtained in these test cases are a good starting point to further investigate more intriguing problems, such as a 3D natural convection (possibly including a turbulence model), or the optimal design of ducted cooling systems such as heat exchangers.

Appendix A

Adjoint equations

A.1 Integration by parts

This section includes parts of the derivation of the adjoint equations omitted from chapter 3. Considering equation (3.7), we show integration by parts. We start from:

1st term

$$\int_{\Omega} \mathbf{u} \cdot (\delta \mathbf{v} \cdot \nabla) \mathbf{v} = \int_{\Omega} u_j \delta v_i v_{j,i} \quad .$$

Be

$$(u_j \delta v_i v_j)_{,i} = u_j \delta v_i v_{j,i} + \cancel{u_j \delta v_{i,i} v_j} + u_{j,i} v_j \delta v_i \implies u_j \delta v_i v_{j,i} = (u_j v_j \delta v_i)_{,i} - u_{j,i} v_j \delta v_i$$

where we have done the hypothesis of divergence free variations δv . Applying the divergence theorem, the *1st term* becomes:

$$\int_{\Omega} (u_j v_j \delta v_i)_{,i} - u_{j,i} v_j \delta v_i = \int_{\Gamma} (u_j v_j) n_i \delta v_i - \int_{\Omega} u_{j,i} v_j \delta v_i = \int_{\Gamma} (\mathbf{u} \cdot \mathbf{v}) \mathbf{n} \cdot \delta \mathbf{v} - \int_{\Omega} (\nabla \mathbf{u} \mathbf{v}) \cdot \delta \mathbf{v} \quad .$$

2nd term

$$\int_{\Omega} \mathbf{u} \cdot (\mathbf{v} \cdot \nabla) \delta \mathbf{v} = \int_{\Omega} u_i v_j \delta v_{i,j} \quad .$$

Be

$$(u_i v_j \delta v_i)_{,j} = u_{i,j} v_j \delta v_i + \cancel{u_i v_{j,j} \delta v_i} + u_i v_j \delta v_{i,j} \quad .$$

As for the previous term, one can obtain:

$$\int_{\Omega} (u_i v_j \delta v_i)_{,j} - u_{i,j} v_j \delta v_i = \int_{\Gamma} u_i \delta v_i v_j n_j - \int_{\Omega} u_{i,j} v_j \delta v_i = \int_{\Gamma} \mathbf{v} \cdot \mathbf{n} \mathbf{u} \cdot \delta \mathbf{v} - \int_{\Omega} (\mathbf{v} \cdot \nabla) \mathbf{u} \cdot \delta \mathbf{v} \quad .$$

3rd term

$$\int_{\Omega} -\mathbf{u} \cdot \nabla \cdot (2\nu D(\delta\mathbf{v})) = - \int_{\Omega} u_j \left(\nu(\delta v_{j,i} + \delta v_{i,j}) \right)_{,i} .$$

Considering the following relation,

$$\left(\nu u_j (\delta v_{j,i} + \delta v_{i,j}) \right)_{,i} = u_{j,i} \left(\nu(\delta v_{j,i} + \delta v_{i,j}) \right) + u_j \left(\nu(\delta v_{j,i} + \delta v_{i,j}) \right)_{,i}$$

the 3rd term becomes:

$$\begin{aligned} & \int_{\Omega} - \left(\nu u_j (\delta v_{j,i} + \delta v_{i,j}) \right)_{,i} + u_{j,i} \left(\nu(\delta v_{j,i} + \delta v_{i,j}) \right) = \\ & \int_{\Omega} \nu u_{j,i} (\delta v_{j,i} + \delta v_{i,j}) - \int_{\Gamma} \nu n_i (\delta v_{j,i} + \delta v_{i,j}) u_j . \end{aligned} \quad (\text{A.1})$$

We now focus on the volume integral on the right-and-side of equation (A.1). We write the following relations:

$$\begin{aligned} u_{j,i} \delta v_{j,i} &= (u_{j,i} \delta v_j)_{,i} - u_{j,ii} \delta v_j \\ u_{j,i} \delta v_{i,j} &= (u_{j,i} \delta v_i)_{,j} - u_{j,ij} \delta v_i \end{aligned}$$

so

$$\begin{aligned} & \int_{\Omega} \nu u_{j,i} (\delta v_{j,i} + \delta v_{i,j}) = \int_{\Omega} \nu \left((u_{j,i} \delta v_j)_{,i} - u_{j,ii} \delta v_j + \underbrace{(u_{j,i} \delta v_i)_{,j}}_{(u_{i,j} \delta v_j)_{,i}} - \underbrace{u_{j,ij} \delta v_i}_{u_{i,j,i} \delta v_j} \right) \\ & = \underbrace{\int_{\Omega} \nu (u_{j,i} + u_{i,j}) \delta v_j}_{\mathcal{T}_1} - \underbrace{\int_{\Omega} \nu (u_{j,i} + u_{i,j})_{,i} \delta v_j}_{\mathcal{T}_2} . \end{aligned} \quad (\text{A.2})$$

Now we integrate by parts the two terms \mathcal{T}_1 e \mathcal{T}_2 , starting from the first one:

$$\begin{aligned} \mathcal{T}_1 : & \int_{\Omega} \nu (u_{j,i} + u_{i,j}) \delta v_j = \int_{\Omega} \left(\nu (u_{j,i} + u_{i,j}) \delta v_j \right)_{,i} - \nu_{,i} (u_{j,i} + u_{i,j}) \delta v_j \\ & = \int_{\Gamma} n_i \nu (u_{j,i} + u_{i,j}) \delta v_j - \int_{\Omega} \nu_{,i} (u_{j,i} + u_{i,j}) \delta v_j \end{aligned}$$

$$\mathcal{T}_2 : \int_{\Omega} \nu (u_{j,i} + u_{i,j})_{,i} \delta v_j = \int_{\Omega} \left(\nu (u_{j,i} + u_{i,j}) \right)_{,i} \delta v_j - \int_{\Omega} \nu_{,i} (u_{j,i} + u_{i,j}) \delta v_j .$$

Equation (A.2) becomes:

$$\begin{aligned} & \int_{\Omega} \nu u_{j,i} (\delta v_{j,i} + \delta v_{i,j}) \\ &= \int_{\Gamma} n_i \nu (u_{j,i} + u_{i,j}) \delta v_j + \int_{\Omega} \cancel{\nu_{,i} (u_{j,i} + u_{i,j})} \delta v_j \\ &+ \int_{\Omega} \cancel{\nu_{,i} (u_{j,i} + u_{i,j})} \delta v_j - \left(\nu (u_{j,i} + u_{i,j}) \right)_{,i} \delta v_j \quad . \end{aligned}$$

Finally equation (A.1) for the 3rd term can be written as:

$$\begin{aligned} & - \int_{\Omega} u_j \left(\nu (\delta v_{j,i} + \delta v_{i,j}) \right)_{,i} \\ &= \int_{\Gamma} n_i \nu (u_{j,i} + u_{i,j}) \delta v_j - \int_{\Omega} \left(\nu (u_{j,i} + u_{i,j}) \right)_{,i} \delta v_j - \int_{\Gamma} \nu n_i (\delta v_{j,i} + \delta v_{i,j}) u_j \\ &= \int_{\Gamma} 2\nu \mathbf{n} \cdot (D(\mathbf{u}) \delta \mathbf{v}) - \int_{\Omega} \nabla \cdot (2\nu D(\mathbf{u})) \cdot \delta \mathbf{v} - \int_{\Gamma} 2\nu \mathbf{n} \cdot (D(\delta \mathbf{v}) \mathbf{u}) \quad . \end{aligned}$$

4th term

$$\int_{\Omega} q \nabla \cdot \delta \mathbf{v} = \int_{\Omega} \nabla \cdot (q \delta \mathbf{v}) - \nabla q \cdot \delta \mathbf{v} = \int_{\Gamma} q \mathbf{n} \cdot \delta \mathbf{v} - \int_{\Omega} \nabla q \cdot \delta \mathbf{v} \quad .$$

5th term

$$\int_{\Omega} \mathbf{u} \cdot \nabla \delta p = \int_{\Omega} \nabla \cdot (\mathbf{u} \delta p) - \nabla \cdot \mathbf{u} \delta p = \int_{\Gamma} \mathbf{u} \cdot \mathbf{n} \delta p - \int_{\Omega} \nabla \cdot \mathbf{u} \delta p \quad .$$

6th term

$$\begin{aligned} \int_{\Omega} T_a \mathbf{v} \cdot \nabla \delta T &= \int_{\Omega} T_a v_i \delta T_{,i} = \int_{\Omega} (T_a v_i \delta T)_{,i} - T_{a,i} v_i \delta T - \cancel{T_a v_{i,i}} \delta T \\ &= \int_{\Gamma} T_a \mathbf{v} \cdot \mathbf{n} \delta T - \int_{\Omega} \mathbf{v} \cdot \nabla T_a \delta T \quad . \end{aligned}$$

7th term

$$\int_{\Omega} T_a \nabla \cdot (K \nabla \delta T) = \int_{\Omega} T_a (K \delta T_{,i})_{,i} = \int_{\Omega} (T_a K \delta T_{,i})_{,i} - T_{a,i} K \delta T_{,i} \quad .$$

The argument of the last term on the right-hand-side of the previous equation reads:

$$-T_{a,i} K \delta T_{,i} = \left(T_{a,i} K \right)_{,i} \delta T - \left(T_{a,i} K \delta T \right)_{,i} \quad .$$

So integrating again by parts, the equation for the 7th term becomes:

$$\int_{\Omega} T_a \left(K \delta T_{,i} \right)_{,i} = \int_{\Omega} \left(T_a K \delta T_{,i} \right)_{,i} + \left(T_{a,i} K \right)_{,i} \delta T - \left(T_{a,i} K \delta T \right)_{,i} .$$

Finally, using the divergence theorem

$$\begin{aligned} \int_{\Omega} T_a \left(K \delta T_{,i} \right)_{,i} &= \int_{\Gamma} K n_i \delta T_{,i} T_a + \int_{\Omega} \left(T_{a,i} K \right)_{,i} \delta T - \int_{\Gamma} K n_i T_{a,i} \delta T \\ &= \int_{\Gamma} K \mathbf{n} \cdot \nabla \delta T T_a - \int_{\Omega} \nabla \cdot (K \nabla T_a) \delta T - \int_{\Gamma} K \mathbf{n} \cdot \nabla T_a \delta T . \end{aligned}$$

Let's consider generic cost functions J of this kind:

$$J = \int_{\Omega} J_{\Omega} + \int_{\Gamma} J_{\Gamma} \quad (\text{A.3})$$

being $\Gamma = \partial\Omega$. After the integration by part performed so far, gathering all the previous contributions, the extended form of the starting equation (3.7) becomes:

$$\begin{aligned} &\int_{\Omega} \left(-(\nabla \mathbf{u}) \mathbf{v} - (\mathbf{v} \cdot \nabla) \mathbf{u} - \nabla \cdot (2\nu D(\mathbf{u})) + \alpha(\rho) \mathbf{u} + \nabla q + T_a \nabla T + \frac{\partial J_{\Omega}}{\partial \mathbf{v}} \right) \cdot \delta \mathbf{v} \\ &+ \int_{\Omega} \left(-\nabla \cdot \mathbf{u} + \frac{\partial J_{\Omega}}{\partial p} \right) \delta p \\ &+ \int_{\Omega} \left(\beta \mathbf{u} \cdot \mathbf{g} - \mathbf{v} \cdot \nabla T_a - \nabla \cdot (K \nabla T_a) + T_a \alpha(\rho) + \frac{\partial J_{\Omega}}{\partial T} \right) \delta T \\ &+ \int_{\Gamma} \left((\mathbf{u} \cdot \mathbf{v}) \mathbf{n} + \mathbf{u} (\mathbf{v} \cdot \mathbf{n}) + 2\nu \mathbf{n} \cdot D(\mathbf{u}) - q \mathbf{n} + \frac{\partial J_{\Gamma}}{\partial \mathbf{v}} \right) \cdot \delta \mathbf{v} - \int_{\Gamma} 2\nu \mathbf{n} \cdot D(\delta \mathbf{v}) \mathbf{u} \\ &+ \int_{\Gamma} \left(\mathbf{u} \cdot \mathbf{n} + \frac{\partial J_{\Gamma}}{\partial p} \right) \delta p \\ &+ \int_{\Gamma} \left(T_a \mathbf{v} \cdot \mathbf{n} + K \mathbf{n} \cdot \nabla T_a + \frac{\partial J_{\Gamma}}{\partial T} \right) \delta T + \int_{\Gamma} K \mathbf{n} \cdot \nabla \delta T T_a = 0 \quad \forall \delta \mathbf{v} \delta p \delta T \end{aligned} \quad (\text{A.4})$$

A.2 Adjoint boundary conditions

In this section we demonstrate equation (3.12) introduced in section 3.1.2 for the computation of the adjoint boundary conditions. We report below the equation:

$$\begin{aligned} \int_{\Gamma} 2\nu \mathbf{n} \cdot (D(\mathbf{u}) \delta \mathbf{v} - D(\delta \mathbf{v}) \mathbf{u}) &= \int_{\Gamma} \nu ((\mathbf{n} \cdot \nabla) \mathbf{u} \cdot \delta \mathbf{v} - (\mathbf{n} \cdot \nabla) \delta \mathbf{v} \cdot \mathbf{u}) \\ &- \int_{\Gamma} \nabla \nu (u_n \delta \mathbf{v} - \delta v_n \mathbf{u}) . \end{aligned}$$

Starting from the definition of the rate of strain tensor, $D(\mathbf{u}) = \frac{1}{2}(\nabla\mathbf{u} + \nabla\mathbf{u}^T)$, the left-hand-side of equation (3.12) reads:

$$\int_{\Gamma} 2\nu\mathbf{n}\cdot(D(\mathbf{u})\delta\mathbf{v} - D(\delta\mathbf{v})\mathbf{u}) = \int_{\Gamma} \nu\mathbf{n}\cdot(\nabla\mathbf{u}\delta\mathbf{v} + \nabla\mathbf{u}^T\delta\mathbf{v} - \nabla\delta\mathbf{v}\mathbf{u} - \nabla\delta\mathbf{v}^T\mathbf{u}) \quad . \quad (\text{A.5})$$

We rewrite the right-hand-side of equation (A.5) in index notation:

$$\int_{\Gamma} \nu n_i u_{j,i} \delta v_j + \underbrace{\nu n_i u_{i,j} \delta v_j}_{\mathcal{T}_1} - \nu n_i \delta v_{j,i} u_j - \underbrace{\nu n_i \delta v_{i,j} u_j}_{\mathcal{T}_2} \quad . \quad (\text{A.6})$$

We now analyze \mathcal{T}_1 :

$$\nu n_i u_{i,j} \delta v_j = n_i (\nu u_i \delta v_j)_{,j} - \nu_{,j} n_i u_i \delta v_j \quad . \quad (\text{A.7})$$

Integrating on Γ the first term on the right-hand-side of equation (A.7) and applying the divergence theorem, we can write:

$$\begin{aligned} \int_{\Gamma} n_i (\nu u_i \delta v_j)_{,j} &= \int_{\Omega} (\nu u_i \delta v_j)_{,j,i} = \int_{\Omega} \nu_{,j,i} \\ &= \int_{\Omega} \nu_{,j,i} u_i \delta v_j + \cancel{\nu (u_{i,i})_{,j}} + \cancel{\nu u_i (\delta v_{j,j})_{,i}} \quad . \end{aligned}$$

The last two terms of the previous equation vanish under the hypothesis of divergence free variations $\delta\mathbf{v}$ and recalling that the adjoint velocity \mathbf{u} is solenoidal. Therefore, integrating on Γ equation (A.7), the term \mathcal{T}_1 becomes:

$$\int_{\Gamma} \nu n_i u_{i,j} \delta v_j = \int_{\Omega} \nu_{,j,i} u_i \delta v_j - \int_{\Gamma} \nu_{,j} n_i u_i \delta v_j \quad .$$

We now analyze \mathcal{T}_2 :

$$- \nu n_i \delta v_{i,j} u_j = \nu_{,j} n_i \delta v_i u_j - n_i (\nu \delta v_i u_j)_{,j} \quad . \quad (\text{A.8})$$

Integrating on Γ the second term on the right-hand-side and applying the divergence theorem, we can write:

$$\begin{aligned} \int_{\Gamma} -n_i (\nu \delta v_i u_j)_{,j} &= \int_{\Omega} -(\nu \delta v_i u_j)_{,j,i} \\ &= \int_{\Omega} -\nu_{,j,i} \delta v_i u_j - \cancel{\nu \delta v_{i,j,i} u_j} - \cancel{\nu \delta v_i u_{j,j,i}} \quad . \end{aligned}$$

The last two terms of the previous equation vanish under the hypothesis of divergence free variations $\delta\mathbf{v}$ and recalling that the adjoint velocity \mathbf{u} is solenoidal.

Therefore, integrating on Γ equation (A.8), the term \mathcal{T}_2 becomes:

$$\int_{\Gamma} -\nu n_i \delta v_{i,j} u_j = \int_{\Gamma} \nu_{,j} n_i \delta v_i u_j - \int_{\Omega} \nu_{,j,i} \delta v_i u_j \quad .$$

Therefore the sum of \mathcal{T}_1 and \mathcal{T}_2 yields:

$$\int_{\Omega} \cancel{\nu_{,j,i} u_i \delta v_j} - \int_{\Gamma} \nu_{,j} n_i u_i \delta v_j + \int_{\Gamma} \nu_{,j} n_i \delta v_i u_j - \int_{\Omega} \cancel{\nu_{,j,i} \delta v_i u_j} \quad .$$

In tensor notation the previous expression becomes:

$$- \int_{\Gamma} \nabla \nu \cdot (u_n \delta \mathbf{v} - \delta v_n \mathbf{u}) \quad (\text{A.9})$$

being u_n and v_n the normal components of primal and adjoint velocities. After substitution in (A.5) of expression (A.9), equation (3.12) can be easily obtained.

Bibliography

- [1] F. Palacios A. Bueno-Orovio C. Castro and E. Zuazua. *Continuous Adjoint Approach for the Spalart–Allmaras Model in Aerodynamic Optimization*. AIAA journal. 2012.
- [2] G. Allaire. *Shape Optimization by the Homogenization Method*. Springer, 2002.
- [3] P. Angot. “Analysis of singular perturbations on the Brinkman problem for fictitious domain models of viscous flows”. In: *Mathematical Methods in the Applied Sciences* 1395-1412 (1999).
- [4] M.P. Bendsøe and O. Sigmund. *Topology optimization by distribution of isotropic material*. Springer, 2004.
- [5] J. Brezillon and R. Dwight. “Discrete Adjoint of the Navier-Stokes Equations for Aerodynamic Shape Optimization”. In: *Evolutionary and Deterministic Methods for Design* (2005).
- [6] F. Palacios C. Castro C. Lozano and E. Zuazua. *Systematic continuous adjoint approach to viscous aerodynamic design on unstructured grids*. AIAA journal, 45(9):2125. 2007.
- [7] A.S. Zymaris E.M. Papoutsis-Kiachagias E.A. Kontoleontos et al. “Constrained topology optimization for laminar and turbulent flows, including heat transfer”. In: *Evolutionary and Deterministic Methods for Design, Optimization and Control* (2011).
- [8] M. Darwish F. Moukalled L. Mangani. *The Finite Volume Method in Computational Fluid Dynamics*. Springer, 2016.
- [9] M.B. Giles and N.A. Pierce. “An introduction to the adjoint approach to design”. In: *Flow, Turbulence and Combustion* 65 393–415 (2000).
- [10] S.J. Wright J. Nocedal. *Numerical Optimization*. Springer, 1999.
- [11] M. Peric J.H. Ferziger. *Computational Methods for Fluid Dynamics*. Springer, 2002.

- [12] K. Lee. *Topology Optimization of Convective Cooling System Design*. PhD thesis, The University of Michigan. 2012.
- [13] S. Nadarajah and A. Jameson. *A comparison of the continuous and discrete adjoint approach to automatic aerodynamic optimization*. AIAA paper 667. 2000.
- [14] *BuoyantBoussinesqPisoFoam*. 2014. URL: <https://openfoamwiki.net/index.php/BuoyantBoussinesqPisoFoam>.
- [15] C. Othmer. “A continuous adjoint formulation for the computation of topological and surface sensitivities of ducted flows”. In: *International Journal for Numerical Methods in Fluids* 58:861–877 (2008).
- [16] C. Othmer et al. *Implementation of a continuous adjoint for topology optimization of ducted flows*. AIAA Computational Fluid Dynamics Conference. 2007.
- [17] A. Quarteroni. *Modellistica Numerica per Problemi Differenziali*. Springer, 2012.
- [18] J. Brezillon R.P. Dwight. *Effect of various approximations of the discrete adjoint on gradient-based optimization*. AIAA 2006-0690. 2006.
- [19] D. Ramajo S.F. Corzo S.M. Damián and M. Nigro. *Numerical simulation of natural convection phenomena*. Mecánica Computacional Vol XXX, p. 277-296. 2011.
- [20] J. Petersson T. Borrvall. “Topology optimization using regularized intermediate density control”. In: *Comput. Methods Appl. Mech. Engrg.* 190 4911-4928 (2001).
- [21] J. Petersson T. Borrvall. “Topology optimization of fluids in Stokes flow”. In: *International Journal for Numerical Methods in Fluids* SE-581 83 (2003).